NASA Research Grant NGR 44-006-088

STRESS CORROSION IN TITANIUM ALLOYS AND OTHER METALLIC MATERIALS

Final Report

summarizing the period of the grant
June 1, 1968 through September 30, 1971

including the work of the following investigators:

F. R. Brotzen, C. G. Harkins, J. W. Hightower, R. B. McLellan,

J. M. Roberts, M. L. Rudee, I. R. Leith, P. K. Basu, K. Salama,

D. P. Parris and J. A. Ehlert

edited by

C. G. Harkins
Senior Research Chemist, Materials Science Group

(NASA-CR-139562) STRESS CORROSION IN TITANIUM ALLOYS AND OTHER METALLIC MATERIALS Final Report, 1 Jun. 1968 - 30 Sep. 1971 (Rice Univ.) 133 p HC $9.75

N74-31005

Unclas
G3/17 46355

Interdisciplinary Research Effort of the Department of Mechanical and Aerospace Engineering and Materials Science and the Department of Chemical Engineering

WILLIAM MARSH RICE UNIVERSITY HOUSTON, TEXAS 77001

TABLE OF CONTENTS

TABLE OF CONTENTS, Continued

Abstract

This is the final report of a three-year interdisciplinary research program on the stress corrosion cracking (SCC) of titanium and titanium alloys. Multiple physical and chemical techniques including mass spectroscopy, atomic absorption spectroscopy, gas chromatography, electron microscopy, optical microscopy, electronic spectroscopy for chemical analysis (ESCA), infrared spectroscopy, nuclear magnetic resonance (NMR), x-ray analysis, conductivity, and isotopic labeling were used in investigating the atomic interactions between organic environments and titanium and titanium oxide surfaces.

Key anhydrous environments studied included alcohols, which contain hydrogen; carbon tetrachloride, which does not contain hydrogen; and mixtures of alcohols and halocarbons. Effects of dissolved salts in alcohols were also studied.

This program emphasized experiments designed to delineate the conditions necessary rather than sufficient for initiation processes and for propagation processes in Ti SCC. Primary results include the following: 1. Molecules initiating SCC of Ti materials (CH_3OH) are strongly chemisorbed on the oxide layer; 2. Oxide film thickness, surface defect orientations, and chemical composition of the oxide film are variables of the initiation process; 3. Photocatalytic properties of the oxide film do not accelerate SCC initiation in pure liquids of either the alcohol or halocarbon class but may facilitate cross reactions in liquid mixtures; 4. In propagation processes, exposed Ti surfaces react directly with the C-Cl bond in CCl_4 and with the O-H bond in CH_3O-H to form Ti compounds. Such direct processes are part of the fundamental chemistry of nonpassivated Ti surfaces and must be included as serial or parallel paths in any generalized TiSCC propagation theory; 5. Chemisorption of CH_3OH and CCl_4 at the Ti surface has the net effect of withdrawing bonding electrons from the metal and localizing them in surface covalent bonds, thereby weakening the metallic bonding and the fundamental strength of the metal at the crack tip; 6. Chemisorption of

molecular hydrogen at Ti surfaces has the opposite effect observed in #5 on the electronic and bonding properties of Ti. While surface hydride is formed and may be passivating, hydrogen removal from the surface by diffusion into the metal phase may facilitate hydrogen embrittlement enhancement of the SCC process; 7. Limited solubility of titanium methoxide provides a passivation process for protection of crack walls in methanol SCC. Variations in this solubility produce a concomitant variation in propagation processes. Presaturation of methanol with $Ti(OCH_3)_4$ inhibits SCC, while increased solubility of Ti, as $Ti(OCH_3)_{4-X}Cl_X$ complexes in chloride solutions, accelerates SCC; 8. In alcohol environments, aluminum is probably not involved in direct surface chemistry of Ti-Al alloys, since presaturation by $Al(OCH_3)_3$ has no effect upon SCC sensitivity; 9. Accelerating effects of chlorine or chloride in the environment on both initiation and propagation steps have been confirmed and extended. Fluoride apparently retarded SCC and pseudohalogens such as azide ion were not observed to alter the SCC process; 10. Alcohols with hydroxyl group acidity less than methanol were not observed to react directly with titanium films except at high temperatures; 11. Alcohols of hydroxyl group acidity greater than methanol should have satisfied thermodynamic requirements for reaction, but SCC testing in alcohols of higher acidity than methanol yielded no SCC. By analogy with other surface chemical processes in porous solids, Ti SCC in organic fluids may be subject to mass transport kinetic control; therefore the proclivity for SCC in CH_3OH and CCl_4 is enhanced by their small molecular size and the correlated ability to diffuse readily within the crack channel.

Minimum requirements for total SCC (initiation plus propagation) in Ti and related materials in organic fluids include: A. Strong chemisorption of organic material and/or halide ions on the protective oxide layer and alteration in mechanical properties of the oxide film by diffusion to defect sites; B. Thermodynamic potential for the organic molecule to undergo strong covalent chemisorption on the metal, thereby reducing the strength of intermetallic bonding; C. Sufficient mechanical stress to develop cracks after alteration in mechanical properties of the solid phases by the chemical interactions; D. Satisfaction of molecular size parameters which allow mass transport to the crack tip in order to sustain the propagation process.

I. INTRODUCTION - SOME FUNDAMENTAL ASPECTS OF STRESS CORROSION

Stress corrosion cracking (SCC) and the resultant failure of modern corrosion-resistant, high-strength materials is a serious technological problem. SCC is also a conspicuous example of technological failure challenging the fundamental understanding of interactions in complex materials systems, requiring and encouraging basic research effort. Stress corrosion has been particularly effective in raising an intellectual challenge as well as a technological challenge simply because the phenomenon is intrinsically multidisciplinary in character, transcending the theory and methods of any one of the traditional scientific and engineering fields.

One consequence of the multidisciplinary aspect of stress corrosion is that the audience most likely to read this report, those currently active in the field, is already heterogeneous in terms of training or experience. Hopefully this report also will reach technical personnel not actively aware of the subtleties of stress corrosion, will whet their scientific curiosity, and will thereby encourage additional input focussed on the fundamental understanding of materials failure and on ameliorating the technological problem of SCC.

To accomodate the expected and desired diversity of readers, this report is written at several levels of consciousness and may be read accordingly. Current experts on titanium stress corrosion and/or those interested only in experimental results may proceed to Section III. In order to minimize extensive digressions in that presentation, much of the background material concerning the system and the chemical properties involved have been extracted and summarized in Section II. Readers familiar with stress corrosion but not with the specific problem of titanium SCC in organic fluids may wish to begin at Section II. Finally, the entire report is for the wider audience unto whom stress corrosion is novel: Section I attempts to summarize the nature of the SCC phenomenon, some approaches to its study, and some relationships to other areas of surface science. Section II introduces a

specific system of technological importance on which these concepts may be tested. Section III reports on the techniques and results of the tests and suggests how these results may refine the concepts of stress corroding systems in theory and in practice.

Any concern for the novice reader outside of the textbook format may seem strange. In part it is compensation for the fact that most science and engineering students will probably never see stress corrosion mentioned in a textbook, especially at the undergraduate level. Texts mentioning stress corrosion do exist, with West [1], Fontana and Greene [2], Uhlig [3], and Scully [4] being notable examples, yet they are relatively specialized texts for corrosion courses, and such courses do not generally exist in United States universities. At a more advanced level several monographs including those by Logan [5], Shvarz and Kristal [6], and Glikman [7] are available. Most of the important information is relatively recent, however, and is available only in the primary journals, in conference proceedings [8,9], or in research reports such as the present one. Considerable effort is required in extracting concepts from the mass of specific detail, and this exercise is often effective in inhibiting the mildly curious from pursuing the topic.

In addition to the experimental effort involved in the present program, we have been involved in a parallel bootstrap educational effort of assimilating a fair portion of the scattered literature on stress corrosion and related topics. This is the basis for the remainder of Section I, and it is a product of the project which, fairly, should be reported. As members of an educational organization we hope that it aids in extending the general appreciation of the stress corrosion phenomenon.

A. Stress Corrosion in Relation to Other Areas of Science and Technology

Stress Corrosion Cracking may be considered part of the generalized concept of "Surface- and Environmental-Sensitive Mechanical Behavior", topic of a recent review essay by Latanision and Westwood [10]. This reference specifically treats neither stress corrosion nor vitreous materials, but it does serve to establish that environment-sensitive mechanical behavior includes more than structural

metals. Numerous examples of environmental-mechanical interactions in ionic solids, such as oxides and chlorides, are cited.

The extension of environmental-sensitive mechanical phenomena to vitreous materials has also been communicated to us by Speidel [11], who indicated that the cracking of rubber in ozone-containing environments and the stress-crazing of plastics, such as polymethyl methacrylate, in organic solvents follows the same macroscopic phenomenology although the microscopic mechanism may be different in that electrochemical effects are minimized.

Since the environmental interaction affecting the strength of materials must proceed through a surface or interface, then environmental-sensitive mechanical behavior along with stress corrosion must be imbedded within the whole panorama of surface adsorption effects on the properties of materials, including the fields of heterogeneous catalysis, corrosion, tribology(friction and wear), and adhesion [12]. Adsorption of molecules at surfaces is the common factor in all of these processes, with many types of surface adsorption states available in the simplest of systems.

The study of detailed mechanisms of adsorption states and adsorption equilibria has perhaps received the most concentrated study in the field of catalysis where the effect of surfaces in accelerating chemical reactions is much more widely known and became the subject of research long before stress corrosion. In the catalysis area, it has already been concluded that that there cannot be a universal microscopic mechanism to explain the catalytic surface phenomenon on all materials [13]. Stress corrosion is a much more complicated effect than catalysis; therefore there is little reason to expect a universal mechanism of stress corrosion either. At least four types of stress corrosion mechanisms have been summarized by Brown [14]: (1) mechano-electrochemical, (2) film rupture, (3) embrittlement, and (4) adsorption. It is likely that under a given set of conditions each is valid, and there is no proof that this is the complete set of physically admissible SCC mechanisms. The critical problem in stress corrosion research is experimentally establishing which mechanisms are operating in a given system under fixed conditions. Only after this information provides a well-understood reference base may this field sucessfully predict stress corrosion effects in novel systems.

B. Macroscopic Phenomenology of Stress Corrosion Cracking

From a technological or design viewpoint, stress corrosion may be summarized in the form of two graphs, shown in Figures 1a and 1b. Figure 1a is pertinent to

uniform cross section tensile specimens such as those shown in Figure 2a, where stress (applied force/unit area) is the mechanical variable and time-to-specimen-failure, t_f, is the response variable. In general, the response curve is a function of bulk alloy composition and thermomechanical treatment, of fluid environment composition, and of the nature and composition of the interface between the metal and the corrosive fluid. One particularly sensitive parameter is the threshold stress, σ_{th}, below which value SCC is not observed.

Existence of such threshold parameters, and the absence of corrosion damage at lower stress levels, is characteristic of stress corrosion, a synergistic process. Some environments are sufficiently corrosive to cause pitting and/or intergranular corrosion in the absence of stress. Acceleration of this process by stress is more accurately called stress-assisted corrosion, and absence of a threshold stress may lead to complications in interpretation.

For purposes of comparing curves on one graph, especially where the composition or heat treatment of the alloy is a variable, then the stress variable on the t_f graph is converted to dimensionless form by plotting as the ratio of applied stress to a yield stress, elastic limit stress, or the breaking stress (if the sample shows no plastic deformation) as measured independently in laboratory air environment.

The design application of such experimental curves is obvious, but the procedure also has its fundamental implications. Smooth uniform samples failing under a given set of conditions indicate that the system has satisfied sufficient conditions for crack initiation and propagation to occur.

It should be emphasized that for the uniform cross section specimens the response parameter, t_f, is a combination of initiation time, t_i, and propagation time, t_p:

$$t_f = t_i + t_p. \qquad [E\text{-}1]$$

This empirical separation into two time factors derives from observation that several fluid environments cannot initiate the stress corrosion of smooth tensile specimens, but the same environments are quite active in promoting subcritical crack propagation in precracked specimens. Other environments can initiate cracks as well as propagate cracks. Two specific examples of these two classes in titanium

SCC are methanol and carbon tetrachloride, the latter fluid being unable to initiate cracks in uniform specimens. Both molecules are active in crack propagation and, as indicated below, crack growth rates at comparable stress intensities may be measured. Data published by Beck and Blackburn [15] indicate the non-initiator, CCl_4, yields higher crack rates. Since the propagation process is undoubtedly associated with breaking of metal-metal bonds in the material, then the absence of initiation by the more active fluid implies some protection of the metal phase during the initiation step. A majority of the alloys sensitive to stress corrosion; such as the stainless steels, and the aluminium, magnesium, titanium, and zirconium alloys; all owe their corrosion resistance to the presence of a protective oxide film. It is logical then to associate the initiation process in these materials with penetration of the protective oxide phase.

One of the paradoxes of stress corrosion testing is that in uniform samples where the initial stress state is easily determined, and where variations in the initiation process may be studied, then evaluation of the relative contributions of the terms in equation [E-1] is difficult. Alternately, in precracked specimens, which must be used with propagation-only fluids, the time to failure variable is simplified:

$$t_f = t_p, \qquad [E-2]$$

but interpretation of the initial stress state becomes complicated.

Qualitatively, introduction of a crack into a uniform cross section specimen under constant load and constant applied tensile stress, σ_{app}, reduces the cross sectional area the plane of the crack; therefore the stress in this region must increase. For purposes of this report we accept that the increased stress cannot be uniformly redistributed over the reduced cross section and the maximum stress concentration or effective stress intensity obtains in the volume of material immediately ahead of the crack tip.* The stress intensity variable is denoted by the symbol $\underline{K}$. $\underline{K}$ must vary as the applied stress varies; it must increase with crack length $\underline{\ell}$, since the reduction in cross section varies with $\underline{\ell}$; and the stress distribution gradient must depend upon sample geometry. It is the domain of linear

*This intensity distribution can be readily observed visually by use of photoelastic models transilluminated by polarized light.

elastic fracture mechanics to consider crack propagation mode, stress state (plane strain vs. plane stress), functional dependence on $\underline{\ell}$ as being $\sqrt{\ell}$, and the geometrical correction factor, $\underline{Y}$. The crack opening mode, termed mode I, is generally assumed, along with plane strain stress state at the crack tip. Incorporation of all these factors is summarized in the equation:

$$K_I = \sigma_{app} Y(\sqrt{\ell}) \qquad [E-3]$$

The geometrical correction factor, $\underline{Y}$, has been calculated only for a few sample configurations, and for quantitative work, it is useful to use those designs. Key references for summaries, explanations, and limitations of precracked designs are Brown and Srawley [16], Brown [17], Hyatt [18,19], and Berggren [20].

Equation E-3 indicates that K_I varies with load just as applied stress varies on the uniform cross section samples illustrated in Figure 1a. A completely analogous time-to-failure curve for the precracked specimens of Figure 2b may be plotted with K_I as a variable and this is illustrated in Figure 1b. The reference stress intensity ($t_f = 0$) in this case is quite clearly the maximum K_I that can be reached before the material yields at the crack tip and the crack becomes unstable. This maximum or critical intensity is given the symbol K_{Ic}. At K_I values below K_{Ic} the crack is stable against propagation unless an environmental interaction changes the strength of the metal at the crack tip region. In the case of stress corrosion as the environmental interaction, a lower threshold value below which crack propagation does not occur is observed, and this design parameter is given the symbol K_{Iscc}.

For additional information on the mechanical aspects of stress corrosion, the reader should refer to the paper of Scully [21] and the references contained therein.

Replotting of Figure 1b in differential form, as in Figure 1c, yields additional insight into stress corrosion processes by magnifying the effects which occur at high stresses. Measurements of crack rate as a function of K_I is facilitated by the double cantilever beam (DCB) precracked specimen illustrated in Figure 2b. Speidel [11,22] has pointed out that region I is the normal stress dependent SCC region with crack rates the order of 10^{-6}—10^{+1} mm/minute.
The inflection leading to stress independent region II represents the onset of mass transport control, since an environment-influenced phenomena cannot occur faster than the environment can migrate to the interface. The upper break in the

curve at K_{Ic} corresponds to the onset of purely mechanical fracture with crack rates $> 10^6$ mm/min., and region III is environment independent. By varying the viscosity of the liquid phase in a series of elegant experiments on aluminum SCC, Spiedel [22] showed directly that the slope of region I remained unaltered while the onset of mass-transport control was affected drastically. Limiting stress corrosion crack velocities (region II) could be altered over two orders of magnitude.

We close this section with comment on the complications introduced if the system is subject to stress-assisted corrosion rather than stress corrosion. Since there is no threshold stress level in the case of stress-assisted corrosion, then time-to-failure studies will be subject to errors dependent upon the time of exposure before load is applied to the specimen and the rates of reaction at zero stress. This pre-corrosion phenomena has been observed experimentally and its implications discussed by Cocks, Russo, and Brummer [23,24]. The latter authors' experience with titanium SCC in CH_3OH/Br_2 solutions [23] is particularly relevant to this report, not because we used this particular environment, but because much of our work on the role of alcohol molecular weight must be compared with systems in which free halogen was added to the alcohols [25]. Addition of free halogens may not be necessary for SCC in higher alcohols, but it is apparently sufficient, since it is sufficient in the absence of stress.

C. Microscopic and Fractographic Examination in Stress Corrosion

In all failure analyses, examination of the fractured surface is a useful process, and this is no less so in stress corrosion. The observed data in this technique is the topological texture of the fracture, and this texture may be correlated with processes occuring at the crack tip as metal-metal bonds were being broken. For example, at stress intensity K_{Ic}, a small zone of ductile (plastic) yielding develops at the crack tip. The size of this zone must be dependent upon several metallurgical factors, but there is a commonality in the resulting fracture texture. Ductile failure at high crack rates generally results in a topology described as "cup and cone" or "dimpled", a characteristic dimple size being in the range 1-10 micrometers. Fracture environmentally induced at subcritical stress intensities $(K_{Ii} < K_{Ic})$, as occurs in stress-corrosion and hydrogen embrittlement

phenomena, is more characteristic of failure in brittle materials such as glass. The resultant texture is jagged with some directional characteristics, as shown in Figures 22 and 23. Invaluable in the interpretation of such data, particularly for the novice, is a dictionary of reference patterns generated under carefully arranged conditions. A key publication of this nature is the Electron Fractographic Handbook by Phillips, Kerlins, and Whiteson [26].

The usefulness of fractrographic methods in SCC lies in a careful interpretation of the one-way correlation between texture and environmental/mechanical interactions. A change in texture of fracture will definitely indicate changes in chemical processes at the crack tip, but a change in chemical mechanism at this interface need not be reflected in a change of fracture mode and texture. From a chemical viewpoint, fractography generally detects the results of a chemical interaction and not the components. It should not then be relied upon to identify species. The exception to this occurs if, in the process of observing textures, one can also identify new solid phases that may have formed at the surface. The papers of Powell and Scully [27] and Gegel, Kirkpatrick, and Swinning [28] provide examples of this latter case, where observation of a hydride phase indicates the presence of a hydrogen reaction.

In pursuing the fractographic technique with the transmission electron microscope, one immediately faces the requirement of a sample which will transmit the electron beam. For direct examination of metals, this requires the thinning of a sample by electropolishing techniques. This procedure is difficult at best, and thinning of a sample while attempting to maintain fractrographic information is probably beyond the state of the art. Direct transmission studies are usually performed upon samples that have been thinned before exposure to corrosion environments, but these specimens are quite fragile. The alternative to viewing the original specimen involves preparation of a metal-shadowed carbon replica of the fractured surface. An intermediate step of casting a plastic negative requires considerable technique by the experimenter, and considerable ability by the replicating material to faithfully duplicate fine detail without the introduction of artifacts. The procedure is tedious at best and misleading at worst.

The possibility of misinterpretation arises not only from replica artifacts, but from the difficulty of correlating a replica geometrically with its equivalent on the original surface.

Recent introduction of the scanning electron microscope has eliminated the thinning and the replicating problem, for the only sample requirement is that it be an electrical conductor. Original fractured surfaces of structural metals may be studied directly, with the dual advantages of large depth of field and absolute geometrical correlation. Comparisons of fractrographs obtained by both scanning electron microscope and replica/transmission electron microscope techniques have been complied and issued by Sloan [29], and this author summarizes the complementarity of the two methods.

D. Metallurgical Variables in Stress Corrosion

Topics I-B and I-C have presented stress effects in SCC in overview form without consideration of the fine structure of the stressed solid. This isotropic continuum approximation applies with little qualification for glasses and most plastics, because of their random atomic and molecular orientation. Metals, forming crystal structures of cubic or lower symmetry, will be anisotropic in the sense that the Young's moduli for elastic deformation under stress, and the energy of dislocation motion (slip) for plastic deformation under stress, will be a function of crystallographic direction.

If many crystallites of random orientation are agglomerated in the solid, which is the case in structural grade metals, these directional effects are averaged out so that at the macroscopic level the isotropic approximation remains useful. Less accurate is the homogeneity approximation for polycrystalline materials due the presence of a large number of complex defective regions, the grain boundaries.

Grain boundaries represent microscopic local perturbations on the average stress field and this has important mechanical and chemical effects. As a simple example we consider the low angle grain boundary consisting of an array of edge dislocations: At each dislocation in the array an extra tensile stress component is added on the missing half-plane side, and a compressive stress component is added on the extra-half-plane side. Stress field interactions stabilize the

array; but, in alloys containing small substitutional atoms or interstitial impurities, chemical interactions can also lower the free energy of the grain boundary. Interstitials collecting at the tension side of the edge dislocation and small substitutional atoms collecting at the compression side produce the volume changes that reduce the inhomogeneity of the stress/strain perturbations.

These effects are related to the nature of crack propagation, hence stress corrosion cracking, in the following way: A crack approaching a grain boundary (more complex than edge dislocations, but containing these as a component) may follow the boundary or enter the next grain, and this is dependent upon the relative strengths of the two regions. In most metals at ambient temperatures the grain boundaries are stronger (being equivalent to work-hardened material) than undeformed grains, and for sub-critical crack propagation ($K_{Ii} < K_{Ic}$) the cracking will be transgranular, usually along preferred cleavage planes. In alloys or materials where chemical impurities have diffused to the grain boundary, new brittle phases may form, and in this case cracking may be intergranular, with failure occurring along grain boundaries normal to the macroscopic stress field.

Impurity effects, hence alloying effects, show up even in the case of transgranular cracking whenever impurities atoms collect along preferred crystal planes and change the slip and cleavage modes of the grain. Such an explanation for the observed SCC cleavage plane in titanium alloys has been described by Mauney and Starke [30].

Since impurity effects are concentration dependent, and diffusion is a limiting factor in assembling high concentration, it is logical that hydrogen as the fastest diffusing interstitial species has maximum effect. Hydrogen embrittlement of the grain or of the grain boundary is an important part of stress corrosion theory.

Accidental or purposeful introduction of interstitial and substitutional impurities to increase the macroscopic strengths of metals does not represent the ultimate in metallurgical practice. Without considering stress corrosion effects, other desired mechanical properties are obtained by alloying and heat treatment which stabilizes or precipitates a second crystal phase in the base metal matrix.

Either phase may be a single metal, an interstitial or substitutional solid solution, or a stoichiometric intermetallic compound. The basic mechanical and chemical properties of each phase, the grain size of each phase and its distribution in the microstructure, and the shape of the grains combine to determine the macroscopic mechanical properties; but each parameter individually may determine the crack propagation and stress corrosion properties.

In two-phase materials, cracks may propagate transgranularly faster in one phase than in the other, yet grain boundary effects and the possiblity of intergranular failure remain. In general the random dispersion of a resistant second phase should impede stress corrosion, while incorporation of a brittle second phase should enhance it, but grain boundary and preferential interstitial solubility effects provide a large number of exceptions.

Multiphase and single phase alloys may have grain size and orientation altered by thermomechanical treatment. Mechanical deformation such as rolling introduces a deformed and oriented grain structure, and the resulting anisotropy is reflected in the stress corrosion response. Time to failure at a given K_{Ii} becomes a strong function of sample orientation with respect to rolling direction of the original material. Sampling is usually done so that the crack plane is parallel or perpendicular to the rolling direction, and such longitudinal, transverse, and short transverse samples demonstrate a dependence in both t_f and K_{Iscc} for crack propagation in the three orthoganol directions. These effects have been demonstrated and summarized by Fager and Spurr [31, 32]. Thermal processing can sometimes be used to offset these effects. Annealing will lead to recrystallization of the deformed grains, reducing the number of crystal defects and randomizing the amount of grain orientation if a sufficient number of small grains are formed. Annealing with production of large grains may decrease failure time if the length of crack necessary for K_I to increase to K_{Ic} runs in a particularly sensitive direction in a large grain.

Thermal processing in multiphase alloys is often used for ageing rather than annealing, with the grain size of the second phase being a function of a time-temperature cycle [33]. Overaging leads to a larger grain size and a softer material, but this loss in mechanical strength is accompanied by a

decreased SCC sensitivity, at least in aluminium alloys [34].

This summary of metallurgical factors is necessarily incomplete; but it should serve to indicate that the solid phase in metals can be very complex and this in turn introduces a complexity to the study of SCC in these materials. Metallurgical techniques have an important experimental role in stress corrosion research ranging from characterization and quality control of test samples to the production of SCC resistant alloys.

E. Chemical and Surface Chemical Aspects of Stress Corrosion

Regardless of the metal phase complexity, sample shape, and stress state, subcritical crack propagation does not occur unless there is a chemical interaction with the material at the crack tip. The reacting environment may diffuse internally to the crack tip region, as in hydrogen embrittlement; or it may diffuse to the crack tip surface from an external source, as in stress corrosion. The most striking features of the SCC phenomenon is the very high specificity with regard to the chemical identity of the environment and the existence of a threshold stress or stress intensity which appears to control the reaction.

The chemical details of stress corrosion, especially the nature of the system as it develops within the crack is perhaps the most empirically studied and least exploited aspect of stress corrosion. Outstanding efforts have recently developed in this area such as the freeze-crack-thaw and the microelectrode probe technique of Brown and colleagues [35,36], and the solvent variation studies and cation variation studies both of Haney [37] and of Sedriks and Greene [38]. Continued effort concerning chemical details has also been facilitated by the discovery of new SCC environments such as organic fluids and the development of samples well-characterized for their stress state as referenced earlier [16-20]. Hopefully some of the techniques exploited in the research effort of this report will be of extended use in this area.

(1) Electrochemical Adsorption

The bulk of fundamental chemical studies in SCC have been electrochemical in nature, a historical requirement since most early observations of stress corrosion and many of the empirical SCC screening tests involved metals in aqueous electrolyte environments. A classic example is stainless steel exposed to boiling $MgCl_2$ solution.

Corrosion chemistry and stress corrosion chemistry is not, however, fundamentally limited to electrochemical processes. The requirements for an elec-

trochemical process are rather extensive, even if they are easily met in practice. Two requirements are basic: an electron-conducting medium and an ion-conducting medium. Commonly cited examples are, respectively, metals and liquid solutions of ions, yet, to place this in general perspective, ionic and covalent semiconductors can just as well serve as electron-conducting phases and defective ionic solids such as doped ZrO_2 and $RbAg_4I_5$ can serve as ion-transport media in place of liquids.

The absence of either conducting medium precludes electrochemical processes. Non-conducting solids such as common plastics, glasses, and insulator crystals cannot crack by an electrochemical mechanism. Neither will metals fail electrochemically in non-conducting fluid environments, especially in non-polar organics which cannot solvate ionic intermediates. Stress corrosion initiation by vapor phase environments may also be free of electrochemical effects.

Several chemical and physical techniques such as impurity additions and irradiation may convert a non-conducting phase into a conductor and allow an electrochemical mechanism to proceed if free energy conditions provide a driving force. A pertinent example would be the introduction of an ionic salt into a polar organic liquid/metal system. Salt dissolution and conversion of the liquid phase into a conducting solution may have either no effect or may introduce an electrochemical process.

Since electrochemical processes are often the likely chemical mechanism or the invoked mechanism in the SCC of metals, some electrochemical details should be kept in mind. One feature is that anodic and cathodic electrode areas exist somewhere within the system. Since a critical process occurs at the crack tip, it is probable, although not necessary, that this region be one of the electrodes. If the crack tip is anodic, stress corrosion includes direct dissolution of the metal. If the crack tip is cathodic and if hydrogen is discharged at that point, the metal may alternately fail by hydrogen embrittlement. The hydrogen-embrittlement hypothesis also provides for subcritical crack propagation if a cathodic region is somewhere near the crack tip so that metal phase diffusion of hydrogen to the stressed region facilitates brittle fracture.

From an electrochemical viewpoint, polycrystalline alloys provide an inhomogeneous system ideal for formation of internal anodic and cathodic areas. Godard [39] has detailed this extensively. Evidently pure grain boundaries with strain

energy stored in the dislocations do not strongly change the reactivity*, but segregation of chemical impurities at the grain boundaries has a major effect. Segregated grain boundaries anodic to the crystallites will facilitate direct intergranular corrosion. Grain boundaries enriched by impurities may also be cathodic with respect to a diffusion depleted layer near the grain boundary. Resulting corrosion of the depleted layer by local cell action leads to essentially the same result as grain boundary corrosion. Both types of intergranular corrosion occur in the absence of stress and are often active in stress-assisted corrosion failures.

In intergranular corrosion internal geometrical limitations restrict the volume of material that is corroded away. In transgranular corrosion there is no such geometrical restriction, and the entire grain interior is subject to dissolution. The latter process would blunt the crack tip and lower the strain intensity as well as perturb the orientation of the non-planar zero isoclinic surfaces as the crack tip approaches a circular contour [40]. In order to explain continuation of the SCC process and absence of grain interior dissolution, passivation of the crack walls by corrosion products or solution impurities is invoked. This is reasonable in the alloys which are quite active with regard to oxide film formation. The crack tip itself would be then subject to passivation, so creation of fresh surface in that region by slip step emergence due to stress/strain effects has been suggested as a mechanism. This model is detailed along with a summary of many electrochemical factors in an article by Scully [41].

These SCC electrochemical mechanisms share a complication common to all electrochemical systems, that of a complex adsorption layer, commonly called the double layer, whose nature can control the electrode kinetics and the mechanism of the chemical reaction. In SCC not only the steady state properties of an existing double layer are involved, but the absorption kinetics for formation of a new double layer on the fresh metal must be considered as a possible rate-controlling step.

---

*The reactivity difference is sufficient to be useful in metallography for revealing the grain structure by etching.

The topic of double layer adsorption kinetics has been presented by Mohilner [42] and a review by Divanathan and Tilak [43] provides additional details and a guide to the extensive literature on the double layer. Double layer adsorption involves formation upon a charged metal surface of inner Helmholtz layer consisting of chemisorbed solvent molecules, perhaps other neutral molecules and, under most conditions, a fractional monolayer of specifically adsorbed desolvated ions. An outer Helmholtz layer (Gouy layer) consists of an ordered adsorption layer of fully solvated ions, and current theory suggests that these ions cannot approach the metal surface more closely than two solvent molecule diameters (one diameter for the solvating sheath, one diameter for the directly adsorbed inner layer). This structure is illustrated in Figure 3, taken from Mohilner [42]. Although the solvent variables listed are for water, the adsorption model is general for all polar molecular solvents.

The key step in electrochemical double layer specific ion adsorption, which distinguishes it from simpler adsorption, is loss of the solvation sheath around the ion, at least in the direction of the metal surface. Only then can the ion penetrate to the inner Helmholtz layer and bond to the metal. Energy considerations suggest that desolvation requires an activation energy proportional to the heat of solvation. Large univalent ions, hence anions such as Cl^-, are therefore most likely to undergo specific adsorption. The exact nature of the ion/metal bonding is still an open question with some evidence that it is covalent [43]. Devanathan states in this same reference that desolvation of the ion is a necessary condition for specific adsorption and covalent ion/metal bond formation is sufficient for specific adsorption.

In summary, the adsorption species which may be present in an electrochemical mechanism to influence the response of the metal to stress includes neutral molecules, solvated ions, and specifically adsorbed ions that may involve covalent bonding. For sake of completeness, we cite that free radical intermediates have also been proposed for organic systems, the Kobe reaction being one example [44]. The difficulties of determining the mechanism in electrochemical systems is difficult enough at exposed electrodes free from

mass transport effects. Electrochemical studies are complicated in stress corrosion by the isolation of the electrode at the crack tip where concentration gradients and electric field gradients with respect to the external environment are likely. T. R. Beck [45] has devoted considerable effort to detailing a mass transport model to consider ion flow in the crack.

If ions and an electrochemical mechanism were absolutely necessary for stress corrosion cracking to occur, then chemical research in SCC would have to live with the complications of ion adsorption. Empirical discovery that titanium alloys might stress corrode in organic environments [46], particularly non-polar organics [46a] and in the vapor phase [46b], indicated that elimination of the complexity of electrochemical aspects of stress corrosion might be an option in this system. If so, the electrochemical adsorption theory outlined above could be replaced by the simpler non-electrochemical theory and techniques widely developed in sister fields of surface sicence. This has been our approach to the titanium/organic system, with electrochemical details being interpreted as an additional rather than an unique adsorption mechanism for SCC.

(2) Direct Molecular Adsorption

Although direct adsorption effects have been recognized in liquid metal embrittlement, and while Coleman, Weinstein, and Rostoker [47] have suggested that direct adsorption of ions or atoms following electrochemical steps is the critical process in SCC, there seems to be no specific statement in the stress corrosion literature regarding the theory of direct adsorption of neutral molecules and the mass transport effect corrections to neutral molecule adsorption in porous solids. This information suggested several of the experiments reported in Section III, and provided interpretation for some of the results; therefore, some aspects of direct adsorption theory is summarized below:

Dowden [48] presented one of the first treatments on the chemisorption of molecules and molecular fragments in which the solid phase was considered as a source or sink of electrons. Physical adsorption, whereby a neutral molecule is held to a surface by weak van der Waals forces, was already recognized as a

precursor state generally available to any molecule. Dowden suggested that only if (1) the electronic energy levels of the physisorbed molecule and the substrate surface are positioned relative to each other that one acts as a donor reactant and the other as an electron acceptor reactant, (2) the physisorbed state bonding distance is sufficiently short for orbital overlap to occur, and (3) the potential barrier separating the crystal levels and the sorbate levels is permeable to electrons, can chemisorption occur. The resulting species may be ionic or covalently bonded in nature, depending on the direction and amount of electron flow, and the kinetics and equilibria are dependent upon the electronic band structure of the substrate solid.

For polyatomic molecules, associative and dissociative chemisorption may be distinguished, depending on whether the molecule is bound as a whole to a single surface site or if original bonds in the molecule are broken. The latter results in multiple bonding for a single molecule or separation and independent bonding of molecular fragments. Recent insights concerning conservation of molecular symmetry during such dissociative processes [49] indicate that the d-electron orbitals of the transition metals are symmetrically favorable for interaction with molecule antibonding states, leading to the dissociation and activation of the latter species. It is consistent to expect that transition metals rather than regular metals would be particularly sensitive to the effects of dissociative molecular chemisorption, depending upon the exact nature of the adsorbed intermediates and the reversibility of the chemisorption reaction. Strongly adsorbed intermediates and extensive rearrangement of bonding in the metal would tend toward irreversible destruction of intermetallic bonding, i.e., corrosion.

The electron transfer processes of chemisorption and intermetallic decoupling have a rate and activation energy determined by electronic potential surface parameters, and this intrinsic maximum rate for whichever step is rate-controlling may be assigned the rate constant, k. This is the fundamental reactivity parameter sought in surface chemical measurements. In a heterogeneous system, however, geometric parameters must also be satisfied; therefore, mass transport and adsorption effects can provide a lower observed rate, k'. Mass transfer control at a

well-exposed surface is best eliminated rather than compensated for in determining k, but mass transport effects are not easily eliminated in porous solids with active surface at the bottom of a pore or crack.

Fortunately Thiele [50] considered this problem of diffusion to internal surfaces several years ago, stating that it was applicable both for corroding and non-corroding porous solids. Its immediate application was to the field of catalysis where porous solids are extensively used, and the treatment of Thiele was expanded considerably by Wheeler [51] for describing pore effects on catalytic rates. The extent and sophistication to which the study of surface reactions in porous media has currently developed may be found in the books of Petersen [52] and Satterfield [53], but the simpler theory is sufficient to explain the current state of mass transport effects observed in SCC:

For reaction in pores or at crack tips, the mass flow is determined by the diffusion coefficient for the molecular species, D; and the crack geometry, whose factors include the length of the pore, L, and the average pore radius, $\bar{r}$. These are correction factors on the intrinsic reaction rate coefficient, k. Thiele and Wheeler showed that these factors may be combined to yield a dimensionless constant, h_o, called the Thiele-Wheeler modulus, and this pure number characterizes the sensitivity of a porous solid undergoing surface processes to mass transport effects.

For psuedo-first order processes this modulus is defined by a combination of the above factors as:

$$h_o \equiv L\sqrt{\frac{k}{\bar{r}\, D}} \qquad [E\text{-}4]$$

By inspection one sees that those factors tending to induce mass transport such as long crack length, small radius, and low diffusion coefficient will correspond to high modulus values; while systems relatively free of mass transfer will correspond to low modulus numbers.

Thiele and Wheeler also show, especially for flat plate samples penetrated by straight pores, that the rate of surface reaction inside the pore, k', is a fraction, f, of the rate at the pore mouth k, as given by the equation:

$$f = \frac{k'}{k} = \frac{\tanh h_o}{h_o} \qquad [E\text{-}5]$$

where tanh = hyperbolic tangent. For low values of h_o, tanh $h_o \rightarrow h_o$, f = 1, and the surface is uniformly reactive. Applied to freely corroding systems with high modulus cracks, equation [E-5] implies that the highest rate of corrosion will occur at the crack mouth, and the lowest rate at the crack tip.

This freely-corroding direct-adsorption model is not consistent with crack propagation, just as in the electrochemical model. We must therefore invoke again crack wall protection by some passivating species. Fortunately this effect and its mass transfer implications were also covered by Wheeler under the theme of pore mouth poisoning. In this case mass transfer control of the internal surface reaction may be even more effective than in the free surface case.

Quantitatively, the Wheeler treatment retains the modulus of Equation [E-4], and introduces activity parameters as shown in Fig. 4a. The fraction of the pore length free to react is symbolized by α, and the fractional length of the poisoning or passivation must be $1-\alpha$. The rate of reactant conversion at the pore tip as a fraction of the unlimited surface reaction is now given by [51] :

$$f = \frac{k'}{k} = \frac{\tanh h_o\alpha}{\tanh h_o \; [1+(1-\alpha)h_o]} \qquad [E-6]$$

The parametric curves of equation [E-6] are plotted for various h_o values in Fig. 4b. In SCC cracks the fraction of the pore passivated is probably large so that mid-value deviations are not so important. Systems of moduli ≤ 10 respond essentially the same as mass-transport free systems, but crack systems of moduli ~ 100 are highly mass-transport limited. Use of this model specifically indicates that the average crack radius or width is an important parameter as well as the length, and that there well may be a critical size opening. If one of the functions of stress in stress corrosion is to hold the crack open, and there is a critical size crack radius, this may be one reason for a threshold stress level.

II. SPECIFIC SYSTEM COMPONENTS: TITANIUM ALLOYS AND ORGANIC FLUIDS

Application of the general principles of Section I toward the design of SCC experiments and the interpretation of the resulting data is ideally done with the goal of determining the microscopic mechanisms in a specific SCC system. Stress corrosion experiments per se are not sufficient to supply all of the microscopic detail necessary to describe the molecular, atomic and electronic properties considered basic to the mechanism. The purpose of this section is to catalogue some of the theoretical and experimental details concerning the components of the system whose stress corrosion mechanisms we are interested in: titanium alloys in contact with organic fluids.

A. Chemical and Mechanical Properties of Titanium

Following our earlier review of this topic [54], we distinguish between state-independent and metallic state characteristics of titanium. Among the state-independent properties is the isotopic composition whose natural distribution is Ti^{46}, 7.93%; Ti^{47}, 7.28%; Ti^{48}, 73.94%; Ti^{49}, 5.51%; and Ti^{50}, 5.34%. In mass-spectroscopic studies, a symmetrical quintet corresponding to this distribution in the cracking pattern is highly specific for Ti-containing species.

The atomic ground state electron distribution in Ti is $[Ar]3d^2 4s^2$, and the valence electron ionization energies are relatively low. Multiple electron loss or sharing is observed, with compounds containing formal oxidation numbers of +2, +3, and +4 all being known. Bonding type within these formal numbers is variable, particularly for the +4 state, where the charge density is extremely high. Such cationic charge density can only be stabilized in a lattice of highly electronegative anions, else the orbitals of the Ti^{+4} core will attract some electron charge density. This is reflected in the ionic bonding of TiO_2, with a lattice melting point of about 1850°C versus the covalently bonded $TiCl_4$, whose intramolecular bonding energy is high, but the intermolecular bonding is so low that solid $TiCl_4$ melts at -25°C. This shift in bonding type occurs at a critical Pauling electronegativity value [55] somewhere between 2.5 (Cl) and 3.0 (O). All compounds containing Ti (IV) must

therefore have some covalent character except for the oxides and the fluorides. The ease of oxidation of titanium compounds and the stability of the ionic oxide lattice, confers on titanium chemistry an extreme sensitivity to an oxygen-containing environment.

The condensed metallic state of titanium is stabilized by overlap interactions among the atomic valence electrons to yield delocalized crystal orbital states of lower kinetic energy. Essentially the atomic s and d discrete energy states split to yield analogous valence bands describing the electron distribution within the metal. These bands for titanium as calculated by Snow and Waber [56], assuming a muffin-tin potential for the ion cores and an attenuated plane wave description for the valence electrons, are shown in Figure 5. Both s and d bands are sufficiently broadened to provide considerable energy overlap, and, as opposed to the isolated atom configuration, the average number of d and s electrons/atom need not be an integer value. The density of states is much higher for a given energy in the d-band than the s-band, and the majority of the electrons for an early transition metal-like titanium are in the t_{2g} d-orbitals (nearest-neighbor bonding) [57].

The energy stabilization due to band formation and electron redistribution in the metallic bonding of Ti is reflected in the increase in the electron binding energy. The first ionization potential for atomic Ti is 6.83 eV, while the Fermi energy E_f, indicated in Figure 5, is -0.92 Rydbergs, equivalent to a 12.5 eV ionization potential. All metallic bonding contributions result in a heat of sublimation for Ti metal of 112.7 kcal/mole.

Unfortunately only a fraction of this interatomic bond strength appears in the macroscopic ultimate tensile strength of a polycrystalline structural titanium, since this engineering parameter is controlled by the nature and mobility of structural imperfections. In the elastic region, however, macroscopic strain does result from a change in interatomic spacings, and the applied stress producing this strain works in opposition to the restoring forces of the metallic bonds [58].

A metallurgically important parameter in titanium is the crystal structure, for this metal shows allotropism, transforming from the low-temperature hexagonal

close-packed phase, denoted as α, to the body centered cubic structure, β, about 880°C. This effect appears in titanium because the Fermi energy, E_f, corresponds so closely with the maximum in the d-band density of states curve as shown in Figure 5. Thermal promotion of electrons to states above the d-band maximum will decrease the d-band : s-band occupation ratio, decreasing the bonding energy since d-character bonding is apparently much more effective than s-type metallic bonding. Since the density-of-states maximum arises from contact in phase space of the Fermi surface with a Brilloun zone, and the shape of the latter is dependent on the crystallography of the metal, a change in crystal structure alters the band shape and shifts the maximum in the density of states curve. In the β structure the maximum is evidently higher with respect to the Fermi level than in the α-phase, so that thermal promotion of electrons above E_f in that structure will reduce the d:s ratio less. In effect, the crystal structure changes to minimize the crystal energy by maximizing the number of bonding d-electrons.

This effect is observed experimentally by measurement of the electrical conductivity during the allotropic transformation. Powell and Tye [59] report a bulk resistivity decrease from 164.4 to 148.4 microhm-cm. for the $\alpha \rightarrow \beta$ transition in pure titanium, indicating an increase in the number of d-electrons at the Fermi level. This interpretation derives from the general formula [60] for electrical conductivity, σ :

$$\sigma = N e^2 \tau / m^* = N e \mu \qquad [E-7]$$

where N = number of electrons/unit volume, e = electronic charge, τ = electron scattering relaxation time, m^* = effective mass of electron, and μ is a combination of the three latter terms designated the electron mobility. For Fermi levels at or below the density of states maximum, the mobility is essentially constant, so that σ measures $N(E_f)$, the number of (essentially d-type) electrons at the Fermi level.

The effect of substitutional alloying by atoms comparable in size to titanium may be systematized within the same rigid band model. Elements with a valence electron/atom ratio < 4 will lower the Fermi level with respect to the band maximum, reducing the requirement for the phase transition, thereby stabilizing the

α-phase. Substitutional alloying of atoms of valence electron/atom ratio ≥ 4 will raise the Fermi level, favoring and stabilizing the β-phase. Multiple alloying element additions combined with suitable thermomechanical processing (cf. Section I-D) provides for an extensive series of single and polyphase alloys for commercial use. The more common of these are listed by composition and phase in Table 1. ASTM standards for the commercial alloys have been published [61] as well as references summarizing the various properties [62,63].

Variations in the non-alloyed (commercially pure) grades are primarily due to dissolved oxygen, which at low concentrations promotes a net proportional increase in yield strength with oxygen content [64]. Commercially-pure grades are therefore coded by yield strength (A-70 = 70 ksi nominal YS). From an electronic band standpoint, the highly electronegative oxygen is an α-phase stabilizer, reducing the number of metallic bonding electrons by localizing them at the oxygen core. However, strain by slip occurs at low stresses in pure metals, and in the titanium α-phase the main slip systems are $(0001)\langle 11\bar{2}0\rangle$, $\{10\bar{1}0\}\langle 11\bar{2}0\rangle$, and $\{10\bar{1}1\}\langle 11\bar{2}0\rangle$. Oxygen at low concentrations is an interstitial species, and as such it impedes slip in these easy directions, thereby increasing the yield strength.

Other impurity atoms small enough to satisfy the interstitial condition (radius of impurity atom ≤ 0.59 radius of Ti [65]) but large enough to inhibit slip should behave in the same manner. This has been observed for nitrogen as well as oxygen [64] along with the observation that the Vickers hardness of α-Ti also increased with the concentration of these two interstitials.

Hydrogen is both smaller in size and lower in electronegativity than oxygen and nitrogen, and therefore differs in mechanical effects. Conser [64] observed neither an increase in yield strength nor Vickers hardness. Hydrogen does, however, tend to form at least two hydride phases in titanium. The most usually cited form is the face-centered cubic γ hydride observed near room temperature. Neutron diffraction studies by Sidhu, Heaton, and Zauberis [66] indicated this form to be analogous to the CaF_2 structure with the hydrogen nuclei residing in tetrahedral holes in Ti lattice. At higher temperatures there is a β hydride phase which is body-centered cubic. Just at the composition TiH_2, the authors of [66] indicate that the fcc γ-lattice undergoes a tetragonal distortion, and

they ascribe the brittleness of this compound to the highly directional bonding suggested by this structure. Korn and Zamir [67] have restudied the phase diagram by use of spin-echo nuclear magnetic resonance and indicate that below 125°C, the α-phase of titanium remains almost hydrogen-free due to the formation of small clusters of γ-hydrides of local composition about $TiH_{1.4}$. This latter observation perhaps explains the lack of an effect on the yield strength and hardness at small H-concentrations. In their explanation of the particular cleavage plane for SCC failure of titanium, Mauney and Starke [30] indicate the γ-hydride precipitates on the $\{10\bar{1}0\}$ and $\{10\bar{1}1\}$ planes to impede that fraction of the number of slip systems.

Electronically, hydrogen is low enough in electronegativity that its bonding to Ti must have considerable covalent character. In sharing its electron with the metallic band, hydrogen ingress raises the Fermi level and serves as a β-stabilizer. Consequently the solubility is higher in the β-Ti lattice, and there is little evidence for immediate hydride precipitation.

The donation of electronic charge to the Ti conduction band by hydrogen will be referred to again in Section III with regard to our thin film conductivity experiments, but there is considerable independent evidence for the validity of this model. Bastl [68] not only measured the conductivity increase in Ti/H solutions, but by the Hall effect determined the carriers were electrons rather than holes. Jones, by studying both magnetic susceptibility [69] and solubility [70] of hydrogen in Ti, showed that when the t_{2g} band received electrons from atoms of valency > 4 the hydrogen solubility was proportionately decreased. The bonding d-subband is filled at the electron/atom ratio closely corresponding to TiH_2, conferring particular stability on that composition. Sidhu [66] indicates that the tetrahedral hole at that composition is too small for a hydrogen atom, suggesting considerable Ti-H covalent bonding. The Ti-Ti bonding also becomes somewhat reduced as indicated by an increase in Ti-Ti distance. Dempsey [71] has generalized the concept of t_{2g} band filling to explain the high melting points and hardness of early-transition-metal borides, carbides, and nitrides; all of which have an electron/atom ratio close to 6 if they are considered to be metallic-bonded compounds.

The internal consistency of the band model is also indicated by the increased α-phase solubility of hydrogen in Ti-Al alloys [72]. Addition of aluminum lowers the Fermi level in the band, increasing the number of states available for the hydrogen.

The independent and the mutual effects of hydrogen and aluminum have developed into a key point in explaining the increased sensitivity of alloys containing ≥ 5% aluminum toward stress corrosion. Mauney and Starke [30] invoke aluminum effects in addition to hydrogen effects for slip impedance on the basal plane of hcp titanium in order that all principal slip planes be blocked and cleavage on the $\{10\bar{1}7\}$ or $\{10\bar{1}8\}$ planes may occur. Sanderson and Scully [73] have shown that the average size of the hydride particles increases as the Al content increases, and they suggest that the addition of Al makes the atomic rearrangements required for the γ-hydride to form in the hexagonal matrix an easier process. Two alternate mechanisms are proposed for this effect: (a) The shift in dislocation structure from a random to a coplanar array as Al content is increased; the hydrides may then segregate on the arrays. (b) The critical Al concentration lies very close to the (α-Ti + δ) phase boundary in the Al-Ti phase diagram [74], the δ-phase being a Ti_3Al superlattice (Strukturbericht DO_{19}) isotypic with Ni_3Sn. This δ-phase may provide nucleation sites for the γ-hydride precipitation.

Separate work on alloys containing about 8 wt % Al [75,76] indicates that the δ-phase precipitates upon low-temperature ageing and this alone is sufficient for embrittlement and the formation of large slip steps upon straining.

Presence of the titanium β-phase adds a predictable complication---the Al will preferentially dissolve in the α-phase and the hydrogen in the β-phase. Tiner, using autoradiography of tritium-doped Ti multiphase alloys has shown [77,78] directly this preferential uptake in the β-phase and α-β grainboundaries of Ti-6Al-4V and Ti-8Al-1Mo-1V alloys. The α/β partition ratio was cited as 1/20 to 10/20 depending upon total hydrogen content in the metal [78]. (Hydrogen content of the β-phase increases more rapidly than the α-phase content). Results similar to those of Tiner for Ti-6Al-4V have also been observed by Toy and Phillips [79] using an independent technique. These investigators coated the alloy

with a thin film of neodymium and determined hydrogen emanation sites by optical determination of the NdH_2 product phase.

In two-phase alloys containing hydrogen, the stress corrosion crack tends to propagate in the α-phase and deviate from the β-phase grains [78]. Extended studies on crack propagation mode has been given by Hickman, Marcus, and Williams [80]. Four modes were observed, and the operative mode was shown to be determined by a combination of alloy chemistry, microstructure, stress intensity, and environmental factors, reemphasizing the complexity of this phenomenon. Transgranular cracking of the α-phase in low alloy or commercially pure titanium (all α-phase) and in α + β alloys where α is the continuous phase remains the most prevalent form and the process of highest research interest.

Additional information on the role of aluminum is available in the above references, especially [75], and in papers by McMahon and Truax [81] and Mauner, Starke, and Hochman [82] and the references contained within these papers.

It is also necessary to cite a 1962 review by Gibb [83] of facts and theories of metallic hydride formation. Arguments presented by Gibb favor the interpretation of active metal hydrides as salts containing the H^- ion, i.e. removal of valence electrons from the metal and localization in s-type orbitals about the hydrogen core. At that time, for titanium, the hydride conductivity and Hall effect [68] information were not available to counter this interpretation. Gibb does, however, cite the size of the H^- ion (radius = 1.40Å) and indicates its comparability to the F^- and $O^=$ ions, two species which do not form interstitial salts. Gibb also reviews methods of hydride preparation including simultaneous reduction of a noble metal oxide (as a catalyst?) during reaction with molecular hydrogen, and electrodeposition at a metal cathode. In both of these procedures, water will be in contact with the metal surface, and H^- ion is extremely unstable in the presence of water. Furthermore, the H^- ion theory hopelessly fails to explain the increased solubility of hydrogen in Ti-Al alloys when AlH_3 is known to be an unstable, covalently-bonded molecule and the solubility of hydrogen in Al metal is from five to eight orders of magnitude less than in titanium [84]. Finally, the analogy between H^- ion and $O^=$ and F^- predicts that hydrogen would be like oxygen, an α-phase stabilizer. This is counter to experiment. Failure of the H^--ion theory to predict solubility, phase change, or electrical conductivity indicates that this model

would be of little value in explaining stress corrosion or hydrogen embrittlement.

An excellent summary of the titanium-hydrogen system is given by Allemand, Fidelle, and Rapin [85] for those wishing to pursue this topic any further.

B. General Corrosion of Titanium

Aerospace structural applications utilizing the high strength-to-weight ratio of titanium alloys accounts for the bulk of titanium consumption [86]. Additional applications, primarily in the chemical process industry, are based on the apparent chemical inertness of Ti-based materials as reflected in their high immunity to general corrosion. This inertness is, of course, inherent to the oxides of titanium rather than the metal, and the corrosion resistance of titanium systems is dependent on the extent to which oxygen can dominate the titanium surface chemistry.

Since a majority of metal-corroding environments are aqueous solutions and electrochemical processes are usually involved, the Pourbaix diagram [87] of Figure 6 summarizes the thermodynamic aspects of corrosion reactions in the presence of water. It is notable that general surface corrosion with generation of soluble Ti(II) and Ti(III) ionic species is possible only at very low pH conditions and at reducing surface potentials (potential with respect to standard hydrogen electrode ≤ 0 volts). At all oxidizing potentials TiO_2 provides a passivating layer, and at slightly reducing potentials in moderately acid and basic solutions the sesquioxide, Ti_2O_3, provides the passivating film. At very reducing potentials, water serves as a hydrogen carrier rather than an oxygen carrier, and the surface becomes coated with the solid hydride, TiH_2. The passivating nature of the hydride phase is still somewhat open to question. At high pH values it makes little difference, and the resistance of this phase at very low and negative pH has only recently been studied. [88].

Very few environments provide the low pH and reducing surface potential required for general corrosion. Hot concentrated solutions of reducing organic acids, such as formic and oxalic acid, are the prime examples [89,90]. Aeration of such solutions (introduction of oxygen) can reduce the corrosion rate [90]. Hydrochloric and dilute sulfuric acid are non-oxidizing acids, and they can promote general corrosion, especially at elevated temperatures [90]. Sulfuric acid is also an environment where purging of the solution with molecular oxygen lowers the rate of corrosion.

Due to the ease of formation of protective TiO_2 at low anodic potentials, titanium is one of the few metals subject to "anodic protection" by purposeful change of the electrode potential of the titanium surface. This protection effect is independent of the source of the potential change, whether it be externally impressed or the result of coupling to a metal more noble than titanium. Since most metals are more noble than titanium and their ions are common contaminants of technical grade acids, corrosion in these environments is inhibited by the deposition of local cathodes and anodic protection of the remainder of the titanium. The more noble with respect to titanium the inhibiting metals are, the more effective as inhibitors. Copper and the platinum metals are well-known inhibitors for hydrochloric and sulfuric acid in contact with titanium [90]. An alternate method for generation of cathodic surface sites is incorporation of noble metal into the metal phase, and for this reason the Ti-0.2Pd alloy is a commercially available material for use in reducing acid environments.

Titanium corrosion in the hydrohalogen acids is rather peculiar, for aqueous solutions of HBr and HI apparently do not attack titanium alloys [90] although they are essentially stronger acids than HCl. Alternately, HF is the weakest of the hydrohalogen acids, while fluoride ion is a very efficient activator for titanium corrosion [89,91]. Strauminis and Chen [91] report the reaction to be:

$$2\ Ti + 6\ HF \rightarrow 2\ TiF_3 + 3\ H_2\uparrow \qquad [E\text{-}7]$$

and show that the rate of this reaction is accelerated by the addition of noble metal cations, the antithesis of the anodic protection results detailed for HCl solutions above.

Little exploration and less explanation seem to have been devoted to the variations of titanium general corrosion in acid solution as a function of halide ion identity, although it will arise as an important aspect of the stress corrosion of titanium. A second interesting observation on the differences in Ti corrosion in HF and HCl is the effect of added nitric acid [92]. The latter is an oxidizing species, and in HCl as little as 1% provides two orders of magnitude reduction in corrosion rate, apparently by surface passivation. Kane [92] mentions that the reaction with hydrofluoric acid, used for pickling titanium, is controlled by the

addition of nitric acid but that five times the HF concentration is suggested.

This information, combined with several other details summarized by Cotton and Wilkinson [93] suggest a more specific mechanism than the general reaction of equation E-7. We recall from Section I-E that ions in solution are solvated, and in aqueous solution all of the dipositive and tripositive ions of the first transition series form complex aquo- ions consisting of six water molecules octahedrally coordinated to the ion [93a]. Thus the ions Ti^{++} and Ti^{+++} listed on the Pourbaix diagram are actually $[Ti(H_2O)_6]^{++}$ and $[Ti(H_2O)_5]^{+++}$. Because of the high charge-to-radius ratio, there is no simple aquo Ti^{4+} ion [93b]. All of these aquo ions are somewhat acidic, dissociating in the manner represented by [93a]

$$[Ti(H_2O)_6]^{+++} \rightarrow [Ti(H_2O)_5(OH)]^{++} + H^+. \qquad [E\text{-}8]$$

Titanium is soluble in aqueous solutions only at high H^+ concentrations which keep the equilibrium of reaction shifted to the left, else the formation and dehydration of the hydroxoaquo complex ion leads to the formation of the insoluble oxide. Halogen ions may replace water as a ligand in the ion coordination sphere, thus in concentrated HCl, titanium remains in solution as chloro complexes such as $[TiCl_5(H_2O)]^-$ and $[TiCl_6]^=$ [93c]. For lighter transition elements the stability trend for coordinating species is $F^- > OH^- > Cl^- > Br^- > I^-$ [94]. Of all the halogens, only F^- ion can compete efficiently for titanium ions in solution, thus the $[TiF_6]^{3-}$ complex ion is both stable and soluble in the presence of water, preventing the formation of a passivating oxide or fluoride film in F^--containing solution.

The general corrosion chemistry of titanium in hydrofluoric acid may then be summarized by:

$$Ti + \underbrace{H_3O^+ + F^-}_{H_2O + HF} \rightarrow [TiF_6]^{3-} + H_2O + H^\circ \downarrow H_2 \qquad [E\text{-}9]$$

The overall reaction is the same as E-7, but E-9 better illustrates that complex ion chemistry is involved, that $[TiF_6]^{3-}$ stability prevents formation of passivating film precursor ions, that noble metals accelerate the reaction by catalytically accelerating the hydrogen atom recombination, and that nitric acid decelerates the reaction by repressing the ionization of the weaker HF ($K_a = 7 \times 10^{-4}$) and lowering the concentration of F^- ions available as a reactant.

Limited stability of all other complex ions with respect to the hydroxyaquo ions, $[Ti(OH)_x(H_2O)_{6-x}]^{2 \text{ or } 3-}$, may account for the suggestion of Wieman [95] that there is a critical titanium concentration for passivation of titanium in aqueous solution corrosion.

C. Stress Corrosion of Titanium

Limitation of general corrosion to the severe conditions outlined in II-B, and the possibility of anodic protection even in strong acids, suggest that titanium and other members of the titanium amily approach the ideal of a universally corrosion-resistant structural or decorative metal. The most serious contraindication to their use is stress corrosion cracking, a problem quite recently recognized for titanium-based materials. As late as 1953, Kiefer and Harple [96] tested commercially pure (Ti-75A) titanium in 23 environments known to cause SCC in other metals, and found it to be immune. Red fuming nitric acid (RFNA) was observed to cause SCC and sodium bromide was found to be an inhibitor. Kiefer and Harple suggested that nitrogen oxides dissolved in the acid were the attacking agents, but they gave no mechanism for corrosion or inhibition. In 1957 [90] failure of Ti-5Al-2.5Sn alloy was reported in a hot solution of 10% HCl, but this may well have been a case of stress-assisted corrosion. Report of a non-acid environment SCC failure of the same alloy was published in 1960 by Brown [97] who found that exposure to trichloroethylene followed by heating to 1500°F caused cracking.

In early 1961 Tomashov and co-workers [98] reported failure in methanol/bromine mixtures. This environment is known to cause corrosion in the absence of stress, but it has nevertheless been used as a stress corrosion test system (cf. Sect. I-B).

By 1963 the stress corrosion of titanium at elevated temperatures (>290°C) with cracks originating at surface deposits of chloride-containing salts began to be observed in the laboratory. This topic, combined with the crack propagation in sea water, essentially meant titanium stress corrosion when the ASTM had a symposium on this topic in 1965 [99].

In the mid-1960's, Mori, Takumura, and Shimose [100] indicated that

both Ti and Zr were susceptible to stress corrosion in methanol solutions containing HCl and H_2SO_4. Included in this report was the inhibiting effects of water, and the indication that Zr would crack in ethanol/HCl solution. The increase of cracking time with an increase in alcohol molecular weight was implicit in this paper.

Particular interest in the methanol environment was triggered in 1966 by failure of an Apollo program tank during proof testing. Details of this failure and some of the initial studies that this observation precipitated have been published by Johnson [101, 102a]. An early symposium on titanium stress corrosion in methanol and other organics remains a most valuable reference source [102] on this topic.

This historical information above combined with other data may be summarized as shown in Table 1. At least six classes of environment are currently known to cause stress corrosion in titanium and its alloys. As indicated in Section I-A, there is little reason to suspect a universal mechanism for all the environments listed, all four mechanisms presented there have been proposed for titanium SCC.

Crack propagation by cadmium and liquid metals probably occurs by the adsorption mechanism. Stress corrosion in aqueous NaCl is ascribed to hydrogen embrittlement [103] but this mechanism has also been rejected [22]. Stress corrosion in methanol/HCl has also been ascribed to hydrogen embrittlement [104], yet propagation in hydrogen-free organics is faster [15].

In hot-salt cracking, the presence of hydrogen at the crack has been observed, and the hydrogen embrittlement mechanism is quite likely [105].

At the moment no mechanism is proven, and it is likely that multiple mechanisms may be active in some environments. There is no reason to expect that the mechanisms currently proposed nor that the six classes of environments listed in Table 1 form a complete set. All of the environments known to be SCC active have been discovered empirically and more are likely to be found in the same way--a fact that should be kept in mind by design engineers.

D. Mechanical and Chemical Properties of Titanium Oxide

The initial response of titanium to an external environment is the response of the oxide; therefore some properties of the protective film and its chemistry are pertinent to interpretation of the stress corrosion of titanium.

The stoichiometric oxides are TiO_2, Ti_2O_3, and TiO.

The crystal structure of the TiO phase is of the rock salt type (Strukturbericht Type B1) in which the large oxide ions form a cubic close-packed structure with the Ti^{+2} ions located in the octahedral holes. There is a marked tendency for lattice vacancies of both cationic and anionic type in this compound.

The sesquioxide, Ti_2O_3, is isomorphic with α-Al_2O_3 (Strukturebericht $D5_1$) in which the larger oxide ions form an hexagonal close-packed structure. The Ti^{+3} cations then reside in the octahedral holes between the oxide layers, filling two-thirds of the total number available. This compound is a classic example in the crystal field theory of transition metal ion compounds, for coulombic interaction between the octahedral field of the oxide ions and the various d-orbitals fo the metal ion result in a splitting of the d-states of the cation. Since the Ti^{+3} ion retains one d-valence electron which has the ability to absorb and reemit light by transition between the lower (t_{2g}) and upper (e_g) states, a broad optical absorption band in the yellow region of the spectrum is present. Ti_2O_3 thus appears to be a dark violet-blue compound, and whereever present contributes this color to the protective film. For the same reasons, octahedrally-coordinated Ti(III) ions in solution are also violet-colored.

TiO_2 is known mineralogically in three different crystalline forms: anatase, rutile, and brookite. Rutile is the most common, and since it is the only modification to have been observed on metals, we limit our attention to this form. The rutile structure is itself a model structure (Strukturebericht C4) in which the oxide ions are essentially cubic close-packed (slight tetrahedral distortion). The Ti^{4+} ions fill one-half of the octahedral holes, and the tetrahedral distortion is such that the apical oxygens are slightly further

from the cation (0.1988 nm) than those at the square plane corners (0.1977nm) [106]. No optical absorption bands exist in this oxide in the visible region, for Ti^{4+} has no d-electron. Likewise solutions containing Ti(IV) complex ions, such as $[TiCl_6]^{=}$, should be colorless.

The Pourbaix diagram, Figure 6, suggests that only one stoichiometric oxide phases coats the metal under a given set of conditions. This occurs if the entire passivating film is generated under a fixed oxidation potential, but, for oxide films formed on titanium metal surfaces by exposure to air or in oxygen-contaminated heat-treating processes, the chemistry and the consequent mechanical properties will not necessarily be homogeneous.

At low temperatures the oxide formed on exposure to air is essentially rutile. Near room temperature the film growth kinetics are of the inverse logarithmic form, with a new film rapidly growing to 12-16 Å in thickness, reaching a thickness of 50 Å over a period of 70 days, and after four years, an essentially limiting thickness of 250 Å [92].

At higher temperatures combined thermal effects lead to a composite film. Oxygen diffusion and dissociation are accelerated, and the thermal creation of point defects in the oxide phase accelerates mass transport. Growth kinetics change from logarithmic to various power law descriptions [107], and films much thicker than those formed at room temperature are formed. An oxygen concentration gradient occurs across these thicker films, providing the whole range of oxidation potentials and thermodynamic stability. A tripartite film consisiting of an outer layer of TiO_2, a central region of Ti_2O_3, and an inner layer of TiO is predicted, and has been observed [108,109,110].

Extensive amounts of the lower oxides in thick films are formed only after long exposure times at high temperatures. Opposing their formation is the considerable mutual solubility between TiO and oxygen-rich Ti. At oxygen concentrations below TiO formation, the oxygen species occupy octahedral holes in the α-Ti hcp lattice, stabilizing the α-phase as discussed in II-A.

At higher temperatures, the simpler rutile film formed at lower temperature will also tend to react with the base metal according to the equation:

$$TiO_2 + \text{xs Ti} \rightarrow 2 \text{ (O dissolved in Ti)}, \qquad \text{[E-10]}$$

according to Hauffe [111a].

Most importantly, the thin rutile formed at low temperatures and the outer layer of rutile that forms a majority of the high temperature oxide is subject to chemical, crystallographic, and mechanical imperfections. Stoichiometrically the defect oxide is TiO_{2-x} and is blue in color. Both properties can be explained either as loss of oxygen from anionic sites and the formation of a blue F-center by the trapping of an electron at the anion vacancy [111b], or by the presence of interstitial Ti^{+3} ions, which would provide the color directly. The blue oxide often observed on titanium samples may be due to several causes, of which interference fringes due to a critical thickness is the least likely, and the presence of Ti^{+3} ions and/or F-centers in defective rutile is the more likely.

The crystallographic consequences of this slightly defective rutile began to be discussed in 1963 after Magneli [112] studied the powder patterns of compositions from $TiO_{1.75}$ to TiO_2. This work supported the concept of Ti^{+3} interstitials, and Magneli proposed that these point defects order into a structural defect termed a crystallographic shear plane. Magneli also indicates that such shear planes are locations susceptible to chemical attack.

An alternate description of the shear plane is a missing layer of oxygen atoms, and considerable effort in following this up has been expended and is discussed in the recent paper of Bursill, Hyde, Terasaki, and Watanabe [113]. Evidently for the slightly defective rutile in the range $TiO_{1.995}$ - TiO_2 that would be of interest to SCC work, the defects consist of randomly spaced and oriented {132} shear planes and some {101} shear planes created by the removal of oxygen layers as indicated in Figure 7 below:

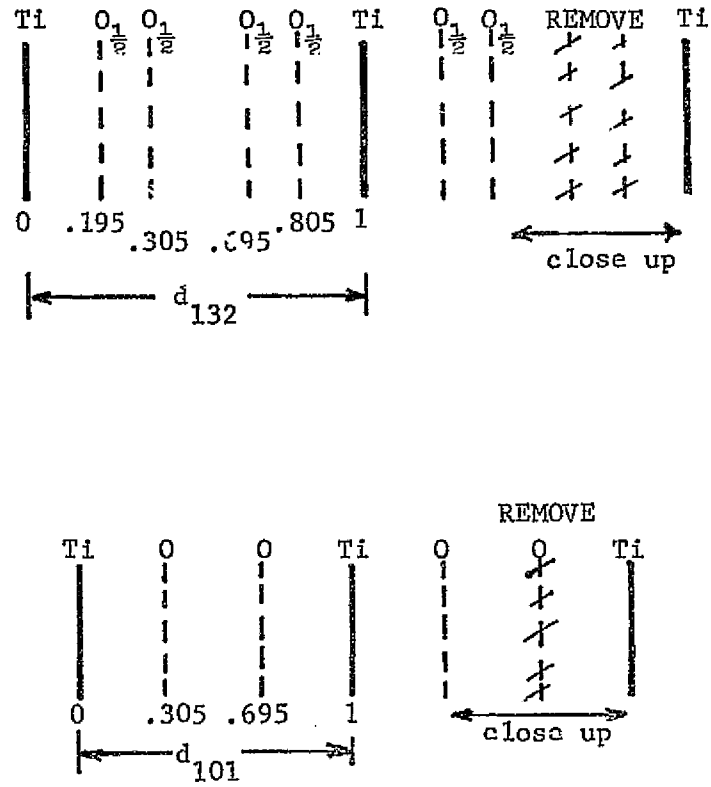

Figure 7. Relative Compositions and Spacings of Atom Planes Parallel to (132) and (101) of Rutile.

(After Bursill, Hyde, Terasaki, and Watanabe [113])

In titanium alloys additional effects may occur. Thin protective films formed on alloys will have a proportional representation of non-titanium ions in the oxide, and, for thick films formed at temperatures where bulk diffusion is possible, selective enrichment or depletion of the mixed ion oxide may occur. Fortunately for titanium alloys the latter situation is a rather simple, for only aluminium and zirconium havea higher oxygen affinity than titanium. The protective film on Ti alloys will tend to be free of cations from less active alloying metals and enriched in Al^{+++} and Zr^{4+}.

Incorporation of zirconium into the alloy and the rutile film would not be expected to have any electronic effects, since no lower oxides of zirconium are known and the Zr^{+4} ion is isoelectronic with Ti^{+4}. The larger size of the Zr^{+4} ion may introduce some lattice strain in the rutile, but this has been shown to affect oxidation rates of alloys only at very high Zr concentrations and at high temperatures [114].

Incorporation of Al^{+3} into the protective rutile layer has both electronic and structural effects, for the oxide most compatible with Al^{+3} is the sesquioxide, Ti_2O_3. Stabilization of the Ti^{+3} state in the presence of Al^{+3} is quite visible in synthetic sapphire where the blue color due to the d-electron absorption band is desired. At lower concentrations present in the oxide film on Ti-Al alloys, the Al^{+3} ions will tend to stabilize the oxygen defect structure [114], increasing the number or the extent of the missing oxygen planes in the defective rutile layer. Theoretically this should increase the oxidation rate, but experiments indicate this is a minor result at temperatures below 800° C and aluminum concentrations below 8% [114].

Defective rutile is an intrinsic n-type semiconductor, and doping with Al^{+3} ion can alter this conductivity. The defective oxide can also be re-oxidized to the white "perfect" TiO_2, and as a result the conductivity and composition are a function of oxygen pressure as well as Al^{+3} concentration. Considerable detail on the high temperature conductivity of pure and Al^{+3}— doped rutile are given in a paper by Yahia [115].

A more direct study of the interactions of oxygen with defects near room temperature is provided by electron spin resonance spectroscopy. Naccache, Meriaudeau, and Che [116], by using oxygen enriched with $^{17}O_2$ as the reactant in their ESR study, were able to show not only that the paramagnetic defect in reduced TiO_2 (assigned to Ti^{+3} interstitials) disappeared upon reaction, but that a triplet spectrum consistent with the formation of a surface O_2^- species then formed. Such a surface species was proposed earlier by Parravano [117] to explain both catalytic oxygen transfer between CO and

CO_2 at doped TiO_2 surfaces and the rates of isotopic exchange between TiO_2 lattice oxygen and molecular oxygen.

Infrared spectroscopy studies have also detailed the considerable interaction of rutile surfaces with small polar molecules, especially those containing hydrogen. Simultaneous papers by Primet, Pichat, and Mathieu [118] and by Jackson and Parfitt [119] report on the spectra due to water adsorption and reaction at the TiO_2 surface. Both investigators observed two O-H absorption bands and proposed interpretation by a model based on the {110} planes which have the highest density packing and compose about 60% of a rutile crystal surface. Exchange with deuterium and assignment of the O-D infrared bands was also noted. The key result is that water chemisorbs at the Ti-O-Ti-O-Ti-{110} surface, dissociating and reacting with it to form the hydroxylated surface, $\begin{matrix} OH & H & OH & H \\ | & | & | & | \\ Ti & O & Ti & O \end{matrix}$.

Infrared spectroscopy studies of the adsorption of ammonia on dry rutile by Parfitt, Ramsbotham, and Rochester [120], indicates the surface reaction is very similar to that of water. Scission of the N-H bond is accompanied by bonding to the oxide surface to yield the structure $\begin{matrix} NH_2 & H & NH_2 & H \\ | & | & | & | \\ Ti & O & Ti & O \end{matrix}$.

The presence of chlorine or chloride ion was observed to perturb the above surface reactions and spectra. Parfitt, Ramsbotham, and Rochester [121] unraveled this aspect by studying the reaction of HCl gas with rutile surfaces. They observed that if no hydroxyl groups were present from previous reaction of the rutile with water, then direct dissociative chemisorption of HCl yielded the surface represented as $\begin{matrix} & & H & Cl & \\ & & | & | & \\ Ti & O & Ti & O & Ti \end{matrix}$. The previously hydroxylated rutile surface reacted with HCl to reform a water molecule and a chloride ion associated with a Ti^{+4} ion, i. e.,

$$\begin{matrix} OH & H & OH & H & OH \\ | & | & | & | & \diagdown \\ Ti & O & Ti & O & Ti \end{matrix} + HCl \rightarrow \begin{matrix} HOH & & Cl & H & HOH & & Cl & H \\ & \diagdown & \diagup & | & & \diagdown & \diagup & | \\ & & Ti & O & & & Ti & O \end{matrix} \qquad [E\text{-}11]$$

reminincent of the ligand stability order discussed in II-B. A similar study by Jones and Hockey [122] confirms this conclusion with the supplementary observation that the presence of Cl^- results in the surface retaining

significantly more water upon attempted dehydration at room temperature than does the chloride free rutile.

Lake and Kemball [123] studied the reaction of water and of hydrogen gas with the rutile by isotopic exchange techniques. H_2/D_2 exchange at 200°-300°C was slow, indicating little dissociative chemisorption of hydrogen. Over the same temperature range Primet, et al. [118] observed reduction of the TiO_2 surface by D_2 gas as detected by appearance of the Ti^{+3} ESR signal. The small amount of H_2/D_2 exchange that Lake and Kemball observed may have therefore proceeded through an adsorbed water intermediate. Lake and Kemball do show that heavy water adsorbs readily and serves as a deuterium carrier for exchange reactions. They suggest that since the rutile surface is very ionic in nature, then in general, heterolytic reactions on TiO_2 should occur much more easily than homolytic bond scission reactions.

Photoeffects: Phototropy of rutile purposely doped with transition metal ions such as Fe^{+3} is known [124], but these reversible bulk effects may be ignored for present purposes since the film formed by oxidation of alloy surfaces is likely to be depleted in transition metal ions. Addition of electromagnetic energy to the system of the rutile film/SCC environment may, however, enhance some of the interactions and reactions at the rutile surface.

Renz [125] some years ago indicated that TiO_2 exposed to the sunlight would darken and release gaseous oxygen when in contact with an easily oxidizable medium, such as glycerol. CO_2 was also identified with the overall reaction. Jacobsen [126] followed up this work using various ultraviolet light sources and showed that under severe conditions the rutile was reduced completely to Ti_2O_3. Formation of the defective rutile structure is a reasonable intermediate in this transformation, and, on exposure to oxygen, reoxidation to the white rutile phase occurs.

Oxygen adsorption on rutile as well as oxygen release is enhanced by near ultraviolet radiation. McLintock and Ritchie [127] studied the room temperature photoadsorption of oxygen, ethylene, and propylene on rutile and correlated this interaction with the photoconductivity of the oxide. They found that illumination enhances the photoconductivity of the intrinsic semiconducting TiO_2. Exposure

to oxygen rapidly reduces this photoconductivity in two steps. First the healing of oxygen vacancies and then the trapping of residual carrier electrons occurs. The latter effect is consistent with formation of the O_2^- species observed directly by Naccache [116]. Adsorption of ethylene and propylene did not affect the conductivity parameter, but these species were readily oxidized by the photo-adsorbed oxygen when hydrocarbon/oxygen mixtures were exposed to irradiated rutile. Stone [128] earlier showed that alcohols, specifically isopropanol, could be oxidized (to acetone) at 0°C by photoadsorbed oxygen species while the thermal conversion did not occur below 150°C. Isopropanol was shown to be strongly adsorbed, more strongly than acetone, but the adsorption of neither organic molecule was photoenhanced.

In the introduction we cited the review of Latanison and Westwood [10] for examples of ionic solids being subject to stress corrosion cracking when suitable chemical interaction with an environment occurs. In this section we have summarized the evidence that rutile (a) will react with small polar molecules, (b) has a tendency to form a defect structure whose presence may be measured electronically, (c) has a defect structure which is altered by solid phase impurities and by reaction with gas phase oxygen. Furthermore the coupling of the electronic properties with the mechanical stress state in semiconducting (defective) rutile films is demonstrated by the piezo-resistive effect measurements of Huber [129]. These combined observations provide strong circumstantial evidence that the chemisorption of small polar molecules on rutile can alter the mechanical properties of this phase, and this effect is basic to the SCC initiation step in environments causing both initiation and propagation.

E. Molecular Properties of Alcohols, Halocarbons, and Alcohol/Halocarbon Mixtures

If chemical interaction with the oxide is basic to crack initiation and chemical interaction with the metal phase is basic to crack propagation in organic environments, then considerable influence on the SCC process should reside in the intrinsic molecular properties of these compounds. Therefore, minor variations in the electronic structure, bond strength, and other molecular parameters of the enviroment should provide an easily controlled and well understood method for probing the SCC mechanism. This has not been a common approach in SCC studies, but it has been incorporated into the research program of this report

and is basic to interpretation of results. For convenience, some of the principles of the molecular properties of organic compounds active and potentially active in titanium stress corrosion are summarized:

1. Heteronuclear Bond Strengths

The organic compounds discussed in this report contain only simple single covalent bonds. Except for the C-C bonds in the higher alcohols, these bonds are all heteronuclear (composed of unlike atoms). Consequently the electron density in the bonds must be displaced toward the more electronegative atom. This polarization increases both the strength of the bond and provides for a dipole moment. If χ_A is the electronegativity of atom A [55], χ_B the electronegativity of atom B in the bond A-B, and $\chi_A > \chi_B$, the electron displacement toward atom A determines the dipole sense, and the increase in bond energy over homonuclear contributions is proportional to $(\chi_A - \chi_B)^2$.

Some values pertinent to the organic fluids used in SCC experiments are summarized in Table 2, derived from Gould [130].

Table 2. Bond Energies of Covalent Single Bonds

Bond	High χ Atom	Low χ Atom	Homonuclear Energy (kcal/mole-bond)	Experimental Bond Energy (kcal/mole-bond)
H-H	H, χ_H= 2.1	same	104	104
C-C	C, χ_C= 2.5	same	80	80
O-O	O, χ_O= 3.5	same	33	33
C-H	C, χ_C= 2.5	H, χ_H= 2.1	92	99
C-O	O, χ_O= 3.5	C, χ_C= 2.5	57	81
O-H	O, χ_O= 3.5	H, χ_H= 2.1	69	110
Cl-Cl	Cl, χ_{Cl}=3.0	same	58	58
F-F	F, χ_F= 4.0	same	37	37
C-Cl	Cl, χ_{Cl}= 3.0	C, χ_C= 2.5	69	77
C-F	F, χ_F= 4.0	C, χ_C= 2.5	59	135
H-Cl	Cl, χ_{Cl}=3.0	H, χ_H= 2.1	81	103

2. Inductive Effects

Polarization in a given bond will be transmitted through the molecular skeleton to alter the polarization of neighboring bonds or functional groups in order that the net energy of the molecule as a whole is minimized. This perturbation on the average bond energies listed above is termed the inductive effect, and the sign of its contribution is correlated with the electronegativity and the direction of the dipole moment of surrounding atoms and functional groups. Two examples illustrate this effect for atoms and functional groups respectively: (a) in the series [CH_4, CH_3Cl, CH_2Cl_2, $CHCl_3$] the C-H bond becomes weaker as the number of C-Cl bonds increase since the electron density increases in the latter bonds at the expense of the C-H bond; (b) in the methanol molecule, CH_3OH, replacement of a methyl hydrogen by an electron donor group, CH_3-, strengthens the O-H bond; alternately, replacement by an electron withdrawal group CF_3- , weakens the O-H bond.

The usefulness of this effect is that selective substitution in a remote corner of a molecule can alter the bond energy at a site actively involved in a chemical reaction, and if stress corrosion is the reaction involved, such substitution should alter the rates of crack initiation and/or propagation.

3. Isotope Effects

Since isotopic substitution cannot perturb the valence electron distribution in a molecule, then any bond energy effects must arise from a mass factor. By the unique infrared absorption spectra of these molecules we know that the heteronuclear bonds are in oscillatory motion, and quantum theory predicts that the zero-point vibrational energy is dependent upon the masses of the oscillators. Increase in oscillator mass, such as substitution of deuterium for hydrogen in a C-H bond, results in a stronger bond. This effect is fundamentally small and dependent upon the square root of the mass difference, so that it is usually considered to be important only for hydrogen isotopes.

4. Intermolecular Effects

The polarity inherent in heteronuclear molecules contributes to the

dipole/dipole components of the intermolecular van der Waals' forces that serve to stabilize condensed states of these materials. In moleclules containing O-H and N-H bonds the attraction of the partially deshielded proton in one molecule for the non-bonded electron pair on the oxygen or nitrogen atom of the second provides an enhanced attraction, so that this particularly strong dipole interaction has been termed hydrogen bonding.

The intermolecular attraction in general and the hydrogen bonding in particular serve to decrease the vapor pressure of liquids and account for the abnormally high boiling points of polar liquids. Water, because it can doubly-bond to form a three dimensional network, shows the maximum effect. Alcohols can only singly hydrogen bond, and are thereby limited to chain [131] or ring structures in the liquid, so that the lighter alcohols have higher vapor pressures than water. Hydrogen bonding in alcohols is nevertheless effective, for ethanol has a molecular weight about one-third that of carbon tetra chloride, yet its boiling point is essentially the same as the non-polar hydrocarbon.

Direct detection of the hydrogen bonding interaction is obtained from the alteration of that portion of the infrared absorption spectrum attributable to O-H bending and stretching when alcohol vapors condense to liquids. Interaction between hydrogen bonding effects and isotopic effects is possible, the perturbation of isotopic effects upon hydrogen-bonding being well enough understood to provide a logical explanation of the vapor pressure differences of the four isotopic methanols CH_3OD, CD_3OD, CH_3OH, and CD_3OD [132]. This same reference indicates no effect by O^{18} and C^{13}, consistent with the comments of Section II-E-3.

Although hydrogen bonding is sufficient to account for large variations in vapor pressure, this strongest intermolecular interaction is still moderately weak compared to the ordinary covalent bond energies of Table 2, ranging from 5 to 10% of the latter values [131]. Hydrogen bonding is therefore quite sensitive to the presence of impurity molecules and the vapor pressure of mixtures is reflective of the change.

In our SCC studies mixtures of CCl_4 and methanol are of specific concern.

Vinogradov and Linnel [133], suggest that in this case the non-hydrogen-bonding halocarbon acts as a simple diluent to reduce the number of hydrogen-bonds between methanol molecules. This is consistent with the endothermic heat of solution observed upon mixing the components. The vapor pressure also shows a large positive deviation from Raoult's law. This is a maximum at the azeotropic (constant boiling point) composition of 20.6% methanol/79.9% CCl_4 boiling (760 torr) at 55.6°C, some 9°C lower than normal boiling point of the methanol [134]. Recent evidence [135] from the more specific and sensitive proton nuclear magnetic resonance studies, however, indicates some weak hydrogen bonding between the methanol O-H hydrogen and the Cl atoms of the CCl_4.

5. Bond Scission Modes

In the corrosion reactions, covalent bonds of the organic species will be broken. Since an electron pair is involved in the bond, it follows that there are two ways the A-B bond can break: homolytic scission, in which the bond electrons are evenly divided between atoms A and B to yield the neutral odd-electron fragments A· and B·; and heterolytic scission, in which both electrons are retained by atom A, and yield the ionic fragments A^- and B^+.

The mechanism and rates of the resulting reactions are quite dependent upon the scission mode and the type of intermediate species formed.

Ionic pair intermediates may react with neutral species to produce more ions, they may recombine, or they may be adsorbed on ionic or polarizable surfaces. In all cases, coulombic attraction tends to localize the reaction to the volume where the intermediates were created.

Neutral odd-electron intermediates (free radicals) are not coupled by coulombic forces and are free to diffuse from their generation site to react at a distant location. A mathematical condition upon the reaction of free radicals is that interaction with a normal electron pair bond always results in an odd-electron fragment. These chain reactions are terminated only by recombination of two radicals or adsorption at a surface. Free radical reactions are therefore subject to initiation by impurity molecules which easily decompose to radicals. Peroxides, containing the weak homonuclear O-O bond (cf Table 2),

undergo thermal homolytic scission and are often used as initiators or accelerators.

In the absence of initiator radicals, heteronuclear bonds will tend to undergo heterolytic scission, since the electron density is biased toward the more electronegative atom. This may be counteracted if the activation energy for scission is supplied by a photon rather than thermally. Free radical generation, i.e. homolytic bond scission, is favored if the photoexcited state just before decompostion is a triplet state with the electrons spin uncoupled

Details concerning the mode of bond breaking during a corrosion reaction can therefore be obtained through studying the response of the system to free radical initiators and irradiation. Free radical mechanisms will be enhanced by these variables, while ionic reactions tend not to be photosensitive.

III. TITANIUM STRESS CORROSION IN ORGANIC FLUIDS: BACKGROUND, EXPERIMENTS, RESULTS, AND DISCUSSION

Among the six classes of stress corrosion environments summarized in Table 1, this research project has concentrated upon the response of titanium to hydrogen-containing and hydrogen-free organic fluids.

A. Background

The interest of NASA and the research community concerning this topic dates from October 1, 1966, when an Apollo spacecraft tank fabricated of Ti-6Al-4V alloy in the solution-treated-and-aged (STA) condition unexpectedly failed while undergoing pressure testing with dry, reagent-grade methanol [101, 102a].

Additional tank testing demonstrated that Freon MF (CCl_3F) would also cause failure, and tensile specimens were observed to crack readily in $CH_3OH + CCl_3F$ mixtures [135, 192b].

Empirical discovery of these two types of organic environments as ambient temperature SCC agents could not have been predicted from the nature of the other known classes of SCC agents (RFNA, hot salt, etc.). The potentially predictive paper of Mori and co-workers [100] concerning methanol may easily be interpreted as requiring the presence of non-oxidizing acids such as HCl or H_2SO_4 for stress corrosion to occur, these acids being known to cause general corrosion (cf. Section II-B). Similarly the extreme temperature conditions required for Brown [97] to observe SCC in Ti-5Al-2.5Sn after exposure to trichloroethylene did not suggest room temperature activity of halocarbons.

Considerable research in many laboratories began immediately and predated the commencement of the research described herein by almost two years. A majority of the results of this earlier work are summarized in References [102] and [9].

Several questions and conflicts had arisen in this earlier work which we hoped to resolve in this research program. These included:

1. The Role of Methanol: There was some question as to whether methanol was a reactant or whether it was just a solvent carrier for an active species such as a halide ion. The work of Haney [102k, 136, 37a] indicated that a trace

of halogen ion was necessary, and that small amounts of water would accelerate the failure process. This was taken to support an electrochemical mechanism for SCC, and Haney [37a] found no cracking in methanol + trace water environments. Alternately, several studies indicated that methanol vapor was sufficient to cause stress corrosion [135, 102b, 102j, 137], suggesting that methanol was truly a reactant, and bringing into question the necessity of an electrochemical mechanism. On the assumption that methanol was a reactant, several proposals that the product was a titanium alkoxide were presented [102c, 102d, 102e]. Sedriks [102j], citing the results of Ambrose and Kruger [137], suggested that dehydrogenation of the methanol to formaldehyde was a possible reaction.

The high specificity of methanol as a stress corrosion fluid in contrast to the other aliphatic alcohols was another peculiar observation. Most experimentalists found stress corrosion in methanol environments; very few observations of cracking in ethanol environments were reported [102c, 102d]; and pure isopropanol was found to be neutral [135] or to inhibit cracking [102d]. Sandoz [102c], using precracked samples of a Ti-8Al-1Mo-1V alloy, is apparently the sole observer of sub-critical crack propagation in alcohols such as n-butanol and t-butanol, and he reports that K_{Iscc} values were much higher for these longer chain alcohols than for smaller alcohols. Sedriks [25], by the addition of molecular bromine or molecular iodine per Tomashov [98], obtained stress-assisted corrosion failure with normal alcohols from methanol through pentanol, but the alcohol was considered to be only a solvent for the halogen in this particular system.

2. The Role of Halogens: There is general agreement that the addition of chloride, bromide, and iodide ions to alcohols accelerates the stress corrosion process. It was very effective to add these species in the form of an acid, but not necessary. Haney [102k, 136] demonstrated that NaCl and HCl additions gave the same t_f values. Sedriks [102j] indicated that NaBr and NaI additions accelerated the stress corrosion, but that the addition of F^- ions, either as HF or NaF, did not promote failure. An analogous result had been observed by Beck [45] in his studies of SCC of titanium in aqueous solution. This halide activity trend directly opposes the order observed in the general corrosion of titanium (cf Section II-B).

3. The Role of Hydrogen: An additional comparison between aqueous chloride stress corrosion and methanolic chloride pointed out by Scully and co-authors [138] consisited of similarity both in fractography (cf Section I-C) and strain-rate dependence of cracking. This was ascribed to a common mechanism of hydrogen embrittlement. Sanderson and Scully [139] suggest that the methoxide formation reaction is the source of hydrogen and that water serves as an inhibitor through methoxide hydrolysis and passivation of the titanium surface. Gegel and Fujishiro [140] observed hydrides directly in the fracture surface of Ti-6Al-4V alloy failed in anhydrous methanol, lending support to the hydrogen embrittlement mechanism theory. Likewise the generation of hydrogen accompanying the formation of formaldehyde [137] would be consistent with this mechanism.

Countering the universality of hydrogen embrittlement are two observations: (a) failure does not occur in HF solutions, even though this reagent is known to introduce hydrogen into titanium [90, 92]; and (b) failure does occur (crack propagation) in such hydrogen-free halocarbons as CCl_4 [102c, 102i], CCl_3F [102b, 135, 141], CF_2Br_2 [142], and $CCl_2F—CF_3$ [102f].

The general inertness of these latter compounds suggested impurity action. The first impurity theory suggested free chlorine as the SCC agent [102], but this was directly disproven by Kamer, Kendall, and Raymond [141]. Raymond and Usell [144] later showed that free Cl_2 would help in the breakdown of a protective oxide film formed on titanium, but it did not alter the propagation process per se. Scully revived the impurity theory by suggesting [143] that hydrogen-containing impurities, particularly water, is the responsible SCC species. This is, of course, related to the possiblity that hydrogen embrittlement is the prime mechanism, the halocarbon serving primarily as the solvent. If so, it is peculiar that closely-related halocarbons such as CF_4 [102f] and $CCl_2F—CClF_2$ [102b, 135, 142, 145] with similar solvent properties do not promote crack propagation. Raymond and Usell [144] also showed that saturation of CCl_3F with water (about 90 ppm) inhibited crack propagation.

4. The Role of Halocarbons: The preceding discussion suggests that the halocarbons may be directly active in stress corrosion. The relationship between

covalently-bonded halogen and ionic halogen (Topic 2) is an open question.

5. The Role of the Oxide Film: Methanol is outstanding in its ability to initiate cracks in smooth specimens. Herrigel [102, p. 58] indicated that the blue oxide coating made Ti-6Al-4V specimens more susceptible to crack initiation, and perhaps made the original suggestion that defect sites in the colored layer (cf. II-D) provided initiation sites for chemical reactions. Early studies at NASA-MSC [145] also indicated that removal of the blue oxide layer retarded crack initiation. This topic does not seem to have been followed up by other investigators.

Although not all of the above questions could be as succinctly stated in early 1968, sufficient kernels of these ideas indicated that considerable fundamental work remained to be done in delineating the mechanisms of titanium stress corrosion, that this work would necessarily involve an interdisciplinary approach, that the organic environments offered several experimental conveniences, and that the study would be relevant to a real technological problem.

As originally proposed, the research program of this report would have as its objectives:

(1) Study of stress corrosion of titanium and titanium alloys in various media from a fundamental point of view.

(2) Extension of these studies to include a wider range of materials.

(3) Attempt the prediction of behavior of materials under stress corrosion conditions, based on the research on mechanisms.

Specific approaches suggested for the first objective included:

(a) Study of the various possible surface chemical reactions, using isotopic tracers (and by implication, mass spectrometric or radiation counting techniques) to determine the chemical mechanism where necessary. Gas chromatography was also proposed to determine impurity compositions.

(b) Study of stress corrosion by transmission electron microscopy, possibly by thinning of bulk samples in order to observe the precipitates and dislocations.

(c) Study of fluctuations in composition, perhaps by use of electron probe analyzer.

(d) Microscopic examination of cracked surfaces to determine the details of slip dislocation configurations near the crack.

(e) Fractography.

As pursued, this research incorporated most of the techniques originally suggested and with varying success. Increased understanding of the problem during the course of the research, however, indicated new techniques and experiments that proved useful in detailing the roles of the various components of the SCC system. The results are described in the remainder of this section and evaluation of the program with regard to its accomplishments and the original objectives is discussed in Section IV.

B. Standardization of Samples and Procedures:

A majority of the stress corrosion testing in this project involved two titanium compositions, the A-70 grade of commercially pure titanium, and the solution treated and annealed (STA) Ti-6Al-4V alloy, in a variety of sample configurations.

The Ti-6Al-4V alloy was used because of its broad range of technological application ·s proven sensitivity to stress corrosion in several media, its specific failure in methanol in the Apollo tank [101, 102a, 135], and the availability from NASA-MSC of materials whose thermomechanical processing was identical to that of the failed tank. As a model system for fundamental studies however, the Ti-6Al-4V system is quite complex. The two-phase metallic structure, combined with the possibility of a three-phase oxide structure (Section II-C), suggests that a crack may pass through five solid phases. In an SCC system where a volatile organic solvent contains non-volatile ionic solutes, as many as seven phases may be present. This situation is represented in Figure 8.

System simplification seemed to be in order--this, combined with the desirability for a readily obtainable and technologically relevant material, lead to the choice of the A-70 commercially-pure grade. Our titanium in this grade was originally produced by Reactive Metals, Inc., Niles, Ohio, and stocked in a variety of rod and fastener forms by a commercial fabricator (Tico Titanium, Detroit, Michigan) from whom it was obtained. While not the highest purity commercially produced, this material is free from the presence of the beta phase and the chemical and metallurgical effects of substitutional elements in the

metal and the oxide phases. Precisely because of the higher yield strength of the A-70 grade, alloy is the basis material for many titanium structural fasteners, and any SCC results obtained on this material would also have technological implications.

1. Materials Characteristics and Sample Characteristics

Ti-6Al-4V alloy was supplied to us in the form of very uniform sheet 0.068 $\pm$ 0.001 in. thick. This sheet had been prepared by the machining on both sides of a large circular tank forging; therefore, our sheet was in fact a small arc from a cylinder, with slight curvature apparent. Post-machining heat treatment (4 hours at 1000°F in air environment) left the sheet faces covered with a thick oxide film of blue-purple coloration (cf p.34). The resultant metallurgy of this aged material is shown in Figure 9a, and is seen to consist of primary α grains the order of 10 micrometers in size dispersed randomly throughout an aged $\alpha' + \beta$ matrix.

A variety of tensile specimens were cut from this material, with side-milling being used to prepare the gauge length and transition sections. A majority of the test specimens were 4 in. long and had a 1.00 in. gauge section 0.125 $\pm$ 0.001 in. wide, as illustrated in Figure 2a.

Two classes of Ti-6Al-4V specimens were prepared and tested. These classes are the parallel sample, where the pre-oxidation machining marks are parallel with the tensile gauge section, and the perpendicular sample, where the pre-oxidation machining marks run across the gauge section width. Figure 10 is a scanning electron micrograph of a failed gauge section which illustrates the surface details in the latter type of sample. In this figure the narrow face of the section contains our sample preparation milling traces, and these are always parallel with the tensile stress direction; the marks on the wide face of the gauge section are the details beneath the blue oxide film whose direction defines the class of the tensile specimen. With respect to the original tank ring, the parallel samples correspond to a circumferential direction and a hoop tensile stress, while the perpendicular samples correspond to an axial direction. Curvature of the original sheet material is most apparent in the

parallel sample, the center of the gauge section being displaced about 1 mm from the centerline defined by the sample loading points. Under load the gauge section is laterally displaced, so that during SCC testing the inner surface is under slightly more tension than the opposite surface.

Response of the material to tensile stress in air environment was determined by loading in an Instron Model TTC tensile testing machine at a strain rate of 0.05 in/min. The stress-strain curve for Ti-6Al-4V STA alloy indicates an extensive elastic region ending at an applied stress about 134 ksi, followed by a limited plastic flow region before failure. The (engineering) ultimate tensile strength was approximately 150 ksi, but for our stress corrosion testing, the 134 ksi elastic limit value was used as the 100% load reference point (cf Section I-B) in time-to-failure testing. In the air environment, the mechanical properties of this material are isotropic with respect to sample orientation, just as one might expect from the isotropic metal phase microstructure of the material.

For the A-70 alloy, the basic tensile sample preforms were standard mechanical fasteners, four-inch long stud bolts in 1/4-20 and 1/2-13 thread sizes. Tensile gauge sections of several sizes and configurations were milled or lathe-turned in the center of these bolts, and the remaining threaded ends provided convenient connection to stressing devices, usually a dead-weight frame. Two sample types, uniform cylindrical cross-section and circumferentially-notched cross-section, are illustrated in Figure 2. The uniform specimen cross-sections are 0.100 ± 0.001 in. in diameter, while the cylindrically-notched version shown in Figure 2b has a large cross-section diameter D, of 0.145 ± 0.005 in. and a notch diameter, d, of 0.100 ± 0.001 in. The stress analysis for this specimen type has been summarized by Brown and Srawley [16] and the d/D ratio of this specimen is within the range for which the stress analysis is considered to be most accurate. Consistent with additional recommendations concerning this sample configuration (page 62, reference [16]) the notch opening angle is 60° and the notch tip radius is 0.003 ± 0.001 in., i.e., within the recommended minimum radius of 0.005 in. For this system the initial stress intensity, K_{Ii}, is given by the equation:

$$K_I = \left(1.72 \frac{D}{d} - 1.27\right) P D^{-3/2} \qquad [E\text{-}12]$$

where P is the force applied to the tensile specimen and $\left(1.72 \frac{D}{d} - 1.27\right) D^{-1/2}$ is a specific form of the geometrical correction factor $Y(\sqrt{\ell})$ referred to in Equation [E-3], Section I-B.

Since all surfaces where stress corrosion might occur on the A-70 samples were machined, it was thought best to anneal these samples to minimize residual stress and surface cold work effects. With due care to avoid contamination, these specimens were vacuum annealed for 1.0-1.5 hrs at 700°C, well below the β-transus and about halfway between the anneal limits suggested by Maykuth [147]. The surface oxide present before annealing diffuses into the bulk of the material at annealing temperatures (cf Equation [E-10] p. 33), and, until opened to the air, the sealed, annealed A-70 samples remain oxide free. Vycor tubes containing these samples were only opened as needed, the samples used within a month, and they never directly heated along the gauge section. From the oxide formation kinetics discussed in Section II-D, it is reasonable to consider these samples to be covered with a pure rutile film about 15-50 Å thick while they were being tested for SCC sensitivity

The metallography of the A-70 samples does not change upon annealing, being consistently represented by the data of Figure 9b. The A-70 titanium consists solely of α-grains of random orientation and of scattered grain sizes in the range of 10-100 micrometers.

The smooth A-70 specimens upon tensile testing in air showed considerable ductility before failure and an engineering UTS of 81 ksi. Fortuitiously, the 0.02% offset yield strength of 56 ksi corresponded to the elastic limit for this material, and this applied stress value was used as the stress corrosion reference state. Immediate plastic deformation effects were thereby excluded, but long term creep under dead weight loading was observed, predominately during the first 100 hrs. under stress.

The air environment stress response for the notched A-70 specimens corresponded to straight line elastic loading to sudden failure. The K_{Ic} value for critical stress intensity was calculated by the above equation to be

24.4 ksi/in$^{1/2}$ and this value is the 100% reference point for the time-to-failure curves generated with this sample configuration.

The metallic component composition of these alloys was not directly analyzed, and must be considered to fall within the nominal standard limits published for such material [61]. These limits set the Al content of the Ti6Al4V alloy at 6.0 $\pm$ 0.40% and the vanadium content at 4.0 $\pm$ 0.15%. Much more of concern was the interstitial impurity content, particularly that of hydrogen because of its relationship to hydrogen embrittlement.

The hydrogen content of various samples was measured volumetrically during high-temperature vacuum extraction with a Laboratory Equipment Company Model 586-100 Hydrogen Analyzer. Multiple determinations gave a bulk average residual hydrogen content of 55 $\pm$ 5 ppm for the Ti-6Al-4V samples as prepared for SCC testing, and a residual content of 38 $\pm$ 5 ppm for the A-70 samples as prepared for SCC testing, i. e. after vacuum anneal in a closed system. The A-70 alloy before anneal contained a hydrogen residual of 74 $\pm$ 6 ppm, indicating that about one-half of the hydrogen was lost during anneal. The values above are consistent within themselves and are quite reproducible, but in an absolute sense may be low by as much as 10%. The sample extraction temperature used in the analyzer was 1200°C, and extraction appeared to be complete in 10 minutes. Specimens of National Bureau of Standards' Standard Reference Material 352 consistently measured 28 $\pm$ 1 ppm in our analyzer while the standard value is 32 $\pm$ 2 ppm. Extraction temperatures in SRM 352 certification averaged 200° higher, however.

An interesting parenthetical study concerning hydrogen analysis of this material developed during the course of this work. It was observed that both lower and more consistent values of hydrogen level were obtained only when the Ti-6Al-4V material was sampled by cutting dry with a hacksaw. An easier method of sampling is cutting with a water-cooled abrasive wheel, but the chips removed by this process (about 0.2 g of metal) showed an increase in hydrogen content of 15-20 ppm, presumably due to reaction of the metal surface with water. The A-70 alloy was not sensitive to this reaction, i. e. residual hydrogen increases were within the 5 ppm scatter band established for analysis of this material. As a result of the experiments, all samples for hydrogen analysis

were prepared dry.

2. Impurity Control Procedures and Analyses

As indicated earlier, impurity effects are often invoked in stress corrosion studies to explain or to avoid the explanation of unexpected experimental results. This hypothesis may always be validly introduced whenever surface phenomena are involved since chemisorption at an interface may lead to high local concentrations of otherwise negligible impurities. The mass action law may still be expected to hold, however, so that reduction of impurity levels reduces the need to invoke impurity effects in detailing the mechanism. Since Haney had previously shown that both water and chloride ion affected the SCC response of titanium alloys to methanol and other organic solutions [37a, 136, 137], purification and processing procedures were incorporated from the beginning of this research program to reduce these particular contaminants to a minimum unless they were purposely added.

All tensile specimens were machined specifically without the use of chlorinated cutting oils; a water:water-soluble oil mixture was used as a machining fluid, coolant, and possible source of residual hydrogen. Machined samples were cleaned in soap and water, rinsed in deionized water and in acetone, and placed in a modified Soxhlet extractor described in a previous report [54]. In this apparatus the specimens were alternately vapor and liquid washed in continually redistilled 2-butanone (methyl ethyl ketone), a solvent suggested by Maykuth [147]. These samples were removed from the extractor while hot (b. p. of ketone = 80°C) and stored in covered glass jar, any residual butanone quickly evaporating during the transfer process. Our ESCA spectroscopy work described later shows that ketones do not strongly adsorb on the titanium (oxide) surface, and tensile testing, including immersion of a precracked Ti-6Al-4V double-cantilever-beam specimen similar to that shown in Figure 2b, indicates no crack initiation or propagation in this fluid.

As a standard procedure the butanone-cleaned samples were handled with forceps until encapsulated in polyethylene and ready for loading into a

stressing device. This served to protect the metal surface from contamination by fingerprints, especially the chloride ion component of a fingerprint.

Most organic fluids, whether used neat or for solution preparation, were dried by refluxing with a dessicant and finally purified by redistillation. For the standard alkyl alcohols, calcium metal was used both as a water-removal and as a halogen-removal agent.

Calcium could not be used as a dessicant for halogenated compounds or unsaturated compounds such as allyl alcohol. In these cases Type 4A Indicating Molecular Sieve in granular form (30/60 mesh) was used as a water absorption agent.

Two exceptions to treatment with water removal agents were 2,2'-dihydroxyhexafluoropropane and carbon tetrachloride. The former compound, as a geminal-diol, is quite unstable toward decompostion by intramolecular dehydration. Furthermore this alcohol is a solid at room temperature (m.p. = 45°C) and it was used in stress corrosion testing only as dissolved in carefully dehydrated ethanol. The carbon tetrachloride starting material we used (Matheson, Coleman & Bell Spectroquality Grade) was free of water as received. The specifications for this material indicate a maximum of 100 ppm water, and our mass spectroscopic analysis gave no increase in the m/e = 18 peak over background, indicating ppm H_2O. Also because carbon tetrachloride contains no hydrogen, the presence of all hydrogen impurities in CCl_4 may be readily detected by nuclear magnetic resonance (NMR) techniques. Our NMR experiments indicated the hydrogen concentration derived from any source including water was less than 25 ppm.

All salts used in making solutions were dried in an oven for 2+ hours at temperatures > 125°C. The dried salts were transferred hot and stored in sealed glass containers, being later exposed to laboratory air only during weighing procedures. Very water-sensitive compounds such as the titanium and aluminium alkoxides were opened, weighed, and processed solely within a glove box containing a dry argon atmosphere.

All redistilled solvents and solutions prepared from them were stored in amber glass bottles sealed with septum stoppers. Removal and transfer of these fluids for testing or analysis was solely by use of glass syringes with stainless

steel needles, these components having been solvent cleaned, baked dry, and stored in a dessicator prior to use.

For stress corrosion testing, a stored tensile specimen was encapsulated along the gauge section with a heat-shrinkable plastic tubing, primarily for the purpose of retaining the test fluid and secondarily to protect the fluid and the gauge section from contamination. This technique had been developed at NASA-MSC, and both the technique and the material facilitating its use, a bulk-irradiated clear polyolefin (FIT-221, Alpha Wire Division of Loral Corp) were suggested to us by Johnson [145]. Our addition to this technique included the use of a surface-irradiated polyolefin (FIT-300, Alpha Wire) to prepare sandwich end seals that were somewhat more reliable against leakage. This polyolefin was a possible source of contamination, but comparison experiments with a Teflon tubing (FIT-500, Alpha Wire) indicated no contribution toward stress corrosion. Corrosion resistance charts for plastics [146] indicate the probable degradation of polyolefin would be absorption of the test solvent accompanied by swelling and loss of strength of the plastic. The only observed effect of polymer degradation observed in this program occurred when pure $CHCl_3$ was irradiated with a high intensity mercury arc, and apparently the free radicals generated reacted with the plastic. Stress corrosion was not observed in this case, nor when the polyolefin was replaced by Teflon.

For post-SCC analysis of products and impurities, the liquid was recovered from the SCC test system and stored in 20 ml. screw top glass vials sealed with a plastic cap carrying an aluminum foil liner. These vessels proved satisfactory except with ($CH_3OH + CCl_4$) solutions which totally destroyed the aluminium cap liner.

For monitoring halide ion contamination (other than fluoride ion) in alcohols, a visual turbidity test based on the precipitation of silver halides by reaction with silver nitrate solution was used. Control tests indicated that as little as 1 ppm chloride ion (10^{-4} wt %) could be detected by this method. All redistilled alcohols used passed this test, as did the fluid recovered after SCC testing.

For the detection of water in solvents, the Karl Fischer method was

originally used, but this was replaced by gas/solid chromatography when a suitable column material for water separation was obtained.

By the appropriate* use of gas chromatography, volatile contaminants in addition to water may be codetermined. The column of widest use in our research was packed with 80/100 mesh particles of a porous organic polymer (Porapak Q, Waters Associates) which is non-polar and preferentially retains non-polar species. Retention time within a homologous molecular series essentially follows molecular weights. The only** shortcoming of this column was its inability to cleanly separate water and formaldehyde, which lead to some confusion.

In the post-SCC analysis of methanol solutions we apparently observed large amounts (1000 ppm) of formaldehyde, somewhat expected as reported by Ambrose and Kruger [138]. Post-SCC testing of ethanol, however, gave smaller amounts of the same product, even though ethanol is not a formaldehyde precursor and does not cause stress corrosion. Water was suspected, and water and formaldehyde were both added and failed to be resolved on analysis. This analytical problem was resolved by use of a column packed with 60/80 mesh particles of a carbon molecular sieve (Carbosieve B, Supelco, Inc.). In contrast to the standard aluminosilicate molecular sieves, Carbosieve B is completely non-polar and has a high affinity for hydrocarbons and halocarbons. This adsorption affinity combined with a pore size of about 12 Å and a surface area of 100 m^2/g resulted in the loss of all compounds less polar than methanol to the column under our analysis conditions; consequently this column was used specifically for the detection of water and formaldehyde in methanol.

---

*Column and operating conditions are chosen so that impurity components elute well ahead of the solvent peak, conferring two advantages: (1) early peaks are narrow, so that the signal is concentrated into producing a peak height, and (2) the column may be flooded with respect to the solvent in order to increase the impurity signal without danger of burying the signal under the solvent peak.

**Porapak Q also fails to separate allyl alcohol and hexafluoroisopropanol under our standard conditions, but this was not a critical analytical problem.

Both the Porapak and the Carbosieve columns were 1 meter in length, and formed from 4-mm i.d. Pyrex tubing. A Perkin-Elmer Model 154 Vapor Fractometer unit provided the column oven, the thermal conductivity detector, and the thermal, electronic, and flow controls. Standard conditions for each column included operation at 150°C and use of high purity helium as a carrier gas at a flow rate of 75 ml/min.

With the careful use of internal standards to verify retention volumes, neither formaldehyde nor CO_2 were detected under any conditions, not even when the stress corrosion cell was irradiated with intense UV light, which Stone [55] suggests promotes the photocatalytic oxidation of alcohols. This finding is in direct contrast to the results of Ambrose and Kruger [138], who report the detection of formaldehyde by gas chromatography. Unfortunately those authors do not report the column, the detector type, nor the instrument operating conditions used in their analysis, so that direct comparison is difficult. Ambrose and Kruger do not report specific action to remove residual water from their reagents, and it is not clear if they ever purposely introduced water and formaldehyde into their system as internal standards. The probability of water being present in their experiments, coupled with our experience in chromatographically distinguishing between water and formaldehyde, strongly suggests that, if these investigators used a thermal conductivity cell detector, then water was the species detected and the formaldehyde reaction is non-existent.

This does not exclude formaldehyde from having been present in their system as an impurity carried by the methanol. Haney [37b] reports traces of formaldehyde to have been detected in all as-received methanol. Evidently Haney was able to get separation of formaldehyde on Porapak Q by using a longer column and lower temperature (115°F) than reported herein. Any formaldehyde present in our starting material was presumably hydrogenated during purification procedures.

Our impurity analyses indicate that water may be formed during the standard stress corrosion test, and definitely indicate that despite careful removal of water from the alcohols, its presence during a standard stress corrosion test is unavoidable. Three possible sources for water appear to be present: (1) water physically adsorbed on the titanium and the plastic encapsulant desorb into the

solvent, (2) water is formed as a byproduct of the chemisorption of the alcohol on the oxide phase, and (3) atmospheric water vapor permeates the walls of the plastic capsule holding the corrodent, the flow rate, $\underline{N}$, for this process being given by the equation [147].

$$N_{H_2O} = \frac{(P_{e,H_2O} - P_{i,H_2O})\ A\ \Pi_{H_2O}}{\tau} \qquad [E\text{-}13]$$

where $\underline{\tau}$ is the thickness of the plastic membrane, $\underline{A}$ is the membrane area, P_{e,H_2O} and P_{i,H_2O} are the external and internal partial pressures of water, and $\underline{\Pi}$ is the permeability coefficient. The permeability coefficient is actually the product of the solubility coefficient $\underline{S}$ and the diffusion coefficnet, $\underline{D}$, i. e.:

$$\Pi = S \times D \qquad [E\text{-}14]$$

and as such is dependent upon both temperature and pressure.

The permeation contribution of water to the system is then, in principle, calculable, but no permeation coefficients were found in the literature for irradiated polyolefin. A permeation experiment to provide an estimate of the upper limit of water ingress was then set up: a glass tube was covered with polyolefin used in the SCC experiments, care being taken to minimize $\underline{\tau}$, increase $\underline{A}$, and minimize the annulus between the plastic and the glass so as to increase the surface/volume ratio of the contained fluid.

Our information concerning water as an impurity may be summarized as follows, with error ranges on the water values of $\pm$ 50 ppm. Most freshly distilled solvents and the solutions made from these solvents tested at less than 100 ppm water. Stored in a septum bottle, solvents picked up water very slowly unless the septum had been punctured many times, in which case one bottle of methanol picked up 200 ppm water in the order of 1 month. In the permeation experiment, methanol containing 150 ppm water was added to the encapsulated glass cell and it immediately assayed 400 ppm water, suggesting process (1) above. Measurements at 5, 23, 47, and 72 hrs gave, respectively, 600, 900, 1000, and 1000 ppm water, indicating a definite permeation effect.

Interestingly, these data plot linearly on semilog paper, but it is only

the slope and not the curve itself which is unique. Since the permeation flow rate N_{H_2O} is equivalent to the increase in internal pressure, dP_i/dt, the general solution of differential equation [E-13] is of the form:

$$P_i(t) = P_e - C_o e^{+kt} \qquad [E\text{-}15]$$

where k incorporates the permeability and dimensional constants, and C_o is an arbitrary constant, essentially the distance from equilibrium at t = 0, whose value determines a specific concentration curve for a specific experiment.

Applying Henry's law to convert from pressures to concentrations, equation [E-15] may be rewritten and explained as:

$$\text{ppm } H_2O \text{ in SCC system at time } \underline{t} \text{ due to permeation} = \text{ppm } (t=\infty) - [\text{ppm } (t=\infty) - \text{ppm } (t=0)]\, e^{+kt} \qquad [E\text{-}16]$$

Occasionally, particularly with solutions containing fluoride ion, the water uptake in a short time was higher than that expected from the upper limit permeation rate experiment. This suggested that water may be produced during the reaction, and for this reason, it was included above as process (2). Similar permeation experiments for the influx of water into CCl_4 showed no uptake within the limits of the analysis (50 ppm) during 48 hours exposure.

3. Baseline Stress Corrosion Experiments

Figure 11 summarizes the results of tensile specimen stress corrosion experiments with purified methanol and methanol + 1 wt % NaCl (0.135N). This data confirms the existence of the SCC phenomena, confirms the results of other laboratories on the efficiency of Cl^- ion incorporation, and, because of the precautions described above to exclude impurity effects, offers what we believe to be some of the best data to suggest that methanol alone is sufficient to cause stress corrosion or subcritical crack propagation in titanium.

Of particular significance is the observation of crack propagation in notched samples of well-annealed, commercially-pure titanium in purified methanol, contrary to the myth that stress corrosion does not occur in unalloyed metals. We did not observe crack initiation of A-70 in purified methanol, but we present evidence in

the next section that this is a property of the oxide film and not of the metal phase.

These data provide within themselves information concerning alloy effects, ion effects, and initiation versus propagation effects. They also suggest additional experiments, and in that case serve as a project reference standard against which other media may be compared.

These data were necessarily generated rather early in the project, and the majority have been previously reported [54]. Some additional data have been added for the purposes of showing scatter or confirming previous trends. Very limited data concerning the susceptibility of a beta-phase alloy show simply that the β-phase is not immune to SCC in methanolic solution, but the chemistry and metallurgy of this alloy do not provide a simpler system for understanding the mechanism.

From the beginning of our program, we appreciated the inhibiting nature of water on the SCC process, were cognizant of the uptake of water from air by methanol in an open cup [148] and aware that a complete covering by plastic reduced this process [148] . In our standard stress corrosion arrangement involving complete encapsulation by plastic, we were confident that the water levels would remain well below the 10^4 ppm water that Johnston, et al. [148] and Haney [37a] showed would cause complete inhibition, and that our starting methanol was well below the 10^3-10^4 ppm range where Haney [37a] was finding minimum failure times then associated with an electrochemical mechanism.

Only well into the program, after sensitive and reliable water analysis was developed, did the data and its mathematical analysis described above lead to full appreciation of permeation processes. During the interim Haney accumulated additional data on the interaction of water and halide ion content, leading to the suggestion [37c] that SCC failure of titanium at chloride concentrations less than 1 ppm (our value) could occur only at water concentrations less than 600 ppm. Applying permeation data in retrospect to our experiments, we obtain a worst case example if considerable water is desorbed from the specimen and plastic. If this provides 400 ppm H_2O, the worst case observed with a glass blank, then the system remains below the 600 ppm level for at least five hours. If the starting water concentration is that of the methanol added, (<100 ppm) then, at maximum permeation, the system should be below the 600 ppm level for at least

40 hours. The fact that we observed in practice crack propagation in A-70 at $K_{Ii} = 80\ \% K_{Ic}$ with failure time of three days indicates that our permeation rates in practice were much lower than the upper limit, or that the Haney criterion is somewhat flexible.

In summary, permeation of water is negligible in short experiments, predictable in long-term experiments, and in practice our prediction data considerably overestimates its concentration.

C. Crack Initiation Studies

The scatter shown in Figure 11 for SCC of Ti-6Al-4V in methanol/Cl^- at low applied stresses disappears if sample orientation is considered. This sensitivity difference as a function of orientation is shown in Figure 12. A similar effect was also reported by Brownfield [135, Table 20, Samples 29 & 30] for the exposure of edge-notched samples of Ti-6Al-4V in reagent methanol. It seems peculiar that the parallel orientation specimen, which undergoes uneven stressing on loading, has the higher threshold stress for SCC. In terms of the original tank failure, this data suggests that axial stresses were more critical than hoop stresses in SCC initiation.

From a fundamental viewpoint, the surface orientation effect indicates anisotropy in the thick oxide film formed upon the machined surface during heat treatment. Such anisotropy may be resident in the defect structure of the oxide. The deep blue color of the oxide film suggests the presence of Ti^{+3} ions and the color centers associated with oxide vacancies. The presence of Al^{+3} in the film, guaranteed by formation on an aluminium alloy, will also tend to stabilize an oxygen defect structure. The shear plane model of such oxide defects, discussed in Section II-D and illustrated in Figure 7, provides such an anisotropic planar variation in chemical and mechanical properties of the rutile film. As an extrapolation of Herrigel's suggestion [102] that defect sites in the colored layer provide chemical initiation sites and Magneli's suggestion [112] that shear planes are susceptible to chemical attack, we specifically suggest that shear plane defects in the rutile film are the protocrack sites for the stress corrosion of rutile in methanol.

The suggestion that the initiation process is equivalent to a stress corrosion process should not be surprising, since we specifically introduced this report (Section I-A) by stating that environment-sensitive cracking was not limited to metals. From this viewpoint equation [E-1] is not an empirical equation but explicitly represents serially-coupled SCC processes. If so, then t_i as well as t_p should be stress dependent, but this has been difficult to measure with composite (oxide + metal) samples. An approximation to the separation of t_i and t_p is resident in the data of Figure 12, however, for the difference between t_f (parallel) and t_f (perpendicular) at a given stress is equivalent to the change in initiation time, Δt_i, i. e.:

$$\Delta t_i = t_f \text{ (parallel)} - t_f \text{ (perpendicular)} \qquad [E\text{-}16]$$

While Δt_i is not the same as t_i, it must be functionally related; and since the Δt_i values in Figure 12 are obviously stress dependent, this implies that the process occurring within the oxide film is stress dependent. This aspect of the initiation process, which seems not to have been proposed elsewhere, is at least subject to direct experimental test in the future. A very direct way of measuring t_i and its stress dependence is elimination of the metal phase, i. e. measurement of environmental sensitive cracking in a rutile crystal, an experiment no one seems to have done yet.

If the initiation step in methanol is equivalent to stress corrosion, then a strong chemical interaction between the material and the environment must be demonstrable. This we have done by the technique of Electron Spectroscopy for Chemical Analysis (ESCA). This method, primarily developed in Sweden over the past 20 years by Siegbahn and co-workers [149], is essentially energy resolution of the photoelectrons emitted by a surface upon irradiation with a soft monochromatic x-ray. The variations in electron energy may be directly related to the electronic binding energy of the surface atoms. ESCA instrumentation necessarily operates at high vacuum (10^{-7} torr) so that any fluid observed on the surface must be strongly chemisorbed. Our results are shown in Figure 13: When a fluid known not to cause SCC, acetone, is exposed to an oxide-covered titanium surface, it desorbs under vacuum, and the ESCA spectrum

shows only the titanium ions and the oxide ions of the clean TiO_2 surface. In a second experiment methanol is seen to be strongly adsorbed on the TiO_2 surface as indicated by the presence of the carbon peak, and the dimunition of the titanium peak. A chemical shift toward higher binding energies is also apparent for the oxygen peak, indicating the oxygen surface species primarily observed is no longer the $O^{=}$ ion, but covalently bonded oxygen and/or the OH^{-} ion.

By analogy to the chemisorption of other polar molecules on rutile discussed in Section II-D, it is likely that methanol dissociatively adsorbs on the (110) surface plane by the following pictorial reaction:

$$\text{Ti-O-Ti-O-Ti} + CH_3OH \rightarrow \text{Ti O Ti O Ti} \quad \text{(O bears } CH_3 \text{ and H)} \qquad \text{[E-17]}$$

so that methoxy groups bond to titanium and hydroxyl species are formed.

Reaction [E-17] is the necessary chemical reaction which occurs on all rutile surfaces (the ESCA measurements were made on zone-refined titanium). Reaction [E-17] alone weakens the ionic surface bonding, but we suggest that, for non-defective rutile, this reaction is not quite a sufficient condition for crack initiation else the smooth A-70 specimen would have failed in pure methanol, since metal phase propagation in A-70 was demonstrated even at lower stress values (see Figure 11). This model is consistent with the earlier proposal concerning Ti-6Al-4V, that defects in the blue oxide film predispose it toward cracking

If rutile defects are necessary, and if aluminium ions in rutile stabilize oxide defects in the Ti-6Al-4V case, then incorporation of aluminium ions into the non-defective film formed on A-70 should promote stress corrosion by promoting the initiation process. This was tested in two series of experiments in which aluminium was added to the rutile film formed on annealed A-70 samples by vacuum evaporation of aluminium metal. The tensile specimens had the gauge length milled to a square cross-section to provide a planar surfaces. In four identical operations in which 99.999% Al wire was wrapped about a tungsten resistance filament to form a point evaporation source and the titanium sample was placed some 20 cm distant, the gauge sections were uniformly coated with

100 Å of Al in one series and 20 Å of Al in the second series.

In the 100 Å series, two post-evaporation treatments were used. These were either vacuum anneal at 625°C (25° below Al melting point) or air anneal at 550°C to convert the aluminum to the oxide. The vacuum annealed samples, stressed to 90% of the elastic limit, were exposed to methanol and to methanol/Cl^-. The sample in methanol did not fail, but one failed in methanol/Cl^- in 383 minutes, about 40 % of the standard t_f for this material (Fig. 11). The air-annealed samples were tested similarly and showed much shorter failure times. The first test in methanol/Cl^- at 90 % elastic limit gave instantaneous failure, and the second test in purified methanol at only 75% of the elastic limit resulted in failure in 2100 minutes, the first case observed of crack initiation and failure of a smooth A-70 specimen in purified alcohol.

These results were encouraging but not conclusive. Consideration of the 100 Å Al thickness versus the probable rutile thickness of 20-50 Å indicated that we were overwhelming rather than doping the rutile layer. This resulted in the 20 Å coating as a compromise between applying too much aluminum and not applying any. Post-evaporation treatment in the 20 Å series included heating to 750°C (well below the β-transus to prevent any recrystallization and grain size effects) in high-purity argon. Two of these samples were tested in purified methanol at 90% of the elastic limit, and failed in times of 112 minutes and 171 minutes, the first sample failing in the vapor phase above the liquid meniscus, a common observation for the uniform cross-section Ti-6Al-4V samples which were tested in purified methanol.

The second set of results do not directly prove the defect structure model but these results do confirm the aluminum effect prediction of that model and thereby lend it credibility.

This raises the question of what special effects might be associated with oxide shear plane defects. The most obvious, of course, is a perturbation on the mechanical properties of the oxide phase. For additional details we turn to the series of papers on rutile defects by Kingsbury, Ohlsen, and Johnson [150, 151, 152]. These authors studied extensively metal ion diffusion in the rutile lattice and they were particularly impressed by the affinity of rutile

for hydrogen atoms, suggesting that rutile or doped rutile would be useful as a semiconductor detector of hydrogen, a prediction fulfilled later by Montgolfier, et al. [153]. Johnson, Ohlsen and Kingsbury [152] indicate : that the diffusing specie in rutile is the H^+ ion, that at rest H^+ is associated with oxygen to yield an O-H stretch infrared absorption band, and that H^+ is preferentially associated with +3 impurity ions (such as Al^{+3}) as determined from the shift in the infrared absorption band when the rutile is doped with aluminum. To apply this information to the initiation of cracking by methanol we refer to equation [E-17], which shows that hydrogen is released by methanol dissociation and is bound as a surface hydroxyl group. Some fraction of this hydrogen may then diffuse to internal sites, preferentially those associated with aluminium ions which, in turn, are preferentially associated with oxygen defects. Further details are that the infrared absorption is almost completely dichroic [152] indicating that the O-H dipoles lie in the basal plane. This would, in terms of the (101) defect shown in Figure 7, additionally reduce the attraction between the cation planes and the anion planes in the (101) direction.

In a sense this is a hydrogen embrittlement mechanism of oxide failure, and is consistent with the observation that in titanium stress corrosion only hydrogen-containing fluids cause crack initiation.

The presence of chloride ions certainly alters the situation, as is evident from the failure of smooth A-70 titanium specimens in methanol/Cl^-, Replacement of oxide ions in a metallic oxide film by chloride ions is almost a tradition within corrosion science to explain pitting effects, and it is reasonable to incorporate the same process in stress corrosion. The measurements of Rideout, Ondrejcin, Louthan, and Rawl [154] on the retention of radioactive $^{36}Cl^-$ ions by the surface of titanium alloy samples show that oxidized surfaces retain more chloride than freshly polished surfaces. They interpret this increase to the absorption of chloride ions into the oxide film, probably into oxide vacancy positions. No particular reason is given in the stress corrosion literature, however, to explain exactly why

this should weaken the oxide phase. It seems to be a particularly appropriate time to recall the basic chemical properties of titanium compounds presented earlier: only fluoride ion and oxide ions have sufficient electronegativities to stabilize Ti^{+4} in an ionic lattice. Substitution of chloride ions will tend to introduce covalent bonding of the type found in $TiCl_4$, weakening the lattice. Any pronounced clustering of these ions, such as at grain boundaries or within the oxygen vacancy planes which are present in defective rutile would seem to be particularly effective.

To enter the oxide lattice, the halide ion would have to lose the solvation sheath surrounding it in solution, and the tendency for an ion to lose this sheath would be dependent upon the structural enthalpy of the ion/solvation-sheath complex. Krishnan and Friedman have measured the trend of this enthalpy, independently of ion-ion effects, by calorimetrically determining transfer enthalpy of various ions between H_2O and D_2O [155] and CH_3OH and CH_3OD [156]. Due to isotope effects (Section II-E-3), intermolecular hydrogen binding and solvation will be approximately 5% stronger in D_2O than in H_2O, and somewhat less different in the isotopic methanols since the latter cannot form three dimensional hydrogen bond structures.

Figure 14, taken from [156] summarizes the enthalpy data of Krishnan and Friedman for the halide series as a function of reciprocal ion size. Fluoride ion differs from the rest of the halide series in that its transfer enthalpy is negative, indicating a particularly high degree of solvent dipole orientation due to the intense electric field gradient about this smallest of the halide ions. This situation is known in solution theory as solvation of the first kind. The other ions, Cl^-, Br^-, I^-, are surrounded by a more diffuse hydrogen-bonded solvent structure which is termed solvation of the second kind. Consequently, it is much easier for the three heavier halides to desolvate and enter the oxide film, and if it were not for ionic size, this process would be favored for iodide ion. Since the results of Haney [35c] indicate that failure times are slightly less in sodium bromide than in sodium chloride, and the results of Sedriks [102j] indicate that

failure in sodium iodide is even slower, then we must assume that ion size is rate-controlling once the solvation sheath is lost.

The data of Figure 14 also show that the solvent isotope effect for F^- ion is smaller in methanol than in water, indicating that water is a preferred solvent. This characteristic may account for the larger amounts of water impurity we observed when testing with 0.1 N methanol/NaF solutions. As shown in equation [E-17], the titanium oxide surface is covered with O-H groups upon methanol chemisorption. The rutile surface is fairly easily dehydroxylated [106]:

$$2\ OH^- \rightarrow H_2O + O^= , \qquad [E\text{-}18]$$

and the small amount of energy process [E-18] costs is partially recovered by exchange of water for methanol in the solvation sheath of the fluoride ion. Equation [E-18] is a spec'fic statement of a process we alluded to earlier as an unavoidable source of water contamination of the fluid phase. It is unavoidable because it is coupled to equation [E-17].

The above data concerning the solvation theory of halide ions in methanol was simply not available until 1971, and the activity trend for SCC enhancement in this series, especially the inactivity of the F^- ion, was confusing. The pseudohalogens, a series of polyatomic species, appeared to be sufficiently related in chemistry [94b] that their activity for SCC enhancement would provide additional points on a trend curve and suggest a mechanism. Consequently the stresscorrosion of titanium in methanol/NaN_3 (sodium azide) was studied. The azide ion, N_3^-, chosen because it best mimicked the properties of Cl^-, was found to have no effect upon the stress corrosion response curves. In retrospect, azide is too big an ion to enter the oxide film. All of the pseudohalogens are larger than I^-.

Alternate Initiation Mechanisms

In the preceding section our observations concerning the initiation process were correlated with the fundamental physical and chemical properties of rutile measured independently of the stress corrosion system. We have indicated that the initiation process within the oxide layer is defect

dependent, is in itself stress-dependent, and that it might be studied independently of the metal phase.

Alternate models exist. One of the incipient biases in the stress corrosion theory of metals is a tendency to explain everything about a system by processes in or requiring the metal phase. An important initiation process from this viewpoint would include slip step emergence from the metal phase at the metal-oxide interface. Dependent upon the size of the step and the elasticity of the protective oxide film, this process would tend to break the inert film and expose a small amount of bare metal on the step face to corrosive attack by the environmental fluid. If an electrochemical corrosion process were necessarily involved, this situation would be particularly favorable, for the small anode/cathode ratio would result in high anodic current densities and rapid rates of crack propagation. Some of the effects favoring the defect structure of the oxide also increase the n-type semiconductivity of the oxide, and this would presumably favor an electrochemical reaction by reducing the solid phase component of the circuit resistance.

With the attitude that slip step breakage of the oxide film was a reasonable initiation mechanism, even if electrochemical processes were not involved, a large portion of research effort on this grant, particularly that of Messrs. Basu, Parris, and Salama, was devoted to the demonstration that slip steps were in fact as well as in theory the key initiation step.

The Ti-6Al-4V alloy served as the basis material, since one of the critical mechanical properties of the titanium-aluminum alloys containing more than 5% Al is the formation of coplanar dislocation arrays (cf. Section II-A). This should result in wide slip steps and account for the increased SCC sensitivity of these alloys.

The experimental technique involved optical analysis of the metal surfaces for slip steps before and after exposure to methanol, and before and after exposure to methanol+stress. Both optical microscopy and electron microscopy were used, the latter process involving the replication of the metal surface (cf Section I-C).

To provide an observation field, an area of the gauge section of standard or double width (1/4 in.) tensile specimens was carefully electropolished in a Carl Zeiss electropolishing microscope. Therein the surface of the sample may be monitored during the polishing operation. The polishing conditions duplicated those of Sanderson and Scully [73], with particular attention being paid to keeping the electropolishing system cold in order to reduce the possiblity of hydrogen contamination and hydride formation in the alloy. The electropolishing solution used consisted of 30 ml of 60% perchloric acid, 175 ml of n-butyl alcohol, and 300 ml of methyl alcohol. In the final development of the technique, the solution was cooled by direct immersion of an aluminum tubing heat exchanger coil into the polishing solution reservoir. Nitrogen gas precooled by liquid nitrogen flowed through the coil at a rate controlled by a temperature sensor and relay operating a solenoid valve. Flow rates of the polishing fluid were sufficient to maintain the sample surface at -30°C. Hydrogen analysis of the electropolished gauge section indicated an hydrogen uptake of approximately 24 ± 5 ppm.

Blank testing in air by observing the surface as a function of load increments established that slip lines observable in a metallographic microscope at 1000 x magnification first began to appear at a stress level 88% of the fracture stress. This value is 96% of the apparent elastic limit stress established earlier as the stress corrosion reference value and a value where we obtained t_f values of less than two minutes. Slip lines first appeared in the alpha grains as would be expected on the basis of crystal structure.

This was followed by testing in methanol/1 wt % NaCl at levels well below where slip bands were observable. This value as, in the more successful experiments, 75% of the fracture strength or 81% of the SCC reference stress. SCC failure times at these stresses were consistently less than ten minutes, but the tests were not considered successful because of the resistance of the electropolished spot to cracking. The gauge section failed in most cases in the regions covered by the blue oxide well remote

of the electropolished area.

Procedures used to force the sample to crack in the electropolished area included the scribing of a notch on the reverse side of the polished area and electropolishing on both sides of the sample to reduce the sample cross section and increase the local stress. These methods were ineffective. In a separate blank experiment in which the gauge section was scribed with a tungsten carbide point, the sample also failed in an unscratched area remote from the scribe marks.

Post-SCC failure examination of samples stressed below 96% reference stress failed to show any slip lines. In one particular case, however, fracture occurred within 2 mm. of an electropolished area. Photographs were taken of this area and some slip lines were observed, but they were not uniformly dispersed. Counts of slip lines versus gauge width, shown in Figure 15, indicate that some 17% of the gauge width was free of slip. Our interpretation of Figure 15 is that the SCC crack initiated before the foramtion of slip lines, as the crack propagated, reducing the cross section and increasing the applied stress on the remaining metal, then normal mechanical slip equivalent to air testing began to occur.

Our interpretation of all surface observation results is that slip line fracture of the oxide film cannot be the initiation mechanism in uniform cross-section samples. This conclusion is subject to the criticism that the slip lines responsible for initiation were smaller than the limit of our observation (step height about 5×10^{-2} micrometers), but the true seeds of doubt about the slip line mechanism do not even require a microscope. Unless there are drastic variations in rutile film elasticity as a function of thickness, the slip step precess should be more effective in exposing fresh metal where the sheared film is thin rather than thick. Our experiments certainly indicate that removal of a high temperature thick oxide and replacement by a low-temperature thin oxide decreases rather than increases the SCC sensitivity as predicted by the slip-step mechanism. The slip step mechanism also fails to explain the anisotropic SCC sensitivity shown in Figure 12, or why failure does not occur in CCl_4 environments if exposure of bare metal

is the major attribute of the slip step process.

In a somewhat related study we attempted to observe stress corrosion cracking effects by transmission electron microscopy. While this may be considered a propagation topic, the thinness of the metal required for electron beam transmission is such that one essentially observes the mechanical response of metal very close to a surface. The planned technique for this study included use of a tensile specimen holder (Ladd Research Industries, Cat. No. 611) incorporating a micrometer screw to provide for sample stressing during electron microscope operation. This unit requires an electrothinned tensile sample 0.1 in. wide by 0.5 in. long.

Preparation of the required thin specimens proved to be a major impediment to the successful completion of this study. Our starting material was an electron beam zone refined titanium of 99.97% purity (Materials Research Corp.) cold rolled to a foil 0.005 in. thick. Use of the Ziess polisher for this application proved unsatisfactory due to the inability of the operator to determine optimum termination of the thinning operation. Mr. Ehlert then designed and built an electropolishing apparatus with dual hollow cathodes to provide for simultaneous thinning of a sample from both sides and transverse illumination of the thinned section. The latter feature enabled the operator to terminate sample preparation at formation of the first pinhole large enough to transmit light.

Additional features from diverse sources were consolidated in the apparatus design of Mr. Ehlert. These included a bridge circuit power supply as described by Hancher [157] for optimum control of electrical conditions, a jet system similar to that described by Gardiner and Partridge [158] to keep the metal surface swept clean of hydrogen, and a hinged electrode holder design similar to that described by Glenn and Rayley [159] to allow the polishing to be terminated by rapid removal from the liquid without interrupting the impressed potential. This latter feature reduces post-thinning surface contamination by chemical attack of the polishing bath.

The polishing solution and the temperature control equipment were the same as that described above for electropolishing the standard tensile specimens.

Large pieces of foil (1/2 x 1 in.) were successfully yielded a thinned

center section, but these thinned areas shattered whenever tensile specimens incorporating them were cut from the larger square. Even the spark cutting of these pre-thinned specimens was not successful. The alternate approach, electrothinning of a tensile specimen precut to the desired size, gave unequal thinning and preferential attack at corners and sides due to the uneven electrical field geometry. In the final series of samples attempted, the foil was carefully annealed in a vacuum furnace before electropolishing to eliminate cold work, then reannealed before cutting to remove any residual hydrogen that may have caused hydrogen embrittlement. The samples were still torn by cutting and handling. Transmission pictures were obtained from these samples, but were uninterpretable; therefore this phase of the research program was terminated.

D. Crack Propagation Studies.

The results of Sedriks [102j] and of Ambrose and Kruger [137] concerning the vapor phase cracking of titanium by methanol strongly suggested that methanol was a reactant rather than an inert solvent component of an ionic conduction medium. Our stress-corrosion testing supported this since several samples tested in purified methanol failed in the vapor phase rather than in the liquid.

We then modeled the conditions at the crack tip (bare titanium metal contacted by methanol molecules) by the evaporation of titanium films under oxygen-free vacuum conditions, and studied the reactions of purified organic fluids with oxide-free and pre-oxidized films.

Much of this work has been published [160], and was included in a previous report [54]. The experimental results obtained principally by Leith are summarized in compact form in Table 3. In this matrix chart a (+) symbol identifies the molecular specie(s) in contact with the film and a (+) or (-) in the film change column identifies whether the film was visually observed to corrode off the walls of the glass substrate. The final column gives additional observations.

As one result, we demonstrated that the fundamental direct chemical reaction between titanium and methanol is:

$$4\ CH_3OH + xs\ Ti \rightarrow Ti(OCH_3) + 4\ (H\ dissolved\ in\ Ti), \quad [E\text{-}19]$$

confirming positively that the proposed methoxide mechanism [102 c, d, e] was correct. In definitely identifying the solid white methoxide, which sublimed and collected in the cooler parts of the reaction vessel, Debye-Scherrer x-ray analysis and mass spectroscopy were used. The powder pattern analysis agreed with a sample of $Ti(OCH_3)_4$ prepared by a wet chemical method (Alfa Chemicals, Beverly, Mass.). The mass spectrum of the compound showed the titanium isotope quintets separated by the 31 m/e units equivalent to CH_3O-. The compound formed with the deuterated alcohol showed quintet separation by 34 units equivalent to the CH_3O- group.

The other isotopic exchange work shows that the O-H bond is the only bond broken by adsorption and reaction of methanol with the titanium surface. This is not predictable from looking at the bond energies of Table 2, but the electronegativities listed in that table also indicate that O-H is the most polarized bond; therefore, the hydroxyl hydrogen is the most electron deficient hydrogen surrounding the methanol molecule. This hydrogen must then see a coulombic attraction for the extra-surface electron density of the highest-kinetic-energy electrons of the metal [161], just as it must be attracted by the excess electron density at the incompletely coordinated surface oxide ion (the $O^=$ surface state, [162]) of the rutile film. It is fundamental and not coincidental that the same bond in methanol is broken in both the initiation reaction [E-17] and the propagation step [E-19].

The energy relationships in this reaction must be quite sensitive. Isopropanol was observed to give no reaction with the titanium film below 300°C. Transport effects cannot be critical in this macroscopic thin film system; therefore, the positive inductive effect (Section II-E-2) of the two additional methyl groups must be sufficient to strengthen the O-H bond and thereby increase the activation energy for the reaction. This correlates with the observations [135, 102d, 163] that isopropanol is not an active

SCC agent at room temperature, and is sufficient to explain a lack of reactivity on unstressed films at higher temperatures.

Several other observations during the thin film work correlate well with tensile testing results: Oxygen and water vapor both inhibited reaction [E-19] while the addition of chlorine as HCl gas accelerated the reaction in proportion to its presence. The presence of HCl also allowed some corrosion to occur through a thin, room-temperature-formed, oxide film in analogy to the initiation and time-to-failure effects on the uniform cross-section A-70 tensile specimens.

The products formed with HCl present were no longer the white methoxide crystal but greenish liquids or solids. The mass spectra showed many peaks with no clear pattern, certainly no evenly spaced titanium quintets. Assuming conservation of mass and chemical identity, the product was obviously a mixture of the several titanium chloromethoxides, in equilibrium given by [164]:

$$TiCl_{4-y}(OCH_3)_y + y\ HCl + z\ CH_3OH \rightarrow TiCl_4 + (y+z)\ CH_3OH \qquad [E\text{-}20]$$

In the absence of methanol, HCl does not seem to react with the oxide-free titanium film at the temperatures studied (150°C). This is consistent with the results of Ondrejcin and Louthan [165], who found that a commercially pure titanium (grade not given) did not crack at 343°C, and that there was a threshold temperature for the cracking of Ti-8Al-1Mo-1V alloy of approximately 245°C. The latter observation suggests that, had we studied the HCl/unoxidized film system at higher temperature, some reaction may have occurred. A high activation energy for this reaction would be consistent with the high bonding energy of HCl (Table 2) if considerable distortion of the HCl molecule were necessary to form the activated complex. In the presence of methanol, predisocciation of the HCl molecule and stabilization due to solvation may occur, so the reaction with titanium will be that of an ionic H^+ and Cl^- species rather than a covalent molecule.

The variations between the SCC susceptibility of commercially pure titanium and the Ti-8Al-1Mo-1V alloy observed by Ondrejcin and Louthan find an explanation in the defective oxide film theory of crack initiation

suggested in the previous section. The susceptibility difference cannot be due to adsorption of HCl on the rutile surface, for the IR spectra of Parfitt, et al. [121] indicates dissociative chemisorption of HCl occurs readily at 45°C. Ondrejcin and Louthan themselves show that diffusion through the oxide on the 8% aluminium alloy affects the failure time, and that the oxide film is considerably enriched (28.6 wt %) in aluminum. Our generalized initiation explanation is that Al^{+3} ions contribute to the defective structure of rutile, allowing faster permeation of the molecular fragments, particularly the H^{+} species, from the surface to the bulk of the rutile. Aluminum doping of the oxide, as described earlier, should also facilitate cracking in this system of the commercially pure alloy. It is otherwise protected by a less-defective oxide film than is the Ti-8Al-1Mo-1V alloy.

The rapid reaction rate we observed with CCl_4 vapor in contact with a thin film at 120°C agrees with the room temperature results of Beck and Blackburn [15] showing the more rapid propagation rate in CCl_4 than in CH_3OH. More quantitative rates of film disappearance determined from resistance measurements as discussed later in the text, suggest that the activation energy for the CCl_4 reaction is slightly less than for methanol. This observation is consistent with the lower bonding energy for the C-Cl bond, but the reaction cannot be directly comparable since a different activated complex must be involved in the mechanism.

As we reported earlier [166], no one seems to have proposed a direct reaction between titanium and CCl_4, the impurity theories (cf. III-A-3, p. 47) having been dominant. From the appearance of the liquid products formed, and their hydrolysis in contact with water vapor, the corrosion reaction results in a covalently bonded titanium chloride which has a mass spectrum similar but not identical to that of an authentic sample of $TiCl_4$ (Matheson, Coleman & Bell, Cat. No. TX 690). A black film, assumed but not proven to be carbon, also formed. The overall reaction between titanium and CCl_4 consistent with the observations is:

$$xs\ Ti + y\ CCl_4 \rightarrow y\ \underline{C} + TiCl_4 + (TiCl_x)\ , \qquad [E\text{-}21]$$

where the unknown product $(TiCl_x)$ is volatile and therefore not $TiCl_2$ or

$TiCl_3$ which are solids. The latter compounds might also have accounted for the black film observed, but these would have immediately reacted with atmospheric moisture upon bulb exposure, while the film observed is quite stable in laboratory air at room temperature.

It was observed that an oxide film prevented the reaction of CCl_4 with the titanium film at temperatures around 150°C, consistent with the earlier observations that CCl_4 will not cause crack initiation in titanium. We also observed, in agreement with Lake and Kemball [123], that hydrogen/deuterium exchange was very slow on the oxided film. Both H_2 and CCl_4 are non-polar molecules; therefore the proposal of Lake and Kemball that the highly ionic rutile dissociates only polarized bonds may be generalized to include the absence of low temperature reactivity of CCl_4 with the oxide.

At high temperatures the story is different. At 350°C a pre-oxidized film readily disappears from the glass surface, leaving no black residue. CO_2 and CO as well as $TiCl_4$ were detected mass spectrometrically. The reaction:

$$CCl_4 + TiO_2 \rightarrow TiCl_4 + CO_2 , \qquad [E-22]$$

should not be surprising when compared with the commercial titanium ore processing reaction,

$$\underline{C} + TiO_2 + 2\,Cl_2 \rightarrow TiCl_4 + CO_2 . \qquad [E-23]$$

One source [167] suggests that CCl_4 may be formed as an intermediate in reaction [E-23] and states that two alternate variations in the synthesis of $TiCl_4$ is the use of either CCl_4 or phosgene, $COCl_2$, in place of the carbon/molecular chlorine combination reactant.

By qualitative observation of film corrosion and quantitative analysis of the products of reaction, primarily by mass spectroscopy, we have then demonstrated a series of chemical reactions [E-20], [E-21], [E-22] which are consistent with observations of stress corrosion in tensile specimens. The questions remain then, what is a more quantitative response of the metal phase to this chemical attack, and what is the role of stress in the metal phase?

To answer this, the thin film technique was expanded to include electrical measurements of titanium phase during the chemisorption and corrosion reaction. The technique and some of the results have been presented for publication [166], and they are summarized as follows:

The experimental apparatus is indicated in Figure 16. It consists of a sorption-pumped and ion-pumped vacuum system, bakeable to 200°C, and, as ordinarily used, provides a background pressure of 10^{-7} torr. The substrate bulb for the thin film contains two sealed tungsten electrodes, so that the film forms one resistance arm of a Wheatstone bridge. To monitor the film, the balance signal for this bridge is fed to a potentiometric chart recorder (Texas Instruments Servo/Riter II) operating at 50 mv. full scale.

The titanium source material, reactants, and procedure are identical to those used in the earlier thin film study [160], except the vacuum system in this case was free of stopcock grease, mercury vapor, and had lower residual pressure before film evaporation. Replacement of the ionization gauge in Figure 16 by a monopole mass spectrometer (Veeco SPI-10) for residual gas analysis indicated that the oxygen levels in the system before film evaporation were less than 10^{-9} torr. The bulk of the residuals were nitrogen (6×10^{-8} torr) water (4×10^{-8} torr) and hydrogen (3×10^{-8} torr). The bulk of the background water vapor effused from the capillary portion of the quartz Bourdon gauge (Texas Instruments Model 245 Precision Pressure Gauge) used to measure the gas reactants and to follow the reaction manometrically. The latter gauge could not be baked and was always closed off during film evaporation and reactant pressurization. In the CCl_4 experiment, small amounts of CCl_4 vapor (system pressure about 5×10^{-5} torr) evidently reduced effusion of residual water from the gauge and lowered the background water peak, simultaneously indicating that water was not a CCl_4 contaminant. The visual results of these experiments were not detectably different from the results shown in Table 3, indicating that the earlier work, performed on a more conventional mercury diffusion-pumped system with standard greased stopcocks, could not be faulted for contaminant effects.

For the electrical conductivity studies, films the order of 500-800 Å thick (5-8 mg weight) were used in order to give an empirically convenient bridge arm resistance the order of 50 ohms after the films were annealed at 225°C to a constant resistance. A normal positive temperature coefficient of resistance indicated the films were continuous.

The recorder traces of the resistance increases of virgin titanium films exposed to spectroscopically pure methanol vapor (18.8 torr) and to spectroscopically pure carbon tetrachloride vapor (1.0 torr) are shown in Figures 17 and 18. The electrical response of the titanium metal to either stress corrosion propagation molecule is seen to be essentially the same--a rapid resistance increase the order of 10%, ocresponding to chemisorption, followed by slow resistance increase, corresponding to film thinning as corrosion products are formed. The electrical response is the same although the chemistry of the two compounds and the activated complexes in reactions [E-19] and [E-21] are different. The methanol reaction in particular should be complicated by the formation of hydrogen, which remains in the metallic phase and is never observed in the gas mass spectrum.

To delineate the hydrogen effect we measured the film response to molecular hydrogen (Pd purified) and found it to be opposite in sign, for the film conductivity increases upon hydrogen chemisorption. The accumulated response for several increments of hydrogen gas is indicated in Figure 19. The hydrogen uptake is irreversible for H/Ti ratios approaching 2 and is reversible above that value. We note that in the earlier thin film work summarized in Table 3, hydrogen/deuterium exchange was observed only after the film was saturated with hydrogen, and Figure 19 explains this system response in terms of reversible and irreversible hydrogen chemisorption.

An insight into stress corrosion propagation theory from an electronic standpoint is possible from these experiments, for the resistance changes corresponding to the chemisorption process may be directly related via equation [E-7] to the electronic band structure of titanium indicated in Figure 5. In Section II-A we have already indicated the evidence that hydrogen uptake donates electrons to the conduction band increasing $\underline{N}$ in

equation [E-7], citing the Hall effect data of Bastl [68] and the magnetic susceptibility data of Jones [69] as independent confirmation of this explanation of resistance decrease we observe with hydrogen.

For the case of methanol and carbon tetrachloride, the localization of titanium valence electrons into surface covalent bonds between titanium and the methoxy fragment or the chlorine atom reduces the number of carrier electrons in the metal, lowering $\underline{N}$ in equation [E-7] and decreasing the conductivity, i. e. increasing the resistance. For titanium, these t_{2g} electrons also provide for the metallic binding [57], so that their removal from the metal phase to the covalent surface bond fundamentally weakens the metal in terms of the tensile strength, $\underline{\sigma}$, between two adjacent atoms at the crack tip. Hydrogen is not required, in fact runs counter to this electronic effect. We conclude therefore, as the CCl_4 data all indicate, that hydrogen embrittlement is not a <u>necessary</u> element of stress corrosion in titanium.

Hydrogen embrittlement may, however, be an accessory process, or perhaps even a sufficient process. This is reconciled by recalling that at the elastic limit the metal may yield by slip, resulting from a resolved shear stress, $\underline{\tau}$, on a slip plane. Kelly, Tyson, and Cottrell [168] have indicated that cleavage fracture of a metal is facilitated by lowering the tensile to shear ratio, σ/τ . Our observed electronic effect lowers this ratio by decreasing σ, while hydrogen localization along a slip plane may lower the ratio by increasing τ. In methanol the hydrogen effect on τ may be present, but the electronic effect on σ is definitely present as indicated by our film resistance studies. In CCl_4 only the electronic redirection of σ may operate, but that is apparently sufficient.

From this electronic viewpoint it is interesting to consider the dual effect of adding aluminium to titanium. First, aluminum incorporation lowers the Fermi level of the alloy, decreasing the number of bonding electrons and fundamentally weakening the material in terms of the interatomic spring constant. Secondly, aluminum increases the solubility of hydrogen in the system, thereby increasing the hydrogen permeability coefficient (Equation [E-14]) and the

flux rate at which hydrogen can move from the crack tip surface where it is generated to the slip planes where it precipitates. These metal phase effects, combined with the defect stabilization in the oxide phase, indicates other multiple reasons why Ti-Al alloy SCC sensitivity increases with Al content.

To complete the electronic aspects of crack propagation, we must indicate another role of stress. Tiller and Schrieffer [169] have published a theoretical paper indicating that in a non-uniform stress distribution such as must occur at the crack tip, electron redistribution must also occur, with electrons flowing into regions of highest tension. This electron density increase at the crack tip will provide for additional overlap with the chemisorbing molecule, lowering the transmission coefficient and/or the activation energy and making the reaction rate stress dependent. For this reason thin films under tension should show near room temperature the effects observed at room temperature with stressed tensile specimens. With unstressed films one must compensate for loss of this activation by heating the system.

We now describe some stress corrosion experiments which are associated with the propagation studies described above:

If reaction [E-19] is involved in the stress corrosion of titanium in methanol, then titanium should be in solution, and may be present in detectable concentrations. We attempted to measure both titanium and aluminum in the alcoholic solution recovered from stress corrosion experiments by the technique of atomic absorption spectroscopy, and should have been able to detect concentrations the order 5 ppm or less in the fluid phase. We did not detect measureable concentrations of either metal. While attempting to prepare suitable atomic absorption standards we then rediscovered the extremely low solubility of titanium methoxide in methanol. Standards were eventually prepared from solutions of titanium isopropoxide (Alfa Chemicals) in isopropanol, and when measured, the solubility of the methoxide in purified methanol was in the range of 20-30 ppm. The solubility essentially doubled, to 40-50 ppm, when 1000 ppm NaCl was added to the methanol. The latter result implied the formation of a more soluble titanium chloromethoxide, and very rapid exchange between halogens and alkoxyl groups has been demonstrated by

Weingarten and Van Wazer [170].

These results have two implications, one of which is that halide ion accelerates the crack propagation by increasing the solubility of the corrosion product, freeing the crack tip surface for continued reaction. The second implication is that saturation of the solution with titanium methoxide should quench the SCC process.

The saturation premise was tested with four samples: two A-70 uniform cross-section and two Ti-6Al-4V in the perpendicular orientation, all loaded to approximately 90% of the elastic limit. One of each type was exposed to $Ti(OCH_3)_4$ - saturated methanol, and the second was exposed to $Ti(OCH_3)_4$ - saturated methanol/1% NaCl. The only sample to fail was the Ti-6Al-4V alloy in contact with Cl^- ion. The Ti-6Al-4V sample exposed to methanol/methoxide was loaded to 92% of the elastic limit and did not fail for 15,000+ minutes, some three orders of magnitude longer than expected time of failure. Discounting part of this resistance to permeation of water into the test cell, we may still suggest with lucid hindsight that incorporation of a few ppm of methoxide may have prevented the tank failure that triggered the research on this topic.

This apparent inhibition is strictly a thermodynamic saturation effect, for just any methoxide will not do. Saturation of methanol with aluminum methoxide (Alfa Chemicals) will not alter the failure time of Ti-6Al-4V, this point also indicating that aluminum does not enter solution during SCC and is not part of the propagation process.

In an attempt to test the hydrogen embrittlement theory further, we ran a tensile failure test with methanol and ethanol solutions of sodium borohydride (Ventron Corporation), $NaBH_4$, which is a hydrogen-releasing reducing agent. No failures were observed, and when the tensile sample gauge sections were analyzed for hydrogen, we found that the samples had lost about 6 ± 1 ppm as compared to the grip section that had not contacted the borohydride solution. A possible explanation for hydrogen loss is that the hydrogen in titanium is protonic in nature, and the borohydride removes it to form hydrogen gas; but this would require more research to confirm and prove.

E. Mass Transport Effects on Crack Propagation

We attempted to extend the number of stress corrosion fluids active with titanium by applying the knowledge that the O-H bond was broken in reaction [E-19] and that the inductive effect explained the inactivity of ethanol, isopropanol, and the higher alkyl alcohols. All that appeared to be necessary for SCC was a reactive O-H bond, and by the substitution of appropriate electron-withdrawing groups, the alcohols could be made more reactive. This reactivity is equivalent to alcohol acidity, or the tendency to lose a proton, i. e.,

$$R\text{-}O\text{-}H \rightarrow R\text{-}O^{-} + H^{+} \qquad [E-\ ]$$

for which an equilibrium constant may be defined by

$$K_a = \frac{[R\text{-}O^{-}]\ [H^{+}]}{[R\text{-}O\text{-}H]}\ , \text{ and} \qquad pK_a = -\log K_a\ . \qquad [E-\ ]$$

The reactivities of alcohols may then be compared by their pK_a values. An extensive compilation of such values and a discussion of this topic has been published by Rochester [171].

The alcohols tested, sample type, stress level, and results are shown in Table 4. Although the same precautions were taken with these experiments as with the preceding methanol studies, no failures were observed until methanol was added to the system.

This inability of the thermodynamically-favored alcohols to react is either an eventually resolvable paradox or an indication of a fundamental misunderstanding of the system. Fortunately this paradoxical situation has arisen before in chemistry, and it usually suggests a complex sterochemistry or the presence of mass transport control. Since the alcohols are fairly simple molecules, we choose mass transport effects, particularly since the reaction site in SCC propagation is subject to extreme geometrical boundary conditions such as at the end of a long pore as indicated in Figure 4a.

For this part of the report the general discussion of Section I-E-2 was incorporated, and we analyze the effect of changing alcohol species on

the SCC response of the system in terms of the Theile modulus, equation [E-4].

Methanol is the smallest stable alcohol molecule, about 4 Å in daimeter Any alteration in structure which affects the acidity of the O-H bond in this molecule must necessarily increase both the molecular size and the molecular weight. The physical parameter of molecular size can have important structural implications in systems the same order of size as the molecule. An excellent example of a size effect involving methanol and ethanol is resident in the β-quinol clathrate structures in which various molecules may be physically trapped [93d]. The trap site is approximately 4 Å in diameter, so that the methanol compound easily forms, while the ethanol clathrate is unknown.

Substitution of a more active alcohol for methanol in a SCC system may affect the Thiele parameter for the crack in the following ways: (a) increase in the molecular weight will lower the diffusivity $\underline{D}$; (b) increase in the reactivity will increase the rate constant, $\underline{k}$; and (c) increase in molecular size will lower the average radius $\bar{r}$, due to the increased thickness of the passivating alkoxide layer lining the crack surface. All three of these effects combine without compensation to increase the modulus and bring the system closer to mass transport control rather than reactivity control.

This application of the Thiele-Wheeler model, which was not originally designed to explain stress corrosion, should nevertheless indicate the correct trends explaining the observed inactivity of the alcohols tested. A more detailed examination of the physical system indicates that the Thiele-Wheeler model represents the limiting case of the non-propagating crack, i. e. $\underline{L}$ fixed. For a propagating crack with parallel walls, increases in L would further increase the Thiele modulus. In practice, the crack mouth may yawn open as the crack propagates, compensating for the modulus increase by an amount dependent upon the crack angle. This question of crack angle is also a point of discussion between Beck and Forty [172] concerning Beck's

electrochemical transport model [45]. A maximum value mentioned is 3°, while Forty contends the deviation is even less. For such small angles it would appear then that the Theile-Wheeler modulus model is relevant if only approximate in suggesting how mass transport control can occur in non-electrochemical stress corrosion systems.

Size effects, and therefore mass transport effects seem also to explain the trend of halocarbon activity outlined on page 47. Except for the special case of CF_4, which contains only very strong C-F bonds, those halocarbons showing SCC propagation activity are all below a critical molecular size, a size about that of the $CFCl_2$-CF_2Cl molecule. Indeed, the small difference in size between $CFCl_2$-CF_3, which showed crack propagation, [102f] and $CFCl_2$-CF_2Cl, which is apparently inactive, indicates that small size variations are extremely important.

F. The Role of Halide Ions

Under Section II-D above we discussed the role of chloride ion as as an initiation species by its interaction with the oxide film. The same ability to aid in the penetration of the oxide film was also observed in the thin film studies.

The thin film studies clearly show, and the rapid failure of two A-70 precracked specimens stressed at 90% K_{Ic} (Figure 11) indicates, that chloride ion serves also as a crack propagation accelerator.

On the other hand, the stress corrosion test of a notched A-70 sample stress at 90% K_{Ic} and exposed to methanol/NaF solution did not fail within 3780 minutes, some 2.5 times longer than the sample should have failed in methanol alone.

A consistent pattern thus emerges in the halide series. In both the initiation process and the propagation process chloride ion is an SCC accelerator while the fluoride ion is either inactive or tends to retard the stress corrosion process. If this pattern is constant, then it would be satisfying if the explanation were constant in both cases.

In discussing the initiation step we earlier suggested that a difference in ion solvation energy was involved, the small fluoride ion retaining

tightly its insulating solvation layer. There is evidence for the same explanation in the propagation step: The formation of chloromethoxides by equation [E-20] in the thin film studies, and the enhanced solubility of titanium methoxide in methanolic chloride solution due to ligand exchange, combine to indicate the ability of the chloride ion to covalently bond to titanium. In terms of ionic adsorption in the double layer diagram of Figure 3, this indicates that chloride ion may lose its solvation sheath and become a specifically adsorbed anion. By the Devanathan criterion [43] covalent bonding is sufficient proof that this desolvation does occur. We mentioned under II-A, however, that fluorine is one of the two elements of sufficient electronegativity so that all bonding to titanium is ionic in nature. Without the ability to stabilize the desolvated F^- ion at the titanium surface by covalent bonding, there is no compensation for the high activation energy of desolvation of this ion and the process is not favorable.

By this argument fluoride ion should be essentially inactive toward the Ti surface, but may induce some retardation simply because of solvent dipole ordering in the liquid. Near F^-, the hydroxyl hydrogen is less likely to be oriented toward the titanium surface as is required for dissociation to form the methoxide.

A common argument for fluoride ion not accelerating stress corrosion is a high activity and blunting of the crack tip. In the blunting argument there must be an assumption that the fluoride chemistry in methanol at the crack tip has something in common with the general corrosion reaction of Equation [E-9]. In the stress corrosion case a very dilute solution of a highly negative ion is not very well attracted to a slightly negative metal surface, while in the general corrosion case a high ionic strength solution of fluoride ions competes with water for a spot in the ligand sphere of a highly positive titanium ion. The two cases are simply not energetically comparable.

G. Mixed Solvent Studies

Out of the frustration of not observing SCC in the high acidity alcohols,

we began to look for new systems to study. CH_3OH and CCl_4 were the only organic compounds in which we had successfully failed titanium, and an observation from the thin film studies (Table 3) indicated that a mixture of these vapors would slowly corrode a pre-oxidized film. This suggested that a mixture of the liquids would provide an SCC initiation medium. The time-to-failure data shown in Figure 20 confirm this prediction for the Ti-6Al-4V alloy and also demonstrate the difference in initiation time between the two sample orientations. The failure times in the mixture were slightly shorter than observed with pure methanol, but we attributed this to the faster propagation rate of carbon tetrachloride.

A real difference in initiation characteristics became apparent when a uniform cross-section specimen failed in 50/50 volume percent methanol/CCl_4. Unless the oxide film were doped with aluminium, initiation by organics only had not been previously observed on unnotched A-70. A second effect not observed previously in the stress corrosion of organics was an apparent photosensitivity of this sytem. This information is summarized in Figure 21, and, as shown there, the time to failure is halved by ultraviolet irradiation of the sample.

This is a particularly good time to discuss the advantages of fractography in stress corrosion studies. Figure 22 is a scanning electron microscope (SEM) fractograph of a notched A-70 speciment which failed in a purified methanol environment after being stress to 90% K_{Ic}. Note the intergranular failure and the extensive secondary cracking between the grains and in the machined notch face. Figure 23 is a similar SEM fractograph of a notched A-70 specimen which failed in CCl_4 under identical stress conditions. Note the similarity in fracture texture and the presence of some, although noticeably less, secondary cracking. The similarity between Figures 22 and 23 are particularly satisfying considering the similar response of the metal phase to the chemisorption of these quite different molecules shown in Figures 17 and 18. The alikeness of these pictures should also serve to emphasize the point that fractography alone may not be able to distinguish between two different corrosion reactions, in this

specific case [E-19] and [E-21].

On the other hand, fractography may predict the presence of a new set of chemical reactions. The SEM fractograph of Figure 24 is of the A-70 unoform cross-section specimen failed in 50:50 $CH_3OH + CCl_4$ and irradiated with UV light. The extensive intergranular corrosion and grain pitting indicates a much more aggressive medium and possible post-failure general corrosion rather than stress corrosion.

This observation resulted in a more careful look at the mixed solvent system and the products formed during corrosion. Some five components, including the two original solvents, were observed by gas chromatographic analysis. Two of the extra three components were identified as H_2O and $CHCl_3$, the latter compound having also been identified in the thin film study. The third product has not yet been positively identified.

It was soon learned that neither presence of stress nor the presence of UV light was necessary for the corrosion of titanium to occur in mixed methanol and CCl_4. It was an unpredictable but interesting result that a combination of two stress corrosion agents resulted in a general corrosion medium when in contact with titanium. A surface catalyzed reaction must be present, for the irradiation of the liquid alone yields no new products.

H. Photochemical Studies

This phase of the research was initiated to determine if any of the intermediates responsible for stress corrosion cracking were operating via free radical intermediates as opposed to heterolytic bond breaking. In particular we thought that some of the halocarbons or molecules such as chloroform, $CHCl_3$, might be activated toward stress corrosion. Chloroform in particular was of interest for the generation of hydrogen atoms which in turn might provide some insight into hydrogen embrittlement.

The technique developed for photochemical stress corrosion involved modification of the fluid environment container by incorporation of a piece of quartz tubing to serve as a UV-transmission window. An illustration of

such a modified sample is shown in Figure 25-a. The quartz is seen to be held in place by the shrinkable tubing, and a portion of the plastic has been removed to expose the window.

The light source used consisted of an Osram 200 watt superpressure mercury arc lamp mounted in a metal shield. This source was mounted on the same optical bench as was a UV-transmitting quartz/fluorite acromat focussing lens used to concentrate the light beam on the sample window. The complete arrangement for irradiation with the sample loaded in a dead weight apparatus is shown in Figure 25b.

As previously mentioned, the only system found to be UV sensitive ($CH_3OH + CCl_4$) was proven to undergo stress-assisted corrosion rather than stress corrosion.

Plenty of free radicals were generated in the chlorinated liquids as shown by the attack upon the plastic tubing, but the rutile film is apparently resistant.

Certainly methanol SCC of titanium was not enhanced by irradiation. In one test a parallel-orientation Ti-6Al-4V specimen was loaded so that the side in maximum tension was irradiated. Upon failure the shear lip was observed to be on that side, indicating that stress corrosion had initiated on the opposite dark side rather than on the illuminated surface.

In retrospect this inactivity is consistent with the initiation requirements mentioned in this report. Some defect structure in the rutile film aids in crack initiation, while irradiation tends to repair the oxide defect structure and retard initiation by facilitating the photoadsorption of oxygen [127, 128] as discussed on page 38-39.

IV. PROBLEMS SOIVED AND PROBLEMS REMAINING

As a result of the research conducted under this grant, the following accomplishments may be summarized:

1. Introduction of stable isotope exchange techniques to stress corrosion studies.

2. Introduction of thin film techniques to stress corrosion research as a method of crack tip modeling.

3. Recognition and emphasis that vapor phase reactions correlate without exception to tensile specimen SCC tests, and that the coordinated study of both methods accelerates mechanism studies.

4. By use of the above methods we unequivocally established the fact of the previously-proposed-but-heretofore-unproven methoxide mechanism and further established that the O-H bond in methanol was the only bond activated in the system.

5. Instituted a regimen of solvent purification, impurity control, and impurity analysis which minimized misinterpretation in both initiation and propagation studies and provided a reference for purposeful introduction of impurities. In particular instituted multiple instrumental analysis techniques concerning the presence of hydrogen in halocarbons.

6. Introduced the question of metal phase electronic effects in stress corrosion theory, introduced and developed the thin film resistance technique for measuring electronic effects under corrosion conditions, and demonstrated by resistance measurements and band theory that chemisorption of organic molecules fundamentally weaken the metal phase bonding. We indicated that this band weakening was the net effect in methanol as well as in carbon tetrachloride, and that from the metal standpoint the effect of both media was the same.

7. As a result of thin film studies, we bypassed the impurity theory of halocarbon SCC and indicate the reaction mechanism of CCl_4.

8. Reemphasized and extended an interest in the initiation process. Specifically incorporated current knowledge concerning physics and chemistry

of the oxide phase, and reemphasized the role of oxide defects in sensitizing initiation. Reemphasized the role of aluminum in the oxide phase as well as the metallic phase, and originated and introduced to stress corrosion research the technique of oxide phase doping to accelerate initiation processes.

9. In confirming the SCC effects of F^- versus Cl^- as impurity halide ions, we recognized the importance of solvation sphere stability effects and correlated this with SCC response in both initiation and propagation processes. This resolved one of the long standing paradoxes between general corrosion of titanium and the stress corrosion.

10. Introduced the concept of the inductive effect in explaining the low activity of higher alkyl alcohols both in tensile and thin film studies.

11. Extended the concept of the inductive effect to the prediction of higher activity for halogenated alcohols, the failure of which prediction has lead to extended emphasis on the various parameters inducing mass transport in SCC. The recognition of molecular size effects lead to an apparent explanation of the variation in SCC propagation response among the various halocarbons.

In the body of the report we specifically suggest four processes where mass transport effects are important. These are (a) permeation of water into the SCC system (b) penetration of halide ions into the oxide film (c) diffusion of organics in cracks and (d) permeation of hydrogen through the alloy.

12. Specifically studied the chemistry of the oxide phase chemisorption and introduced use of the ESCA technique to stress corrosion research for this purpose.

13. Introduced the question of bond scission mode to stress corrosion, and introduced and developed the photochemical technique for studying this question. Demonstrated that free radical mechanisms are apparently not involved in the initiation process and suggested that photoadsorption of oxygen heals defects on oxide surface to reduce SCC initiation sensitivity.

14. Used fractographic, photochemical, and thin film techniques to discover cross reactions between CCl_4 and CH_3OH were catalyzed by titanium oxide, and that the resultant mixture is a general corrosion environment.

15. Demonstrated thermodynamic inhibition effects by saturation of SCC environment with a specific corrosion product.

16. Developed an integrated viewpoint on the multiple roles of system constituents, i. e. Al affects the sensitivity of both oxide and the metallic phase. Likewise Cl^- ion has a dual role in promoting initiation as well as propagation processes.

We suggest that these 16 points fulfill the prime purpose of the grant, a study of stress corrosion from a fundamental and novel point of view.

An auxiliary purpose of the grant, extension to a wider range of materials, was specifically done for zirconium. Response of a zirconium film to methanol correlated exactly to the titanium studies in that the film corroded and a methoxide was formed. Given the similarity in chemistry and in the electronic bond structure of the two metals, the results for titanium SCC reported herein may with few exceptions be assumed to hold for the stress corrosion of zirconium and its alloys.

A second auxiliary purpose of the grant--prediction of behavior of materials under stress corrosion conditions--is essentially fulfilled by the synthesized concept of minimum requirements for stress corrosion presented in the abstract. The mass transport effects and molecular size effects indicated in 13 above are not specific as to chemistry and may be generally expected in any SCC system. Likewise the dual roles of stress in the system (a) keeping the crack open and (b) increase of electron density in the metal phase at the crack tip is likewise not chemically specific and may be expected to be important in any SCC system.

Our results also indicate that for either direct molecular adsorption, or for ionic adsorption as might occur in an electrochemical process; covalent bonding between the ion or molecule is of fundamental importance in SCC sensitivity.

Some areas of research remain to be pursued, however: (1) We have proposed and given circumstantial evidence that the initiation process is fundamental to the oxide phase and that this process may be studied in the absence of the metal phase. This is definitely a testable hypothesis. (2) We have been unable to correlate the results of Haney on the interaction of halide ions and water to produce a minimum in the time to failure with our thin film studies where water is observed to be a definite inhibitor. Brown [36] has indicated that water enables methanol solution to wet the crack tip, lower the pH, and initiate the dissolution of Aluminum as well as titanium.

This implies an electrochemical process which, for the sake of simplicity, was excluded from our study. A problem remaining to be solved then is a reconciliation of the principles elucidated in this research with the processes which occur in aqueous solution.

(3) We have suggested that stressing of thin films would enhance their reactivity. This remains an area open to additional research.

ACKNOWLEDGEMENTS

Many people have contributed to the education of our group in the area of stress corrosion. We specifically thank Dr. J. C. Scully, Dr. E. Floyd Brown, Dr. Marcus Spiedel, Dr. T. P. Haar, and Dr. M. Pourbaix for their visits to our laboratory and the time spent in discussing corrosion and stress corrosion.

We have especially enjoyed the interest, support and cooperation of the Structure and Materials Branch personnel at NASA-MSC. They have willingly supplied us with materials, suggestions, and experimental support during the course of this research. Dr. J. L. Youngblood was particularly helpful in fractography studies and Mr. Lubert Leger aided in atomic absorption spectroscopy and infrared spectroscopy analysis.

Mr. R. E. Johnson, as technical monitor, constructive critic, and encouraging friend is especially thanked for his attributes of patience and helpfulness which were certainly tested during the course of the research program.

We thank Varian Associates for the opportunity to use their Induced Electron Emission Spectrometer during a demonstration session to implement our stress corrosion studies.

Finally we thank NASA for Grant NGR 44-006-008 which initiated and supported the bulk of this research. For the sake of completeness, however, we must also thank NASA for grants ~~NsG-6-59~~ and NGL 44-006-033 which provided additional support for maintaining and extending our interest in the stress corrosion of titanium.

REFERENCES

[1] J. M. West, Electrodeposition and Corrosion Processes, 2nd Ed. London: Van Nostrand Reinhold Company, 1971.

[2] M. G. Fontana and N. D. Greene, Corrosion Engineering. New York: McGraw Hill, 1967.

[3] H. H. Uhlig, Corrosion and Corrosion Control. New York: John Wiley & Sons, Inc., 1963.

[4] J. C. Scully, Fundamentals of Corrosion. Oxford: Pergamon Press, 1966.

[5] H. L. Logan, The Stress Corrosion of Metals. New York: John Wiley and Sons, Inc., 1966.

[6] G. L. Shvartz and M. M. Kristal, Corrosion of Chemical Apparatus. New York, Consultants Bureau, Inc., 1959.

[7] L. A. Glikman (trans. J. S. Shapiro), Corrosion-Mechanical Strength of Metals. London: Butterworths, 1962.

[7b) I. A. Levin, Ed., Intercrystalline Corrosion and Corrosion of Metals under Stress. New York: Consultants Bureau, 1962.

[8] W. D. Robertson, Editor, Stress Corrosion Cracking and Embrittlement. New York, John Wiley and Sons, Inc., 1956.

[9] R. W. Stahle, A. J. Forty, and D. van Rooyen, Proceedings of Conference: Fundamental Aspects of Stress Corrosion Cracking. Houston, National Association of Corrosion Engineers, 1969.

[10] R. M. Latanision and A. R. C. Westwood, Advances in Corrosion Science and Technology, 1, 51-145 (1970).

[11] M. O. Spiedel, Lecture Notes, Fundamentals of Corrosion Short Course, Rice University, July, 1969.

[12] C. G. Harkins, "Surface Properties of Metals," Lecture Notes, Recent Developments in Materials Engineering Short Course, Rice University, July, 1971.

[13] A. G. Oblad, Oil and Gas Journal, 53, 198 (1955).

[14] B. F. Brown, "Stress Corrosion Cracking, A Perspective View of the Problem," NRL Report 7130 (June 16, 1970). Washington, D. C.: Naval Research Laboratory.

[15] T. R. Beck and M. J. Blackburn, AIAA Journal, 6, 326 (1968).

[16] W. F. Brown, Jr. and J. E. Srawley, Plane Strain Crack Toughness Testing of High Strength Materials, ASTM STP 410. Philadelphia: American Society for Testing and Materials, 1966.

[17] W. F. Brown, Jr., Review of Developments in Plane Strain Fracture Toughness Testing, ASTM STP 463. Philadelphia: American Society for Testing and Materials, 1970.

[18] M. V. Hyatt, Corrosion, 26, 487 (1970).

[19] M. V. Hyatt, Corrosion, 26, 547 (1970).

[20] J. Berggreen, Werkstoff und Korrosion, 8, 640 (1970).

[21] J. C. Scully, Corrosion Science, 8, 759-769 (1968).

[22] T. R. Beck, M. J. Blackburn, and M. O Speidel, "Quarterly Progress Report No. 11, Contract NAS-7-489." Boeing Scientific Research Laboratories, March, 1969.

[23] F. H. Cocks, J. F. Russo, and S. B. Brummer, Corrosion, 24, 206 (1968).

[24] F. H. Cocks, J. F. Russo, and S. B. Brummer, Corrosion, 25, 345 (1969).

[25] A. J. Sedriks, Corrosion, 25, 207 (1969).

[26] A. Phillips, V. Kerlins, and B. V. Whitson, Technical Report ML-TDR-64-416, Air Force Materials Laboratory, 1965. NTIS Document AD612-912.

[27] D. T. Powell and J. C. Scully, Corrosion, 25, 483 (1969).

[28] H. L. Gegel, H. B. Kirkpatrick, and C. M. Swinning, Corrosion, 25, 215 (1969).

[29] R. D. Sloan, "A Comparison of Scanning and Transmission Electron Microscopy as Applied to Failure Analysis in Metals." Santa Barbara, Sloan Technology Corporation, 1970.

[30] D. A. Mauney and E. A. Starke, Jr., Corrosion, 25, 177 (1969).

[31] D. N. Fager and W. F. Spurr, The Science, Technology and Application of Titanium. Oxford: Pergamon Press, 1970. pp. 259-261.

[32] DNF & WFS, Trans. Amer. Soc. Met., 61, 283 (1969).

[33] W. G. Moffatt, G. W. Pearsall and J. Wulff, Structure and Properties of Materials, Vol. 1. New York: John Wiley and Sons, Inc., 1964. pp. 183-198.

[34] R. D. Townsend, Ed., ARPA Coupling Program on Stress Corrosion Cracking (Seventh Quarterly Report). NRL Memorandum Report 1941, October, 1968. Available from NTIS as Document AD 681727.

[35] B. F. Brown, C. T. Fujii, and E. P. Dahlbert, Electrochem. Acta, 116, 218 (1969).

[36] B. F. Brown, "Crack Tip Solution Chemistry Studies," Paper 6, International Symposium on Stress Corrosion Mechanisms in Titanium Alloys, Atlanta, January, 1971.

[37] E. G. Haney, Semi-Annual Progress Reports on NASA Research Grant NGR-39-008-014. Mellon Institute, Pittsburg, 1966-1970.

(a) Report #4.

(b) Report #6.

(c) Report #7.

[38] A. J. Sedriks and J. A. S. Green, Corrosion, 25, 324 (1969).

[39] H. P. Godard, "Localized Corrosion," Chapter 9 in NACE Basic Corrosion Course. Houston, National Association of Corrosion Engineers, 1969.

[40] B. C. Syrett and L. P. Trudeau, Corrosion, 27, 216 (1971).

[41] J. C. Scully, Corrosion Science, 8, 513 (1968).

[42] D. M. Mohilner, Electroanalytical Chemistry, 1, 242 (1966).

[43] M. A. V. Devanathan and B. V. K. S. R. A. Tilak, Chem. Rev., 65, 635 (1965).

[44] A. K. Vijh and B. E. Conway, Chem. Rev., 68, 623 (1968).

[45] T. R. Beck, Ref. [9], p. 605.

[46] DMIC Memorandum 228, Battelle Memorial Institute, March, 1967.

(a) K. E. Wever, p. 39.

(b) A. J. Sedriks, p. 43.

[47] E. G. Coleman, D. Weinstein, and W. Rostoker, Acta Met., 9, 491 (1961).

[48] D. A. Dowden, J. Chem. Soc., 1950, 242 (1950).

[49] R. G. Pearson, Accts. Chem. Research, 4, 152 (1971).

[50] E. W. Thiele, Ind. Eng. Chem., 31, 916 (1938).

[51] A. Wheeler, Advances in Catalysis, 3, 250 (1951).

[52] E. E. Petersen, Chemical Reaction Analysis, Englewood Cliffs: Prentice-Hall, 1965.

[53] C. N. Satterfield, Mass Transfer in Heterogeneous Catalysis. Cambridge: MIT Press, 1970.

[54] C. G. Harkins, F. F. Brotzen, J. W. Hightower, R. B. McLellan, M. L. Rudee, J. R. Roberts, I. R. Leith, and P. K. Basu, Progress Report #2, NASA Grant NGR 44-006-088.

[55] L. C. Pauling, The Nature of the Chemical Bond, 3rd Ed. Ithaca: Cornell University Press, 1960. Chapter 3.

[56] E. C. Snow and J. T. Waber, Acta Met., 17, 623 (1969).

[57] J. B. Goodenough, Phys. Rev., 120, 67 (1960).

[58] H. W. Hayden, W. G. Moffatt, and J. Wulff, The Structure and Properties of Materials, Vol. III. New York: John Wiley & Sons, Inc., 1965. pp 28-29.

[59] R. W. Powell and P. P. Tye, J. Less-Common Metals, 3, 226 (1961).

[60] N. F. Mott and H. Jones, Theory of the Properties of Metals and Alloys, New York: Dover Publications, Inc., 1958. p. 247.

[61] Book of ASTM Standards, Part 7. Philadelphia: American Society for Testing and Materials, 1966. pp 359 ff.

[62] R. A. Wood, "Tabulation of Designations, Properties, and Treatments of Ti and Ti Alloys." DMIC Memorandum 171, 1963.

[63] A. W. Hodge and D. J. Maykuth, "Properties of New High Temperature Titanium Alloys." DMIC Memorandum 230, 1968.

[64] B. W. Gonser, Ind. Eng. Chem., 42, 222 (1950).

[65] R. C. Evans, An Introduction to Crystal Chemistry, 2nd Ed. Cambridge: Cambridge University Press, 1966. p. 344.

[66] S. S. Sidhu, L. Heaton, and D. D. Zauberis, Acta Cryst., 9, 607 (1956).

[67] C. Korn and D. Zamir, J. Phys. Chem. Solids, 31, 1172 (1971).

[68] Z. Bastl, Coll. Czechoslov. Chem. Commun., 36, 1172 (1971).

[69] D. W. Jones, J. Less Common Metals, 6, 100 (1964).

[70] D. W. Jones, N. Pessall, and A. D. McQuillan, Phil. Mag., 6, 455 (1961).

[71] E. Dempsey, Phil. Mag., 8, 285 (1963).

[72] J. W. Berger, D. N. Williams, and R. I. Jaffee, Trans. AIME, 212, 509 (1958).

[73] G. Sanderson and J. C. Scully, Trans. AIME, 239, 1883 (1967).

[74] R. Hultgren, R. L. Orr, and K. K. Kelley, Supplement to Selected Values of Thermodynamic Properties of Metals and Alloys. Berkeley: University of California, Constant Publication.

[75] M. J. Blackburn and J. C. Williams, "Strength, Deformation Modes, and Fracture in Titanium-Aluminium Alloys." Available from NTIS as document AD 683 484. January, 1969.

[76] J. D. Boyd and R. G. Hoagland, "The Relation Between Surface Slip Topography and Stress Corrosion Cracking in Ti-8wt % Al." Paper 14, International Symposium on Mechanisms of Stress Corrosion Cracking in Titanium Alloys, Atlanta, 1971. To be published by NACE, Houston.

[77] N. A. Tiner, Reference [9], p. 602.

[78] N. A. Tiner, "Microprocesses in Stress Corrosion of Titanium Alloys." Paper 10, International Symposium on Stress Corrosion Mechanisms in Titanium Alloys, Atlanta, 1971.

[79] S. M. Toy and A. Phillips, Corrosion, 26, 200 (1970).

[80] J. C. Williams, H. L. Marcus, and B. S. Hickman, "The Influence of Microstructure on the Stress Corrosion Susceptibility of Titanium Alloys." Paper 15, International Symposium on the Stress Corrosion Mechanisms of Titanium Alloys, Atlanta, 1971.

[81] C. J. McMahon and D. J. Truax, "Mechanisms of Stress Corrosion Cracking of Titanium-Aluminum Alloys in Methanol-HCl Solutions." Paper 15, International Symposium on the Stress Corrosion Mechanisms of Titanium Alloys, Atlanta, 1971.

[82] D. A. Mauner, E. A. Starke, and R. F. Hochman, "Hydrogen Embrittlement and Stress Corrosion Cracking of Ti-Al Binary Alloys." Paper 21, International Symposium on the Stress Corrosion Mechanisms of Titanium Alloys, Atlanta, 1971.

[83] T. R. P. Gibb, Jr. "Primary Solid Hydrides," Progress in Inorganic Chemistry, 3, 315 (1962).

[84] W. M. Mueller, J. P. Blackledge, and G. G. Libowitz, Metal Hydrides. New York: Academic Press, 1968. pp. 573-575.

[85] L. R. Allemand, J. P. Fidelle, and M. Rapin, Colloque sur L'Hydrogene dans les Metaux, Valduc, 1967. (Publisher, Centre d'Etudes de Bruyéres-le-Chatel.) pp. 242-279.

[86] R. A. Wood, DMIC Review of Recent Developments, December 10, 1971.

[87] M. Pourbaix, Corrosion, 25, 267 (1969).

[88] A. Pourbaix, M. Marek, and R. Hochman, Proceedings of International Symposium on Stress Corrosion Mechanisms in Titanium Alloys, Atlanta, 1970. To be published by NACE.

[89] H. B. Bomberger, Fundamentals of Corrosion of Titanium. Report RMI TR D-7. Reactive Metals, Inc., Niles, Ohio (1965).

[90] J. D. Jackson and W. K. Boyd, Corrosion of Titanium, DMIC Memorandum 218, 1966.

[91] M. E. Straumanis and P. C. Chen, J. Electrochem. Soc., 98, 234 (1951).

[92] R. L. Kane, Chapter 33, The Corrosion of Light Metals, ed. by H. P. Godard, W. B. Jepson, M. R. Bothwell, and R. L. Kane, New York: John Wiley, 1967.

[93] F. A. Cotton and G. Wilkinson, Advanced Inorganic Chemistry, 2nd Ed. New York: Interscience, 1966. (a) p. 153 (b) p. 803 (c) p. 801 (d) p. 225.

[94] T. Moeller, Inorganic Chemistry, New York; John Wiley and Sons, Inc., 1952. (a) p. 236. (b) p. 263.

[95] S. H. Weiman, Corrosion, 22, 98 (1966).

[96] G. G. Keifer and W. W. Harple, Metal Progress, 63 No. 2, 74 (1953).

[97] H. Brown, DMIC Memorandum 60, 1960. Available from NTIS as Document PB 161 210.

[98] N. D. Tomashov, R. M. Al'tovskii, and V. B. Veadmirov in Korroziya i Zashchita Kinstruktsionnykh Metallichoskikh Materialov, Moscow (1961), cited in reference [90].

[99] Stress Corrosion Cracking of Titanium, STP 397. Philadelphia: American Society for Testing and Materials, 1966.

[100] K. Mori, A. Takamura, and T. Shimose, Corrosion, 22, 29 (1966). Reference [70] also cites S. Segawa, K. Mori, and A. Takamura, Corrosion Engineering, 13, 214 (May, 1964).

[101] R. E. Johnson, "Ti Alloy Pressure Vessels in the Manned Spacecraft Program," in The Science, Technology, and Applications of Titanium, R. E. Jaffee and N. Promisel, eds. New York: Pergamon, 1970. pp. 1175 ff.

[102] "Accelerated Crack Propagation of Titanium by Methanol, Halogenated Hydrocarbons, and Other Solutions," DMIC Memorandum 228 (March, 1966).

(a) R. E. Johnson, pp. 2-7.

(b) R. O'Brien, pp. 3-9.

(c) G. Sandoz, pp. 10-15.

(d) H. Herrigel, pp. 16-19.

(e) C. C. Seastrom and R. A. Gorski, pp. 20-28.

(f) J. Schwartz, pp. 29-33.

(g) B. Lisagor, p. 34.

(h) R. G. Rowe, pp. 35-38.

(i) K. E. Wever, et. al., pp. 39-42.

(j) A. J. Sedriks, pp. 43-47.

(k) E. G. Haney, pp. 51-53.

(l) A. Hurlich, pp. 54.

[103] G. Sanderson and J. C. Scully, Corrosion Science, 8, 541 (1968).

[104] D. T. Powell and J. C. Scully, Corrosion, 24, 171 (1968).

[105] H. R. Gray, "Role of Hydrogen in the Hot-Salt Stress Corrosion of Titanium Alloys." Paper 25, International Symposium on the Mechanisms of Stress Corrosion in Titanium Alloys, Atlanta, 1971.

[106] P. Jones and J. A. Hockey, Trans. Faraday Soc., 67, 2669 (1971).

[107] P. Kofstad, High Temperature Oxidation of Metals. New York: John Wiley, 1966. p. 169.

[108] Kofstad, ref. [107], citing W. Kinna and W. Knorr, Z. Metall., 47, 594 (1956).

[109] Kane, ref. [92] quoting N. D. Tomashov, Dokl. Akad. Nauk. (USSR), 141, #4, 2 (1961).

[110] K. Hauffe, Oxidation of Metals. New York: Plenum Press, 1965. p. 211. [quoting P. H. Martin and W. H. Baldwin, Trans. Am. Soc. Met., 44, 1004 (1952).]

[111] Hauffe, ref. [110], p. 212.

[112] A. Magneli, "Crystallographic Principles of Some Non- Stoichiometric Transition Metal Oxides," Paper 9 in Proceedings of Buhl International Conference on Materials. New York: Gordon and Breach, 1964.

[113] L. A. Bursill, B. G. Hyde, O. Terasaki, and D. Watanabe, Phil. Mag., 8th Ser., 20, 347 (1969).

[114] J. M. Ferguson, "Oxidation and Contamination of Titanium and Its Alloys," DMIC Memorandum 238, 1968. p. 3.

[115] J. Yahia, Phys. Rev., 130 1711 (1963).

[116] C. Naccache, P. Meriaudeau, M. Che, and A. J. Tench, Trans. Faraday Soc., 67, 506 (1971).

[117] D. Y. Cha and G. Parravano, J. Catalysis, 11, 228 (1968).

[118] M. Primet, P. Pichat, and M. V. Mathieu, J. Phys. Chem., 75, 1216 (1971).

[119] P. Jackson and G. D. Parfitt, Trans. Faraday Soc., 67, 2469 (1971).

[120] P. Jackson, J. Ramsbotham, and C. H. Rochester, Trans. Faraday Soc. 67, 841 (1971).

[121] P. Jackson, J. Ramsbotham, and C. H. Rochester, Trans. Faraday Soc., 67, 3100 (1971).

[122] P. Jones and J. Hockey, Trans. Faraday Soc., 67, 2669 (1971).

[123] I. J. S. Lake and C. Kemball, Trans. Faraday Soc., 63, 2535 (1967).

[124] W. A. Weyl and T. Forland, Ind. Eng. Chem., 42, 257 (1950).

[125] C. Reuz, Helv. Chem. Acta, 4, 961 (1921).

[126] A. E. Jacobsen, Ind. Eng. Chem., 41, 523 (1949).

[127] I. S. McLintock and M. Ritchie, Trans. Faraday Soc., 61, 1007 (1965).

[128] F. Stone, "The Photocatalytic Oxidation of 2-Propanol at Titanium Oxide Surfaces," preprints of Ipatieff Centennial Symposium on Catalysis, Northwestern University, Evanston, Illinois, September, 1967.

[129] F. Huber, J. Electrochem. Soc., 115, 203 (1968).

[130] E. S. Gould, Mechanism and Structure in Organic Chemistry. New York: Holt, Dryden, 1959. p. 37.

[131] L. B. Clapp, The Chemistry of the OH Group. Englewood Cliffs: Prentice-Hall, 1967. p. 18.

[132] J. L. Borowitz and F. S. Klein, J. Phys. Chem., 75, 1815 (1971).

[133] S. N. Vinogradov and R. H. Linnell, Hydrogen Bonding. New York: Van Nostand Reinhold, 1971. pp. 38-39.

[134] M. Lecat, Tables Azeotropiques, 2e Ed. Bruxelles: Chez l'Auteur, 1949. Table 60, p. 72.

[135] C. D. Brownfield, "The Stress Corrosion of Titanium in Nitrogen Tetroxide, Methyl Alcohol, and Other Fluids." Report SD 67-213A, Space Division of North American Rockwell Corporation, June, 1968 (revised version).

[136] E. G. Haney, Corrosion, 25, 87 (1969).

[137] J. R. Ambrose and J. Kruger, Corrosion Science, 8, 119 (1968).

[138] D. T. Powell and J. C. Scully, The Science, Technology, and Application of Titanium, p. 247 ff.

[139] G. Sanderson and J. C. Scully, Corrosion Science, 8, 541 (1968).

[140] H. L. Gegel and S. Fujishiro, J. Less-Common Metals, 17, 305 (1969).

[141] K. Kamber, E. G. Kendall, and L. Raymond, The Science, Technology, and Applications of Titanium. Oxford: Pergamon Press, 1970. pp. 293-298.

[142] M. Vialatte, Corrosion--Traitements-Protection-Finition, 16, 246-252 (1968).

[143] J. C. Scully and D. T. Powell, Corrosion Science, 10, 719 (1970).

[144] L. Raymond and R. J. Usell, Corrosion, 25, 251 (1969).

[145] R. E. Johnson, et. al., personal communication.

[146] Corrosion Resistance Charts for Plastics available in 1970 Catalogue, United States Plastic Co., Lima, Ohio, pp. 103-107. Original source not cited.

[147] Permeability equation modified from one presented in General Electric Permselective Membranes, Publication GEA-8685, General Electric Co., Schenectady, 1968, p. 4.

[148] R. L. Johnston, R. E. Johnson, G. M. Ecord, and W. L. Castner, NASA Report S-148, 1967.

[149] K. Siegbahn, et al. , Electron Spectroscopy for Chemical Analysis, Tech. Report AFML-Tr-68-189, 1968. Available as NTIS Document AD844-315.

[150] P. I. Kingsbury, Jr., W. D. Ohlsen, and O. W. Johnson, Phys. Rev., 175, 1091 (1968).

[151] Ibid. P. 1099.

[152] Johnson, Ohlsen, and Kingsbury, p. 1102.

[153] Ph. de Montgolfier, P. Dumont, Y. Mille, and J. Villermaux, J. Phys. Chem., 76, 31 (1972).

[154] S. P. Rideout, R. S. Ondrejcin, M. R. Louthan, Jr. and D. E. Rawl, Reference [9], p. 650.

[155] C. V. Krishana and H. L. Friedman, J. Phys. Chem., 74, 2356 (1970).

[156] C. V. Krishnan and H. L. Friedman, J. Phys. Chem, 75, 388 (1971).

[157] R. L. Hancher, Metallurgia, 49, 47 (1954) .

[158] R. W. Gardiner and P. G. Partridge, J. Sci. Instruments, 44, 63 (1967).

[159] R. C. Glenn and J. C. Raley, Advances in Techniques in Electron Metallography, ASTM-STP 339. Philadelphia: American Society for Testing and Materials, 1963. pp. 60-68.

[160] I. R. Leith, J. W. Hightower, and C. G. Harkins, Corrosion, 26, 377 (1970).

[161] C. Herring, "The Atomistic Theory of Metallic Surfaces," Metal Interfaces. Cleveland: American Society for Metals, 1952. pp. 1-19.

[162] C. G. Harkins, W. W. Shang, and T. W. Leland, Jr., J. Phys. Chem., 73, 130 (1969).

[163] J. G. Williamson, NASA Technical Memorandum Report No. 53971. Marshall Space Flight Center, November 19, 1969.

[164] D. C. Bradley, "Metal Alkoxides," Preparative Inorganic Reactions, 2, 169 (1965).

[165] R. S. Ondrejcin and M. R. Louthan, Jr. "Role of Hydrogen Chloride in Hot-Salt Stress Corrosion Cracking of Titanium-Aluminum Alloys," NASA CR-1133, issued originally as USAEC Rep. DP(NASA)-1130. Available from National Technical Information Service.

[166] C. G. Harkins, "Chemical Reactions of Organic Fluids with Titanium and Titanium Oxide Surfaces." Paper 5, Proceedings of International Symposium on Stress Corrosion Mechanisms in Titanium Alloys, Atlanta, 1971. To be published by NACE.

[167] H. F. Walton, Inorganic Preparations. Englewood Cliffs: Prentice-Hall, Inc., 1948. p. 107.

[168] A. Kelley, W. R. Tyson, and A. H. Cottrell, Phil. Mag. 15, 567 (1967).

[169] W. A. Tiller and R. Schrieffer, Scripta Met., 4, 57 (1970).

[170] H. Weingarten and J. R. Van Wazer, J. Am. Chem. Soc., 87, 724 (1965).

[171] C. H. Rochester, "Acidity and inter- and intra-molecular H-bonds," Chapter 7 in The Chemistry of the Hydroxyl Group, S. Patai, editor. London: Interscience Publishers, 1971. pp. 327 ff.

[172] Reference [9], p. 617.

Figure 1. Stress dependence of stress corrosion on time-to-failure

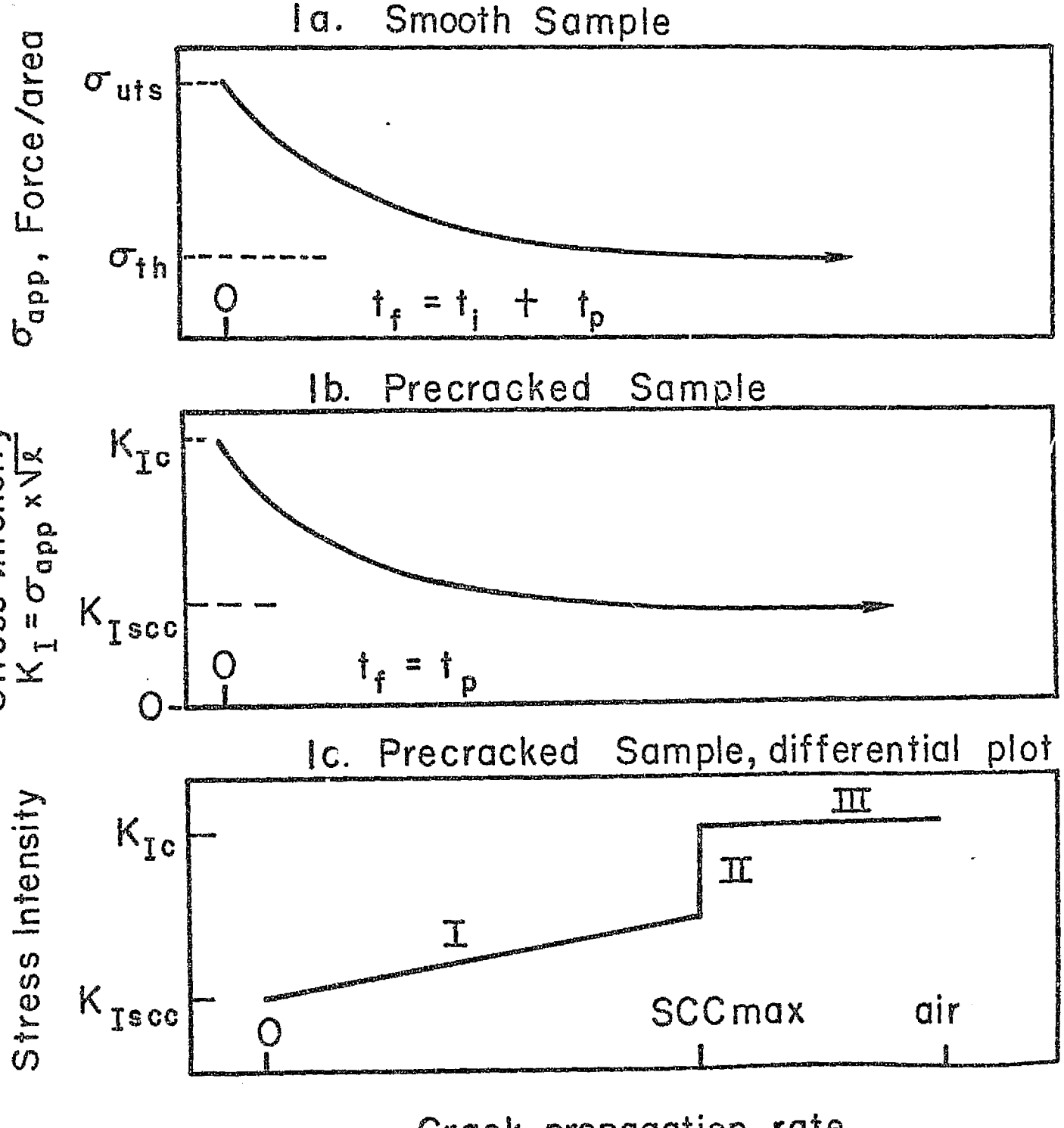

FIGURE 2: STRESS CORROSION SAMPLE CONFIGURATIONS

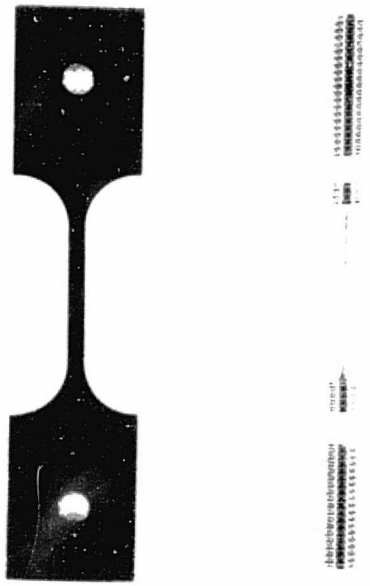

2a. Uniform Cross-Section Samples

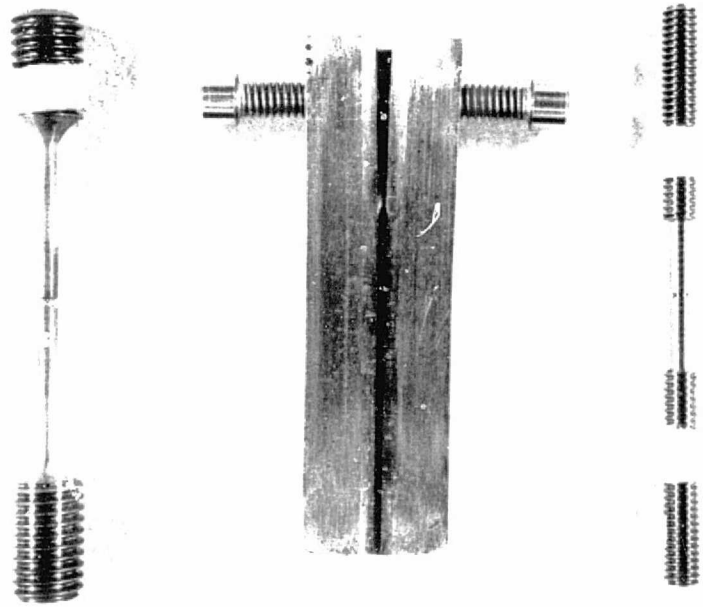

2b. Notched or Pre-cracked Samples

Figure 3. Electrochemical Double Layer Adsorption Model

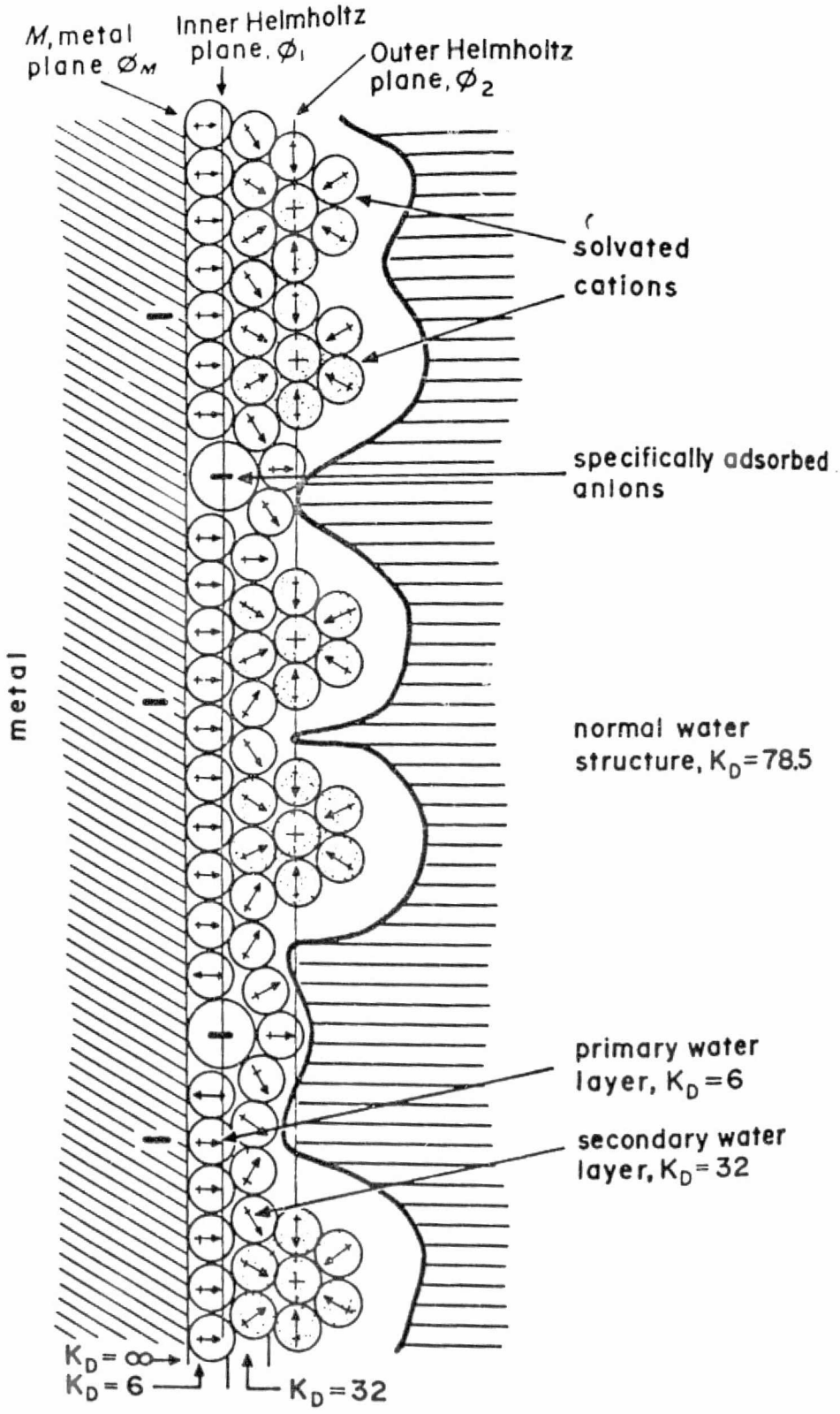

FIGURE 4. Pore Parameters And Effect Of Wall Passivation On Surface Reaction Rates Inside Pores

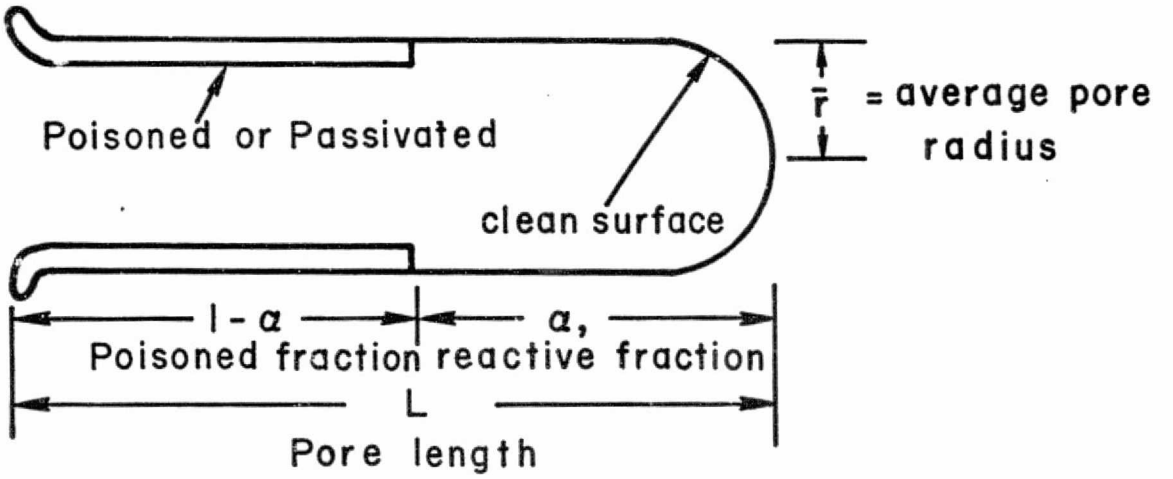

4a: Pore Model

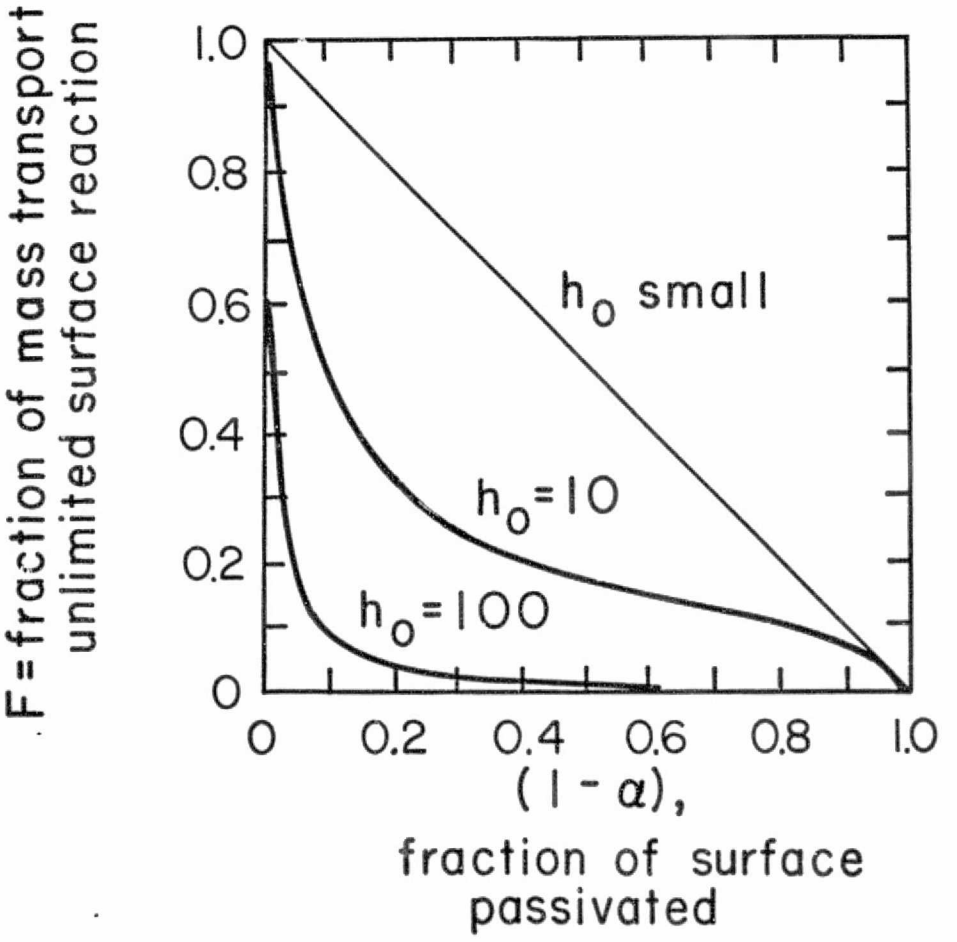

4b: Mass Transport Effects on Pore Model

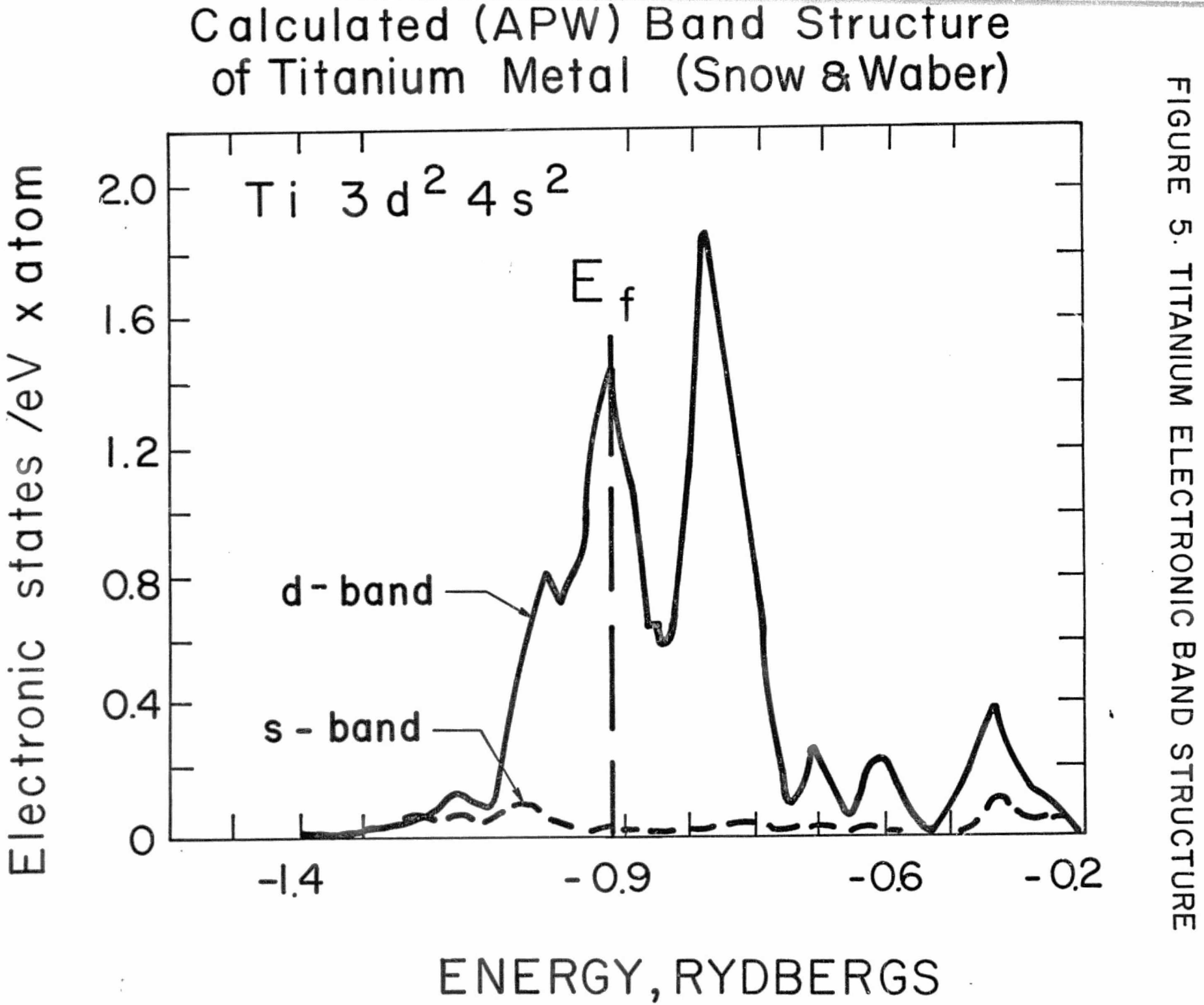

FIGURE 5. TITANIUM ELECTRONIC BAND STRUCTURE

Table I.

SUMMARY OF OBSERVED STRESS CORROSION CRACKING CONDITIONS FOR TITANIUM

ALLOY	PHASE	METALS T°C	HOT SALT T°C	STRONG OXIDIZERS T°C	AQUEOUS SOLUTIONS T°C	HYDROGEN CONTAINING ORGANICS	ACCELERATORS	T°C	HYDROGEN FREE ORGANICS	T°C
Ti 35A	α					EtOH, CH_3OH, n-PrOH, n-BuOH, $n\text{-}C_5OH$	I_2 + Br_2; Fe^{+++}, Pd^{++}, Au^{+}, Cl^-			
Ti 55A	α									
Ti 65A	α									
Ti 75A (A-70)	α	Mg 25		RFNA		CH_3OH		RT		
Ti 100A	α				SEA WATER 25		H_2O			
Ti -0.2Pd	α					CH_3OH	Cl^-			
Ti -4Al-3Mo-1V	α + β				10% HCl	CH_3OH		RT		
						CH_3OH		RT		
Ti -5Al-2.5Sn	α	Ag 468		RFNA 25		C_2H_5OH	Br^-	RT	CCl_4	
					SEA WATER	CH_3CCl_3	I^-	370	CF_2Br_2	25
Ti -5Al-5Sn-5Zr	α									
Ti -6Al-4V	α + β	Hg 25		N_2O_4 30-75	SEA WATER 25	CH_3OH	HCl	RT	CF_3CCl_3	RT
		Cd 25		RFNA 25		CH_3CCl_3	H_2SO_4	370	$CFCl_3$	RT
Ti -6Al-6V-2Sn	α + β				SEA WATER 25					
Ti -6Al-2Sn-4Zn-2Mo	α+lean β									
Ti -7Al-4Mo	α + β	Ag 468							$CCl_2F\text{-}CF_3$	
						C_6H_{14}	C_3-OH	RT		
						CH_3OH		RT		
						C_2H_5OH		RT		
Ti -8Al-1Mo-1V	α+lean β	Hg 25			HCl gas 340	CH_3CCl_3		370	CCl_4	RT
		Cd 25			SEA WATER 25	$(CH_2OH)_2$		RT		
Ti -4Al-3Mo-1V	α + β					CH_2FCCl_3		700		
Ti -8Mn	α + β	Cd 320		RFNA 25	SEA WATER 25					
Ti -13V-11Cr-3Al	all β	Hg 370			5% HCl 25	CH_3CCl_3		370		

ALL ALLOYS 290°C

OXYGEN NECESSARY

H_2O CRITICAL

FIGURE 6

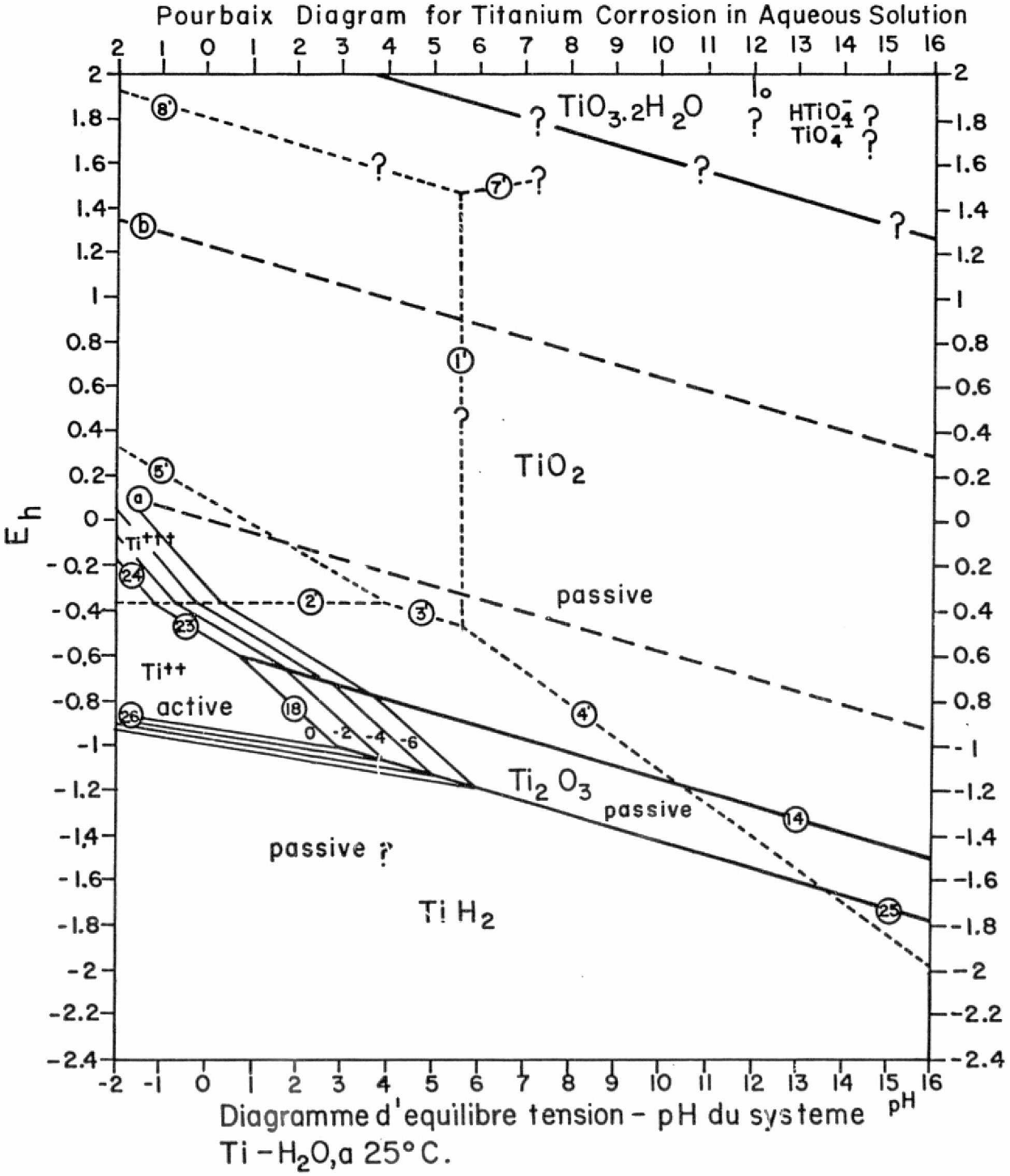
Pourbaix Diagram for Titanium Corrosion in Aqueous Solution
$TiO_3.2H_2O$
$HTiO_4^-$?
TiO_4^- ?
TiO_2
passive
Ti^{++}
active
Ti_2O_3 passive
passive ?
TiH_2
E_h
pH
Diagramme d'equilibre tension - pH du systeme Ti - H_2O, a 25° C.

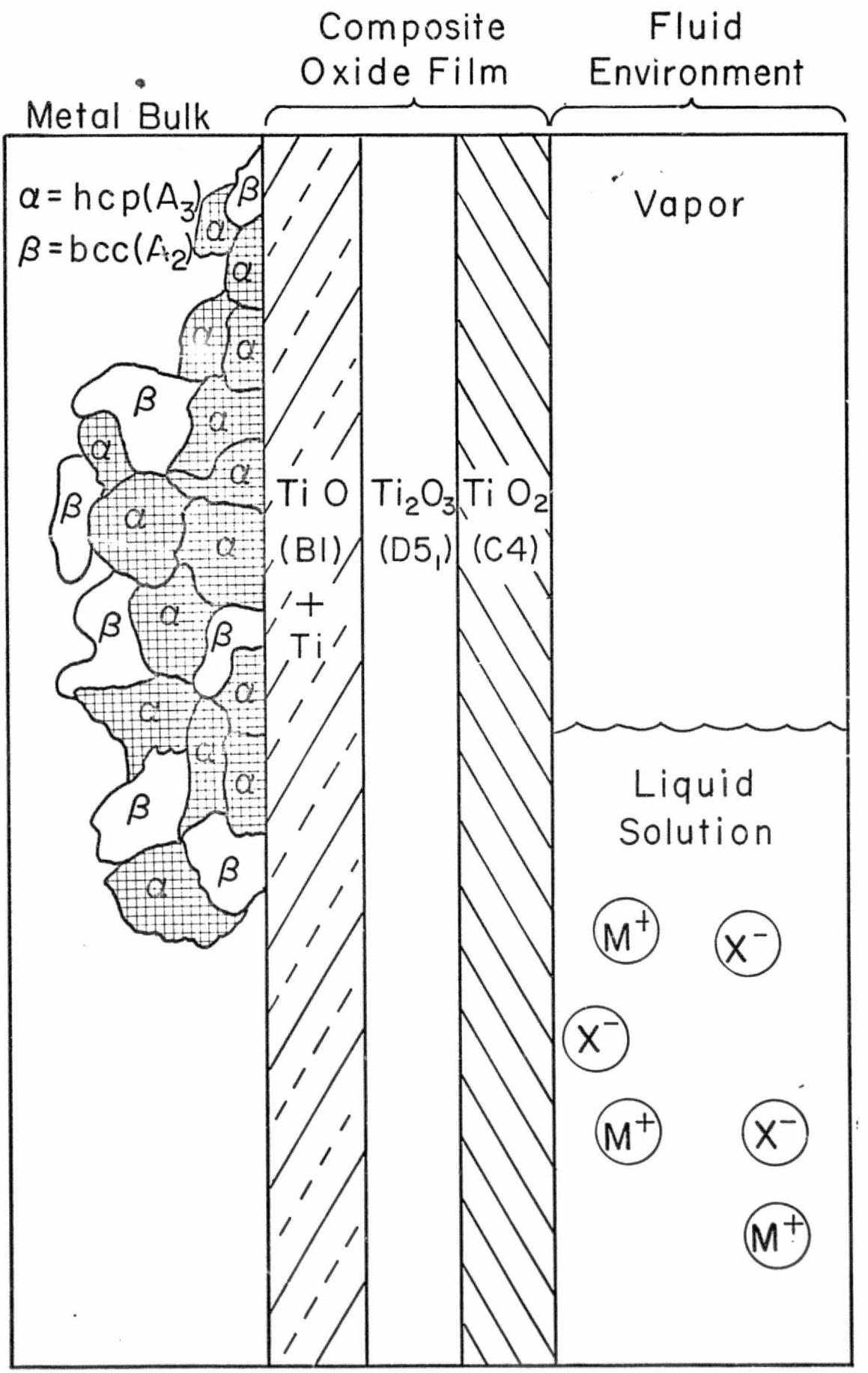

Seven Phase System
Stress Corrosion of Ti

Figure 8

FIGURE 9. METALLOGRAPHY OF TITANIUM SAMPLES

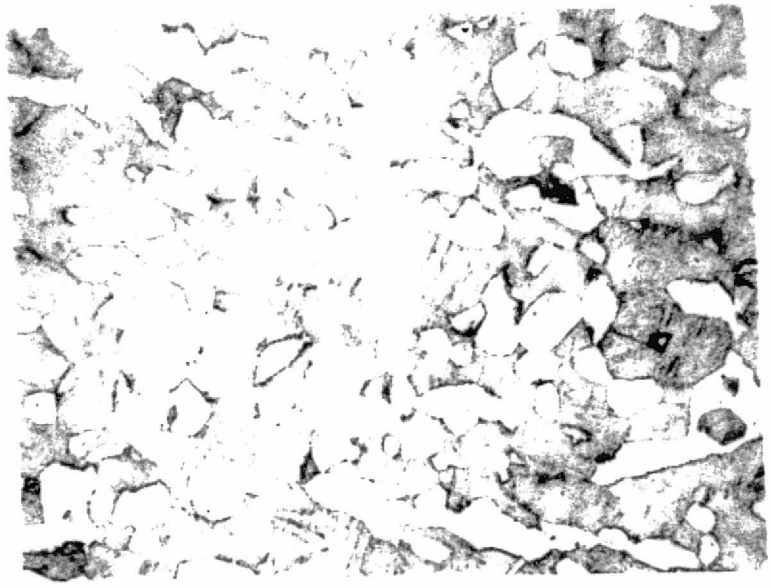

9a. Ti-6Al-4V (STA)

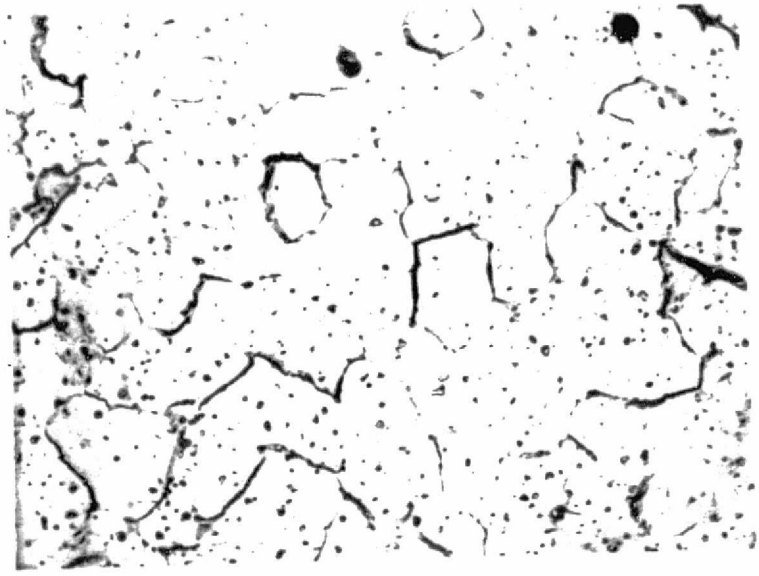

A-70 Grade, Comm. Pure Ti
(Annealed)

FIGURE 10. SURFACE DETAIL OF Ti-6Al-4V TENSILE SPECIMEN

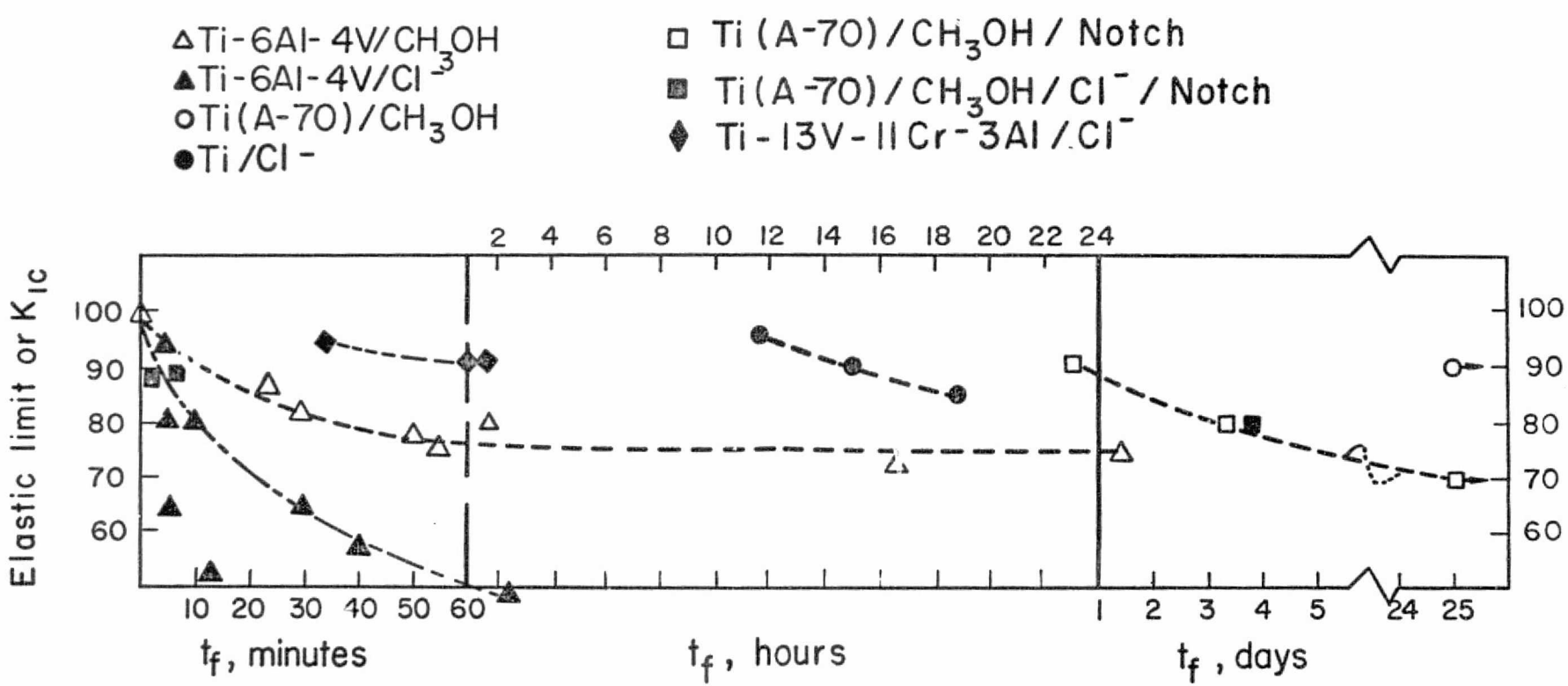

Time-to Failure Data
Titanium Alloys
in CH_3OH and 1% NaCL/CH_3OH

Figure 11

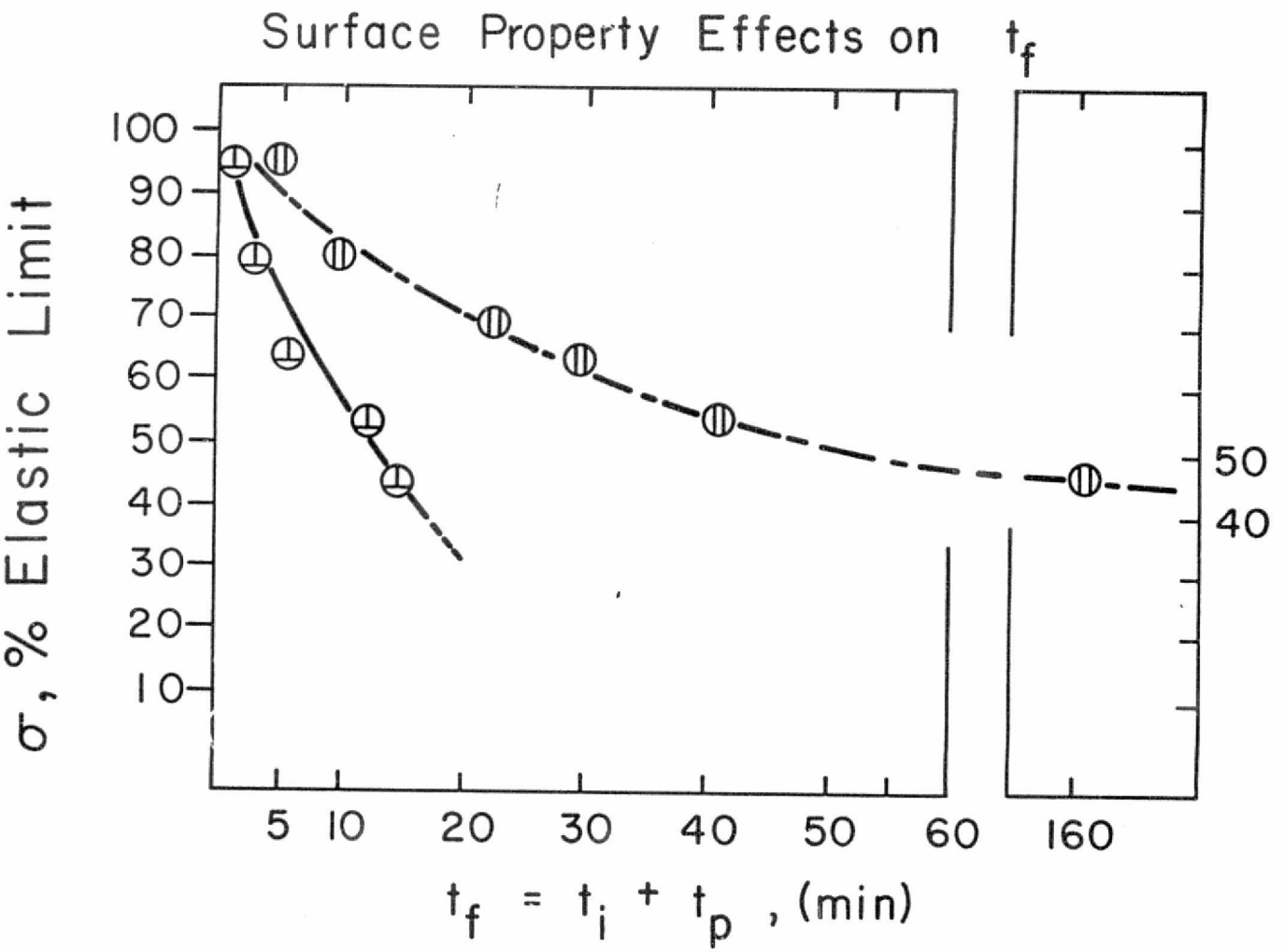

Ti-6-4 in 1% Cl⁻/Me OH as $f(\sigma, t)$

Figure 12

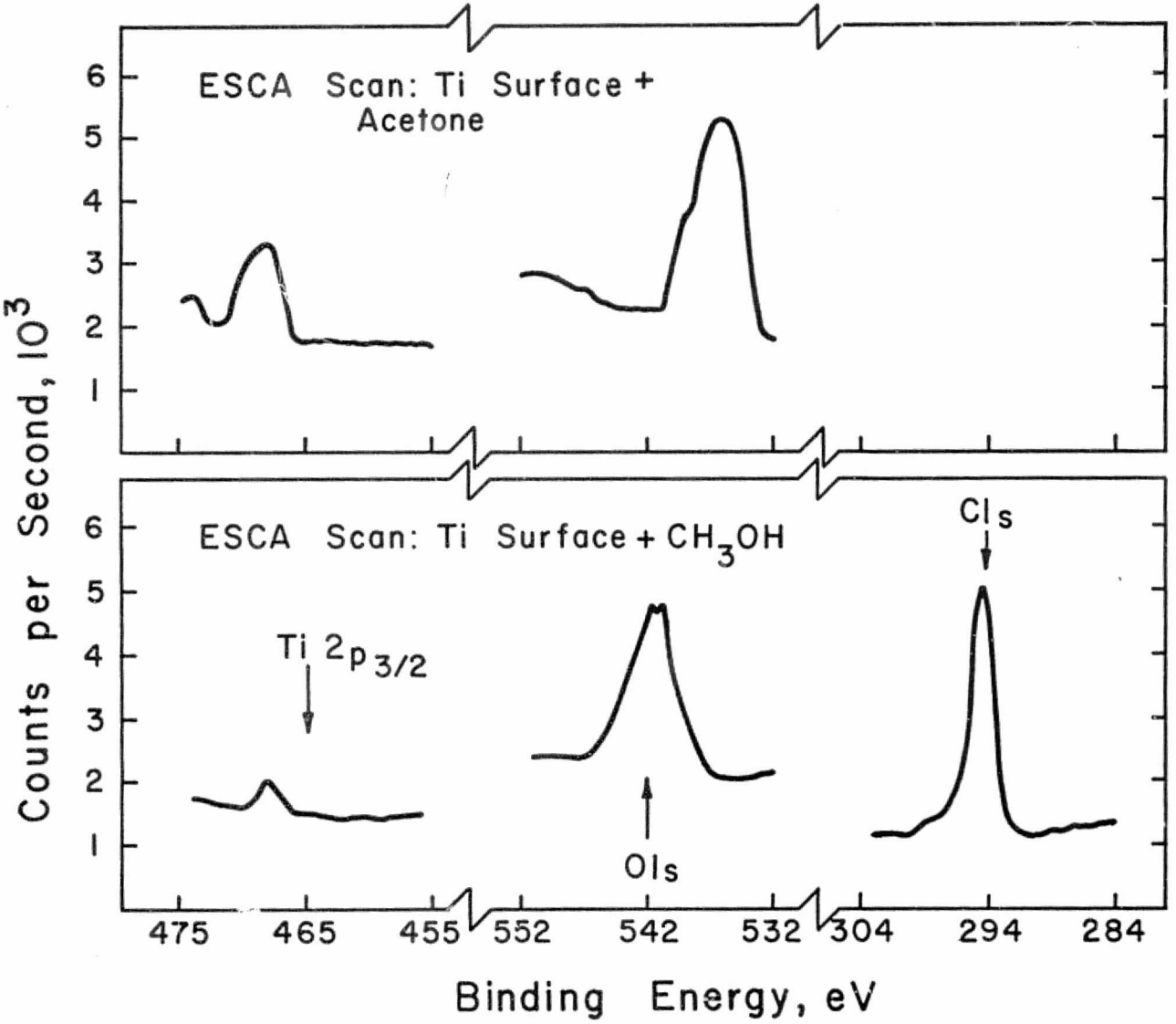

Figure 13. ESCA Spectra of Ti O_x Surfaces

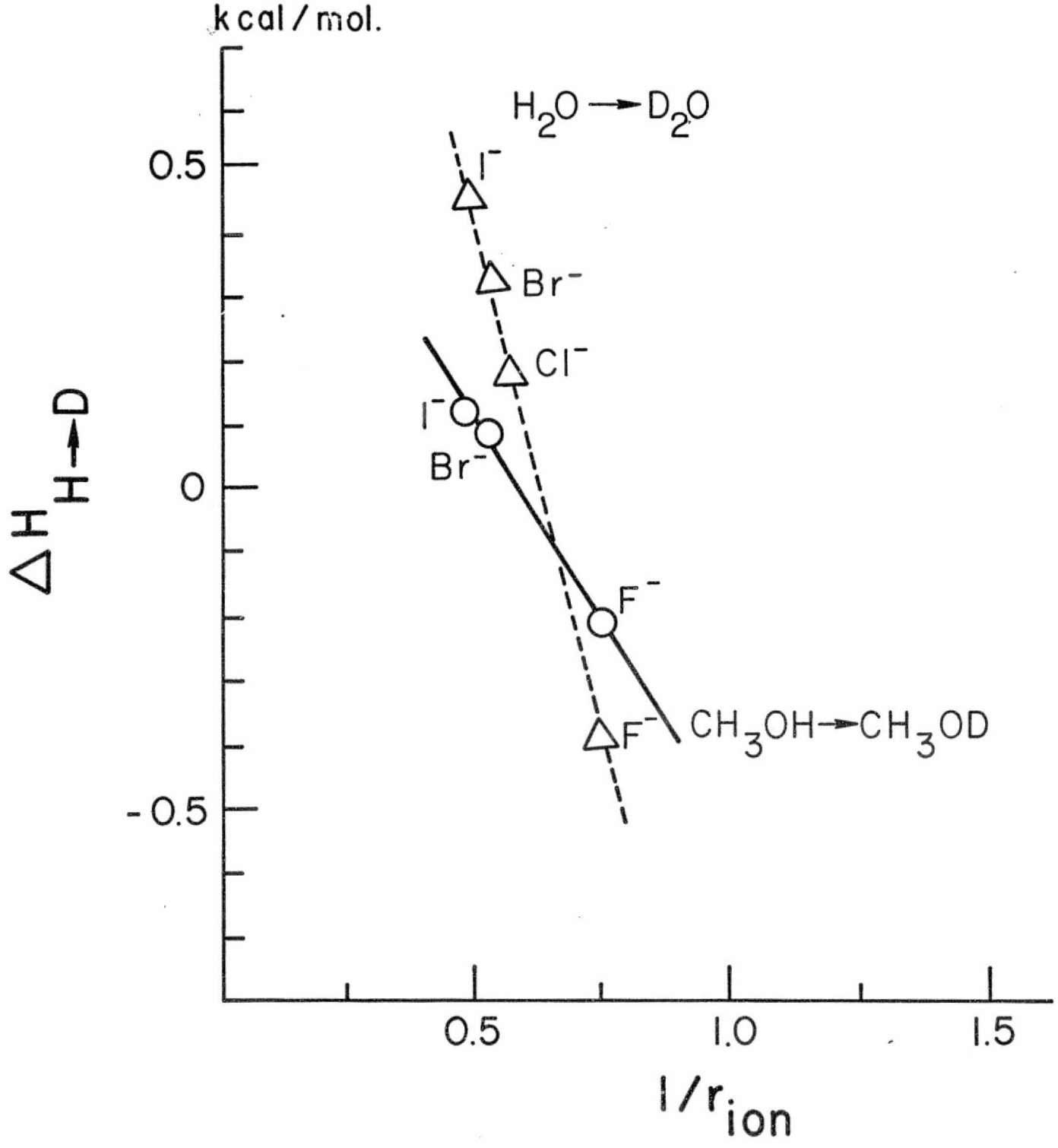

Figure 14. Isotopic Solvation Enthalpies Halide Ions in Water & Methanol

* Krishnan & Friedman, J. Phys. Chem. 75, 388 (1971)

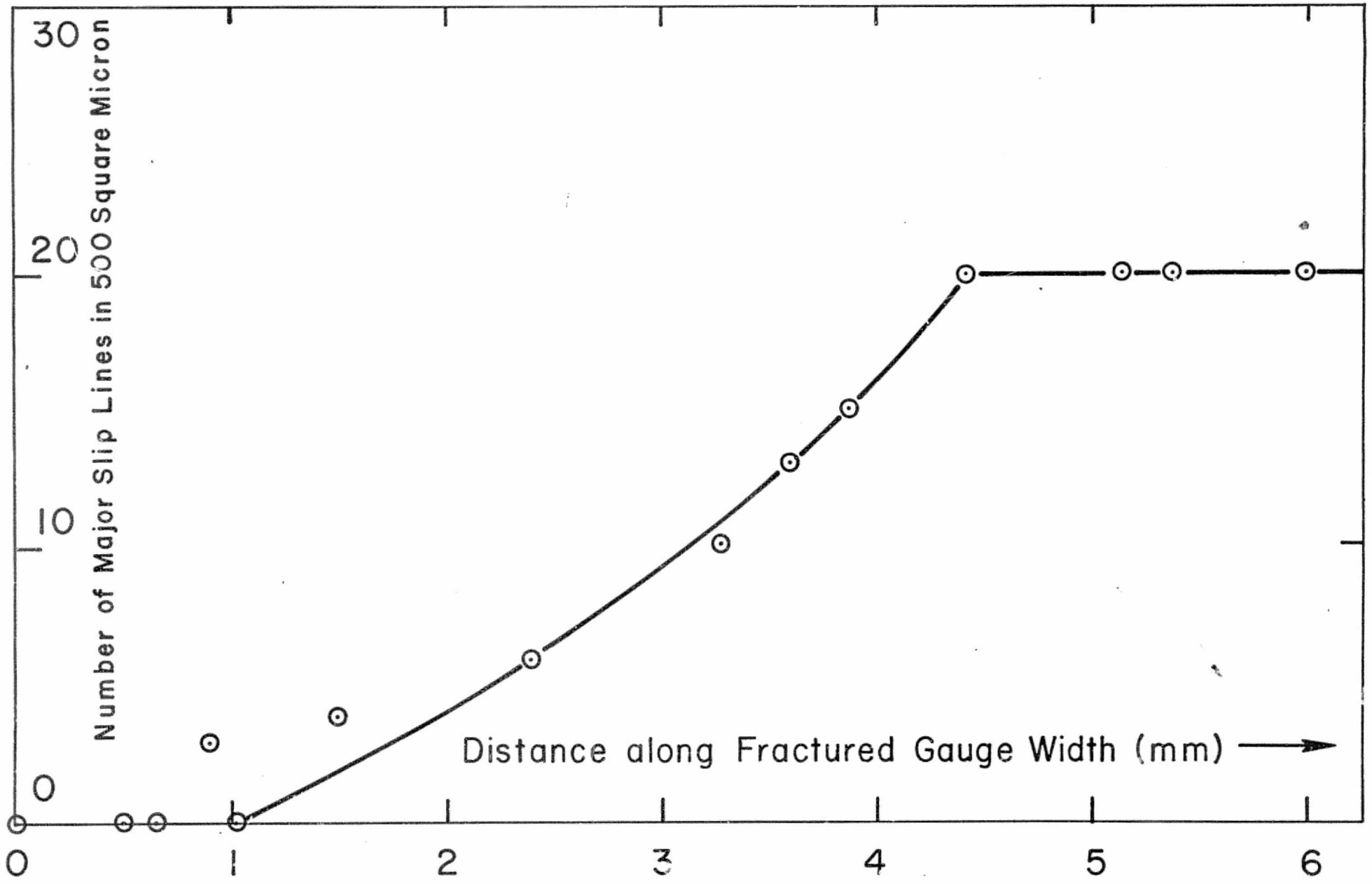

Figure 15. Inhomogeneous Slip Line Distribution, Ti SCC in Methanol/Cl

TABLE 3. QUALITATIVE Ti + gas phase REACTIONS

SURFACE	O_2	H_2O	CH_3OH	CD_3OD	$^{13}CH_3OH$	$H_3C^{18}OH$	HCl	i-PrOH	H_2	D_2	CCl_4	Δ-Film	RATE	PRODUCTS
Glass			+											no reaction <274 °C
Glass			+							+				no xcgn, CO>310°C
Ti			+									+	slow	@ 150. $Ti(OCH_3)_4$
Ti				+								+	slow	$Ti(OCD_3)_4$
Ti							+					−		no reaction
Ti								+				−		no reaction < 300°C
Ti											+	+	fast	@120. C, yellow liquid
Ti			+	+								+	slow	no H/D exchange
Ti					+	+						+	slow	No $^{13}CH_3{}^{18}OH$
Ti	+		+									−		no reaction
Ti		+	+									−		no reaction
Ti			+				1%					+	fast	@ 120°C
Ti			+				5%					+	fast	green solid
Ti			+				10%					+	fast	@ 25°C
Ti	+		+				+					+	slow	trace CH_3Cl
Ti	+										+	−		no reaction @ 150°C
Ti	+										+	+++	?	$TiCl_4$, CO, CO_2 @ 350
Ti				+			+				+	+	med	min. H/D exchange
Ti	+								+	+		−		no H/D exchange
Ti	+			+						+		−		no H/D xgn @ 300°C
Ti	+							+		+		−		no H/D xgn @ 200°C
Ti									+			−		approx TiH_2
Ti				1st					2nd			+		$Ti(OCD_3)_4$; no HD
Ti				2nd					1st			?		HD, D_2, m/e 20 pk

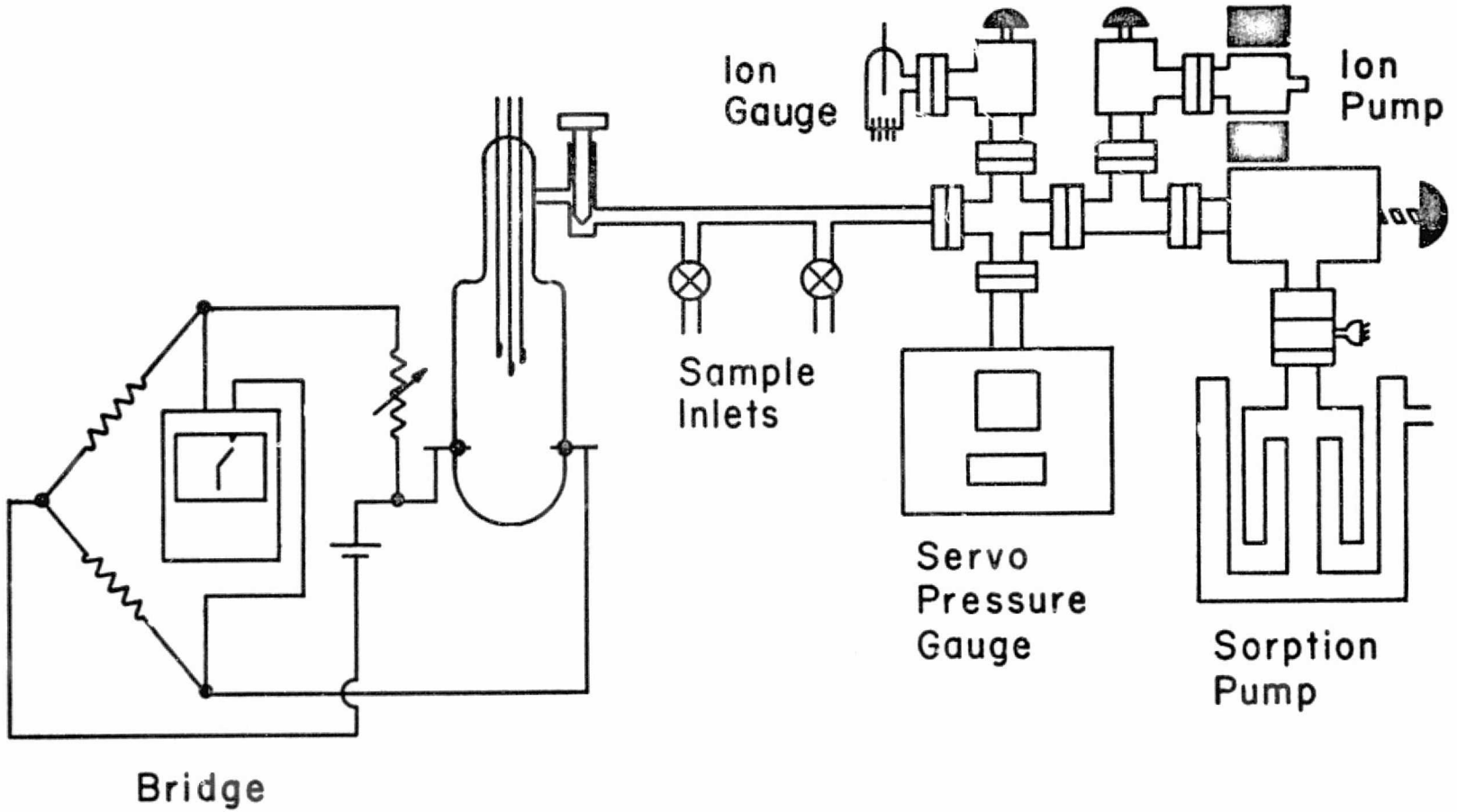

Electrical & Vacuum Circuits

Figure 16

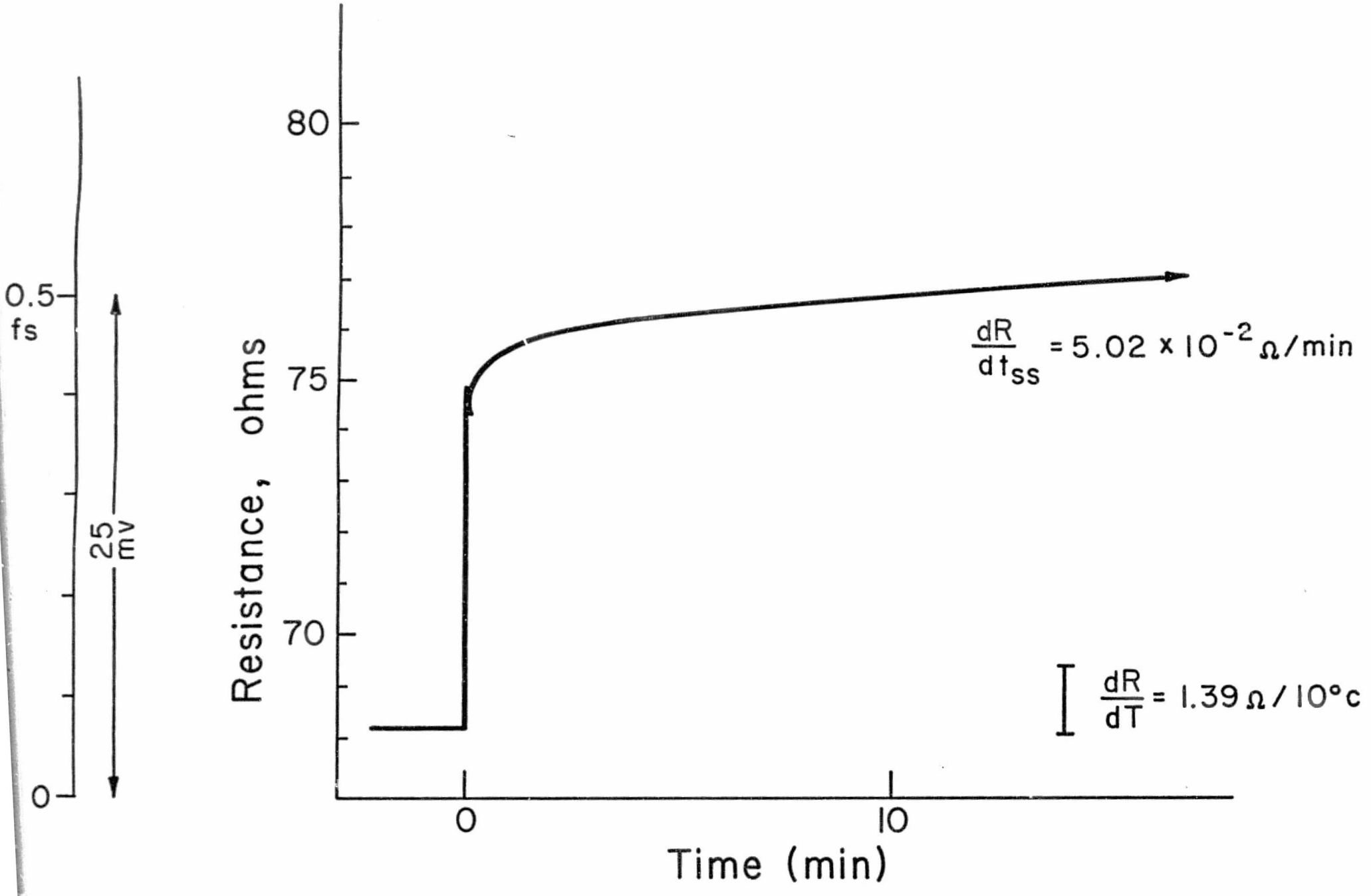

CH_3OH Chemisorption on Ti (145°C)

Figure 17

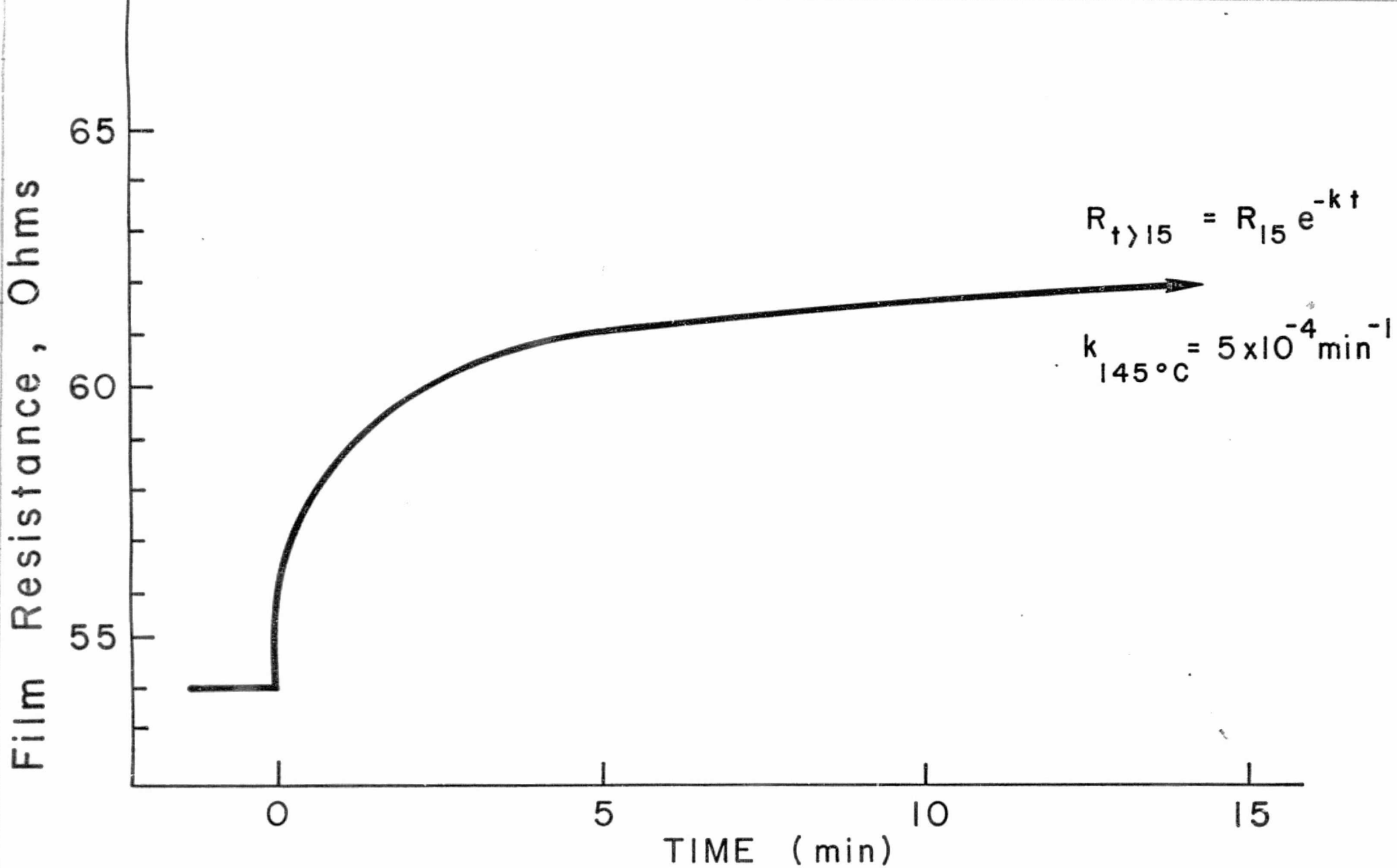

CCl_4 Chemisorption on Ti (145°C)

Figure 18

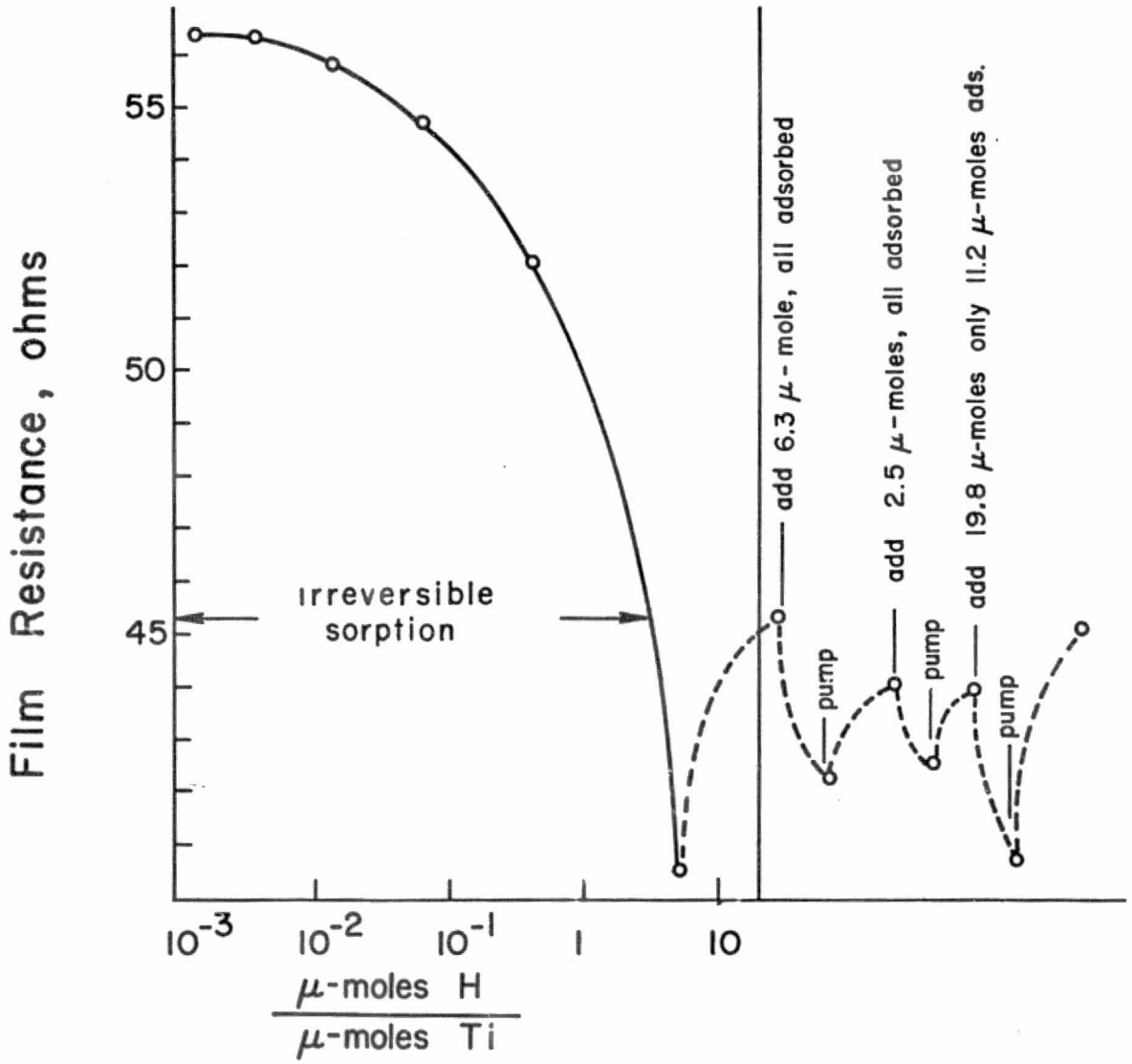

Irreversible & Reversible H_2 Chemisorption on Ti

Figure 19

Table 4

Stress Corrosion Sensitivity To Alcohol Acidity

Alcohol	pK_a, 25°C	Sample	Additions	t_f
CH_3OH	15.5	Ti-6Al-4V, 85% load		28 min
		Ti-A70, 90% load		> 24 days
CH_3CH_2OH	15.9	Ti-6-4, ⊥, 86%		$> 6 \times 10^3$ min
CF_3CH_2OH	12.4	Ti-6-4, ⊥, 86%		$> 5 \times 10^3$ min
		A-70, 90%		$> 7 \times 10^3$ min
		A-70, 90%	+ CH_3OH	$> 7 \times 10^3$ min
$CF_3-\overset{OH}{\overset{\vert}{C}}-CF_3$	9.30	Ti-6-4, 90%		$> 5 \times 10^3$ min
$H_2C=CH-OH$	15.5	Ti-6-4, ⊥, 86%	NaCl	$> 11 \times 10^3$ min
		Ti-6-4, ⊥, 86%	CH_3OH	19 min, vp
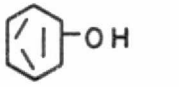	9.99	Ti-6-4, ⊥, 86%		> 20 days
		Ti-A-70, ⊥, 90%		> 20 days
$CF_3-\overset{OH}{\overset{\vert}{\underset{OH}{\underset{\vert}{C}}}}-CF_3$	6.58	Ti-6-4, ⊥, 86%	ε+OH	$> 1.3 \times 10^{+3}$ min
			MeOH	$> 9 \times 10^3$ min

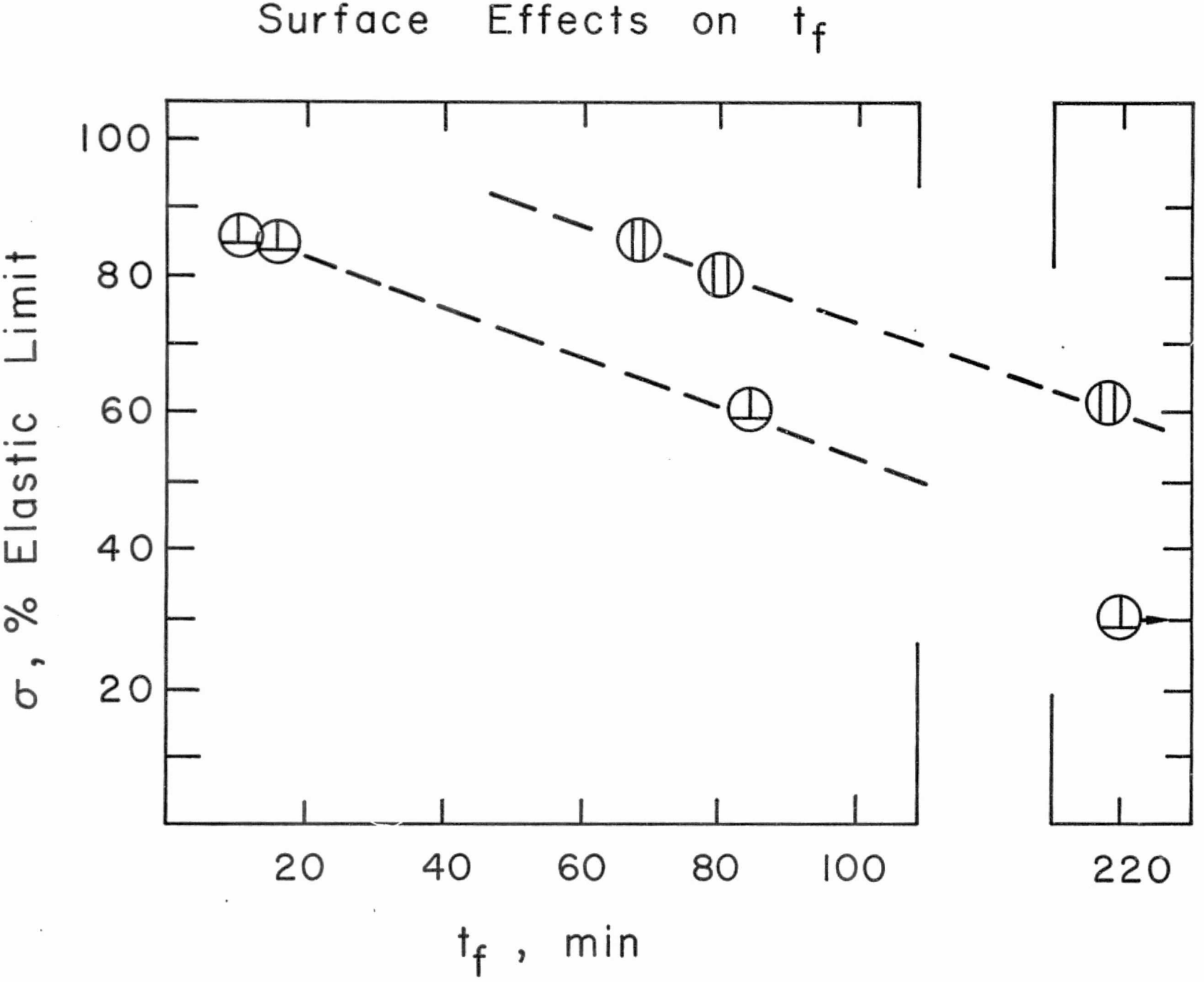

Ti-6-4 Alloy in 50:50 vol % CH_3OH / CCl_4

Figure 20

Figure 21. SCC Response of Titanium Alloys to CH_3OH/CCl_4 Solutions

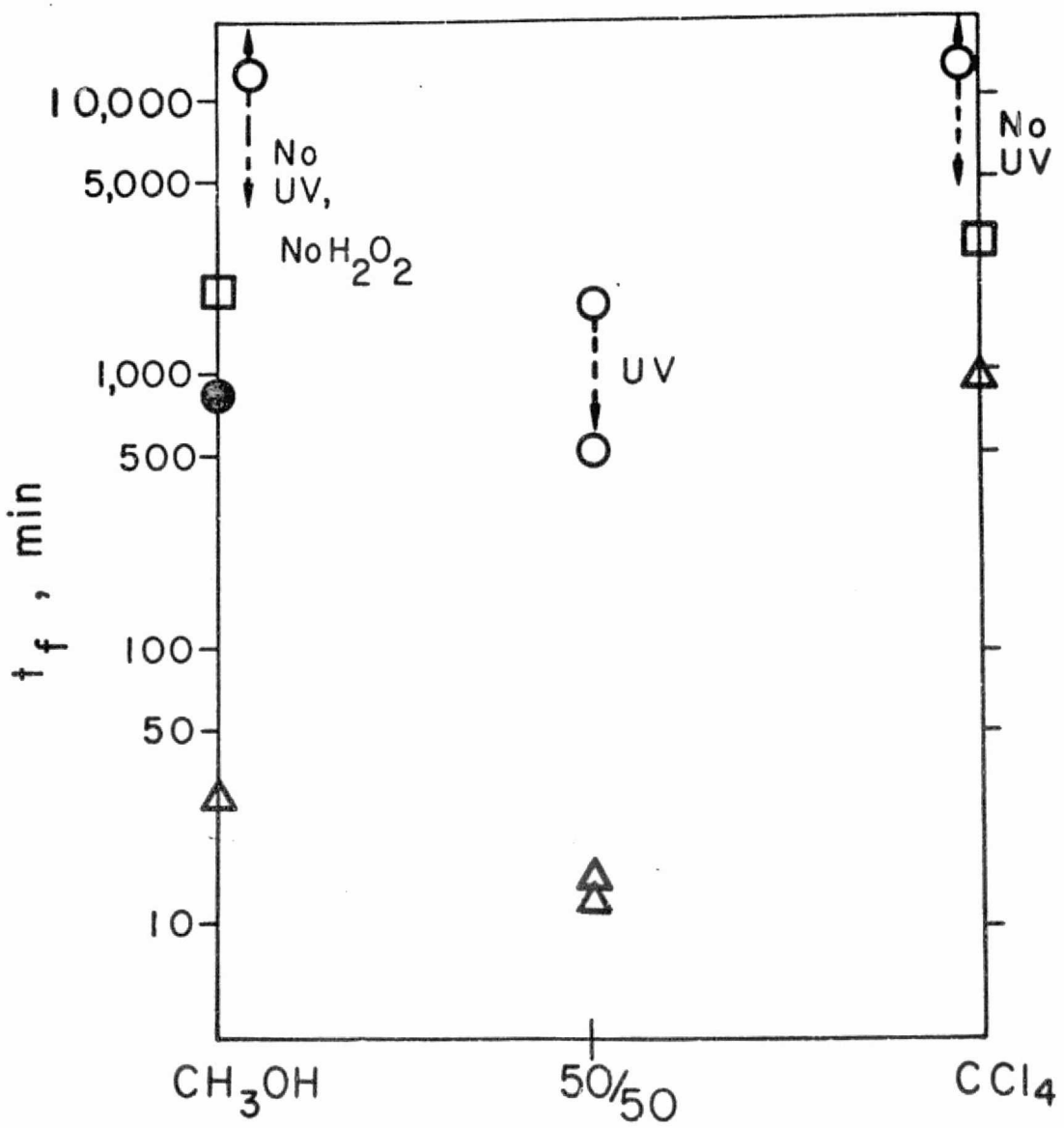

FIGURE 22. FRACTURE SURFACE OF A-70 Ti SCC IN PURIFIED METHANOL

FIGURE 23. FRACTURE SURFACE OF A-70 Ti SCC IN PURE CCl_4

FIGURE 24. FRACTURE SURFACE OF A-70 Ti IN $CH_3OH + CCl_4$ (IRRADIATED)

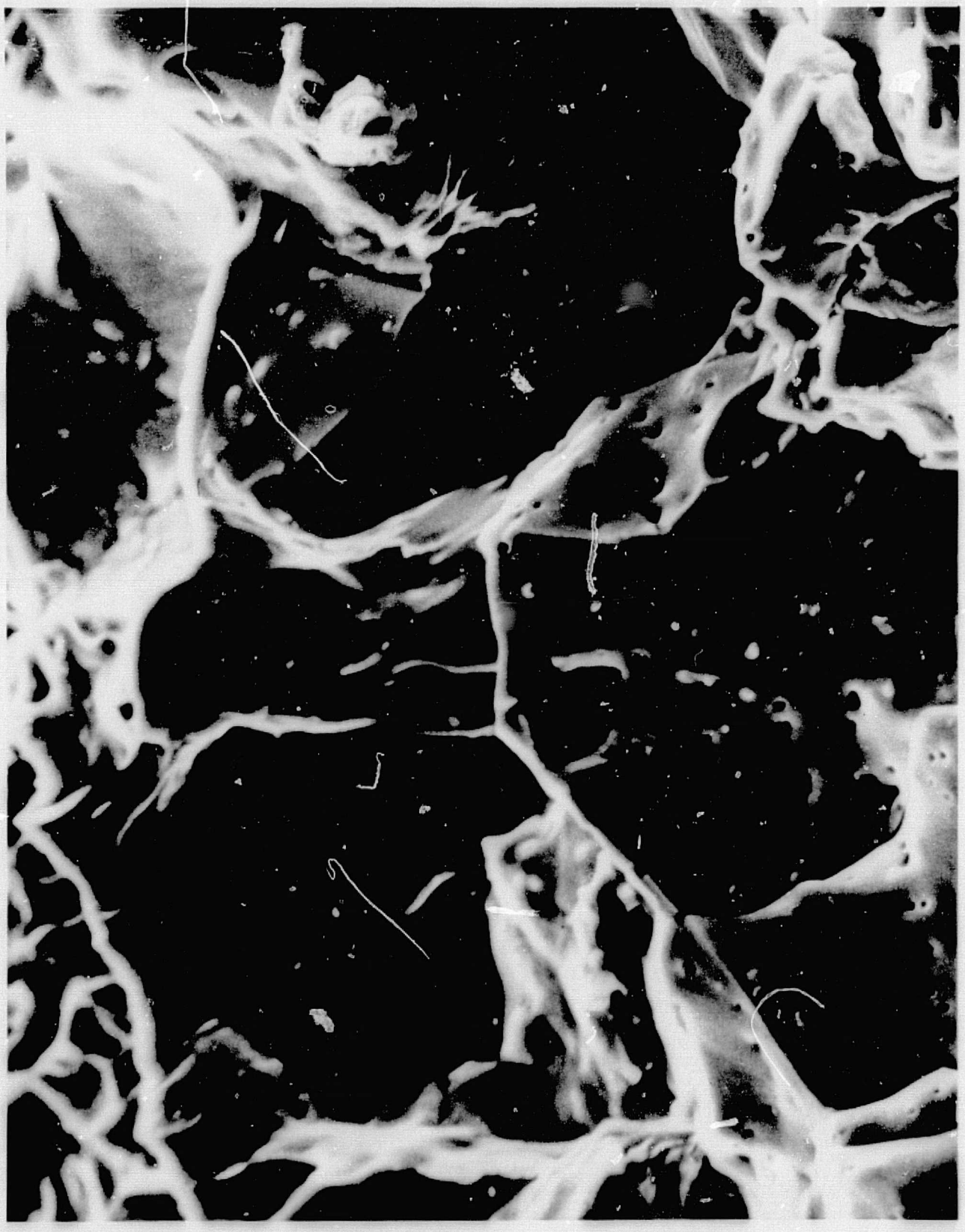

FIGURE 25. MODIFICATIONS FOR PHOTOCHEMICAL EFFECTS STUDIES

25a. Quartz-windowed Sample

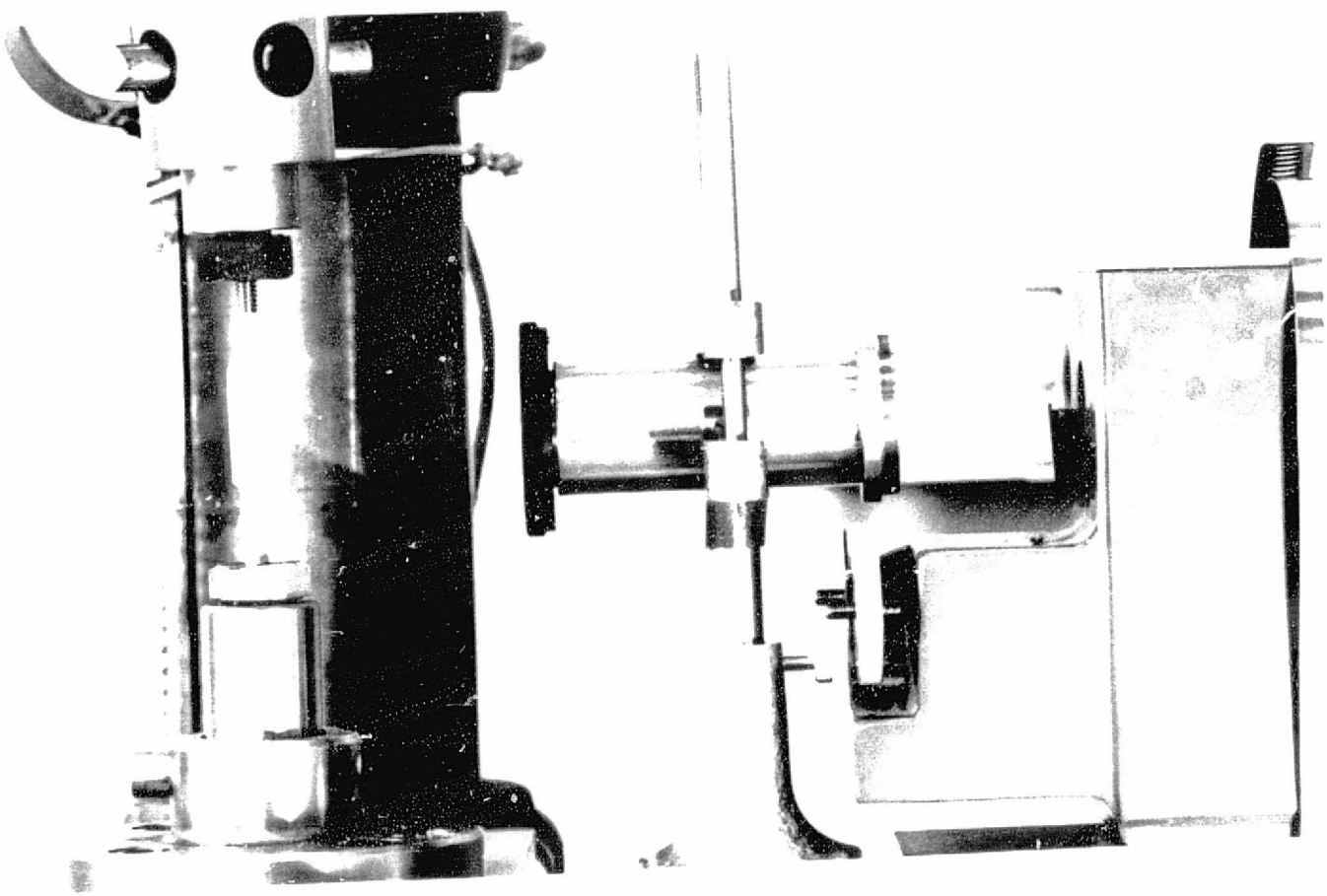

25b. Irradiation Arrangement During SCC Test